ANALYSIS AND DESIGN OF A SUBSTRATE INTEGRATED WAVEGUIDE MULTI-COUPLED RESONATOR DIPLEXER

AUGUSTINE ONYENWE NWAJANA

A thesis submitted in partial fulfilment of the requirements of the University of East London for the degree of Doctor of Philosophy

July 2017

Abstract

A microwave diplexer achieved by coupling a section of a dual-band bandpass filter onto a section of two single-bands (i.e. transmit and receive) bandpass filters is presented. This design eliminates the need for employing external non-resonant junctions in diplexer design, as opposed to the conventional design approach which requires separate non-resonant junctions for energy distribution. The use of separate non-resonant junctions in diplexer design increases the design complexity, as well as gives rise to bulky diplexer devices. The proposed design also removes the too much reliance on the evaluation of suitable characteristic polynomials to achieve a diplexer. Though the evaluation of complex polynomials to achieve a diplexer is seen as a viable option, the technique is hugely dependent on optimisations which come with loads of uncertainties.

This thesis relies on well-established design formulations to increase design reliability, as well as simplicity. A 10-pole (10^{th} order) microwave diplexer circuit has been successfully designed, simulated, manufactured and measured. The measured results have been used to validate the circuit model and the electromagnetic (EM) simulated results. The diplexer is composed of 2 poles from a dual-band bandpass filter, 4 poles from a transmit bandpass filter and the remaining 4 poles from a receive bandpass filter.

The design was initially implemented using asynchronously tuned microstrip square open-loop resonators. The EM simulation and the measurement results of the microstrip diplexer were presented and show good agreement with the proposed design theory. The design was also implemented using the substrate integrated waveguide (SIW) technique and results presented and discussed. In comparison to the results achieved with the microstrip diplexer, the EM simulation and the measurement results realised with the SIW diplexer, show that a slightly better insertion loss was attained across both the transmit and the receive channels, respectively.

Table of Contents

List of Figures

List of Tables

List of Symbols and Abbreviations

2D	Two-Dimensional
3D	Three-Dimensional
AC	Alternating Current
ADS	Advanced Design System
BPF	Band-Pass Filter
BSF	Band-Stop Filter
C	Capacitance of a capacitor
C_0	Speed of light in free space
CAD	Computer-Aided Design
CPW	Co-Planar Waveguide
CR	Common Resonator
d	Diameter of metallic post (or diameter of via)
dB	Decibel
DBF	Dual-band Bandpass Filter
DC	Direct Current
D-CRLH-MTM	Dual Composite Right-Left Handed Metamaterial
E	Electric
ED	Energy Distributor
EM	Electro-Magnetic

EMPro	Electro-Magnetic Professional
f	Frequency
f_0	Fundamental resonant frequency (or cut-off frequency)
FBW	Fractional Band-Width
FEM	Finite Element Method
f_H	Higher frequency boundary
f_L	Lower frequency boundary
f_r	Resonant frequency
FSIW	Folded Substrate Integrated Waveguide
GCPW	Grounded Co-Planar Waveguide
GHz	Giga-Hertz
GIPD	Glass-based Integrated Passive Devices
h	Substrate thickness
HMSIW	Half-Mode Substrate Integrated Waveguide
HPF	High-Pass Filter
HTS	High-Temperature Semiconductor
IEEE	Institute of Electrical and Electronic Engineers
IL	Insertion Loss
J-inverter	Admittance inverter
k	Coupling coefficient

K_a	Asynchronous coupling coefficient
K-inverter	Impedance inverter
K_s	Synchronous coupling coefficient
L	Inductance of an inductor
l	Length
LCP	Liquid Crystal Polymers
l_{eff}	Effective length
LKPF	Leiterplatten-Kopierfräsen
LPF	Low-Pass Filter
LTCC	Low-Temperature Co-fired Ceramics
M	Magnetic
MatLab	Mathematical Laboratory
MEMS	Micro-Electro-Mechanic Systems
MHz	Mega-Hertz
MMT	Mode Matching Technique
mm-Wave	Millimetre Wave
nH	Nano-Henry
p	Pitch (or distance between two metallic posts)
PCB	Printed Circuit Board
pF	Pico-Farad

PIM	Passive Inter-Modulation
P_r	Passband ripple
Q	Quality factor (or unloaded quality factor)
Q_{ext}	External quality factor
Q-Factor	Quality Factor
Q_L	Loaded quality factor
R	Resistance of a resistor
RF	Radio Frequency
RL	Return Loss
R_s	Skin Resistance
R_x	Receive
s	Spacing (or separation distance)
S_{11}	Simulation / measurement return loss
S_{21}	Simulation / measurement transmit band insertion loss
S_{31}	Simulation / measurement receive band insertion loss
S_{32}	Simulation / measurement isolation between transmit and receive bands
SIR	Stepped Impedance Resonator
SIW	Substrate Integrated Waveguide
SLR	Slot-Line Resonator
SMA	Sub-Miniature version A

SOLR	Square Open-Loop Resonator
t	Tapping distance (also, signal line thickness)
T	Transfer function
tan δ	Loss tangent
TE	Transverse Electric
TEM	Transverse Electro-Magnetic
TL	Transmission Line
TM	Transverse Magnetic
T_x	Transmit
V	Voltage
w	Width
w_{eff}	Effective width
Y_L	Load admittance
Y_s	Source admittance
Z	Impedance
Z_0	Characteristic impedance
Z_L	Load impedance
Z_s	Source impedance
α_c	Conductor loss mechanism
α_d	Dielectric loss mechanism

α_r	Radiation loss mechanism
ε_{eff}	Effective permittivity (or effective dielectric constant)
ε_r	Relative permittivity (or relative dielectric constant)
λ	Wavelength
λ_g	Guided wavelength
μ_r	Relative permeability
σ_c	Conductivity of copper
ω	Angular frequency
Ω	Low-pass prototype frequency domain
ω_c	Cut-off angular frequency
Ω_c	Low-pass prototype cut-off frequency
ω_r	Angular resonant frequency

Acknowledgements

I would like to thank my director of studies (i.e. my first supervisor), Dr Kenneth S. K. Yeo for his wonderful guidance and support throughout the period of my PhD research. He did not only act as my lead supervisor but also went extra miles in ensuring that my work was fabricated, in the absence of the workshop technicians. I would also like to thank my second supervisor, Dr Wada W. M. Hosny for his advice at the beginning of my research journey. His feedback during my transfer from MPhil to PhD was very helpful.

My sincere gratitude also goes to Professor Allan J. Brimicombe who taught me on the research method module in the first year of my research. His guidance and support helped me through the process of registering my PhD research topic with the UEL graduate school.

Finally, this acknowledgment will be incomplete without the mention of my research colleague, Amadu, who has been a member of my research team since the start of this project in 2013. He is a wonderful gentleman to have as a team mate. Thank you for being there.

Dedication

This thesis is dedicated to my lovely wife, Mrs Amaka Calista Nwajana (a.k.a. AsaFano) who shouldered most of the responsibilities of taking care of our wonderful kids (Muna & Ife) while I accomplish this profound task. I also like to welcome Onyie to our lovely family. This research work is for you as you decided to join the family in this particular month that I am submitting my thesis. Welcome home, daddy loves you.

Chapter 1: Introduction

1.1 Background

The need to miniaturise in size, as well as reduce the design complexity of microwave and millimetre-wave components, circuits and devices; while maintaining (or even improving on) the quality of such components, circuits and devices has recently drawn a lot of attention from researchers in this research field. The term microwave, in this context, is used to describe electromagnetic (EM) waves with frequencies beginning from 300 MHz and ending at 300GHz. The microwave frequency range (i.e. 300 MHz to 300 GHz) corresponds to the free space wavelengths of 1 m to 1 mm as shown in Figure 1.1 (Hong and Lancaster, 2001). EM waves with frequencies ranging from 30 GHz to 300 GHz are also referred to as millimetre-waves as a result of their wavelengths being in the millimeter range i.e. 1 mm to 10 mm. According to Hong and Lancaster (2001), the radio frequency (RF) spectrum lies below the microwave frequency spectrum. However, the boundary between the RF and microwave frequencies is arbitrary and depends on the particular technology developed for the exploitation of the given specific frequency range (Hong and Lancaster, 2001). It is important to note that the frequency values in Figure 1.1 increase in the reverse direction to the wavelength values. This is in agreement with Eqn. (1.1) where c_0 is the speed of light in free space, f is the frequency, and λ is the wavelength.

$$f = \frac{c_0}{\lambda} \tag{1.1}$$

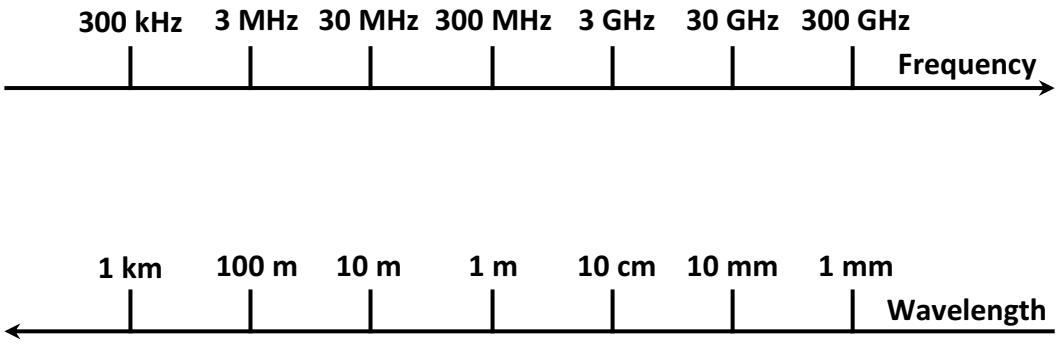

Figure 1.1: Radio frequency and microwave spectrums (Hong and Lancaster, 2001).

Microwave diplexer is a device that has attracted a lot of interest due to its ability to allow two separate components to share one communication medium (Nwajana and Yeo, 2016). The aforementioned advantage makes the diplexer a cost effective and less bulky alternative to communicating through two separate transmit and receive channels. Due to the vast applications of diplexers in communication engineering, researchers have been coming up with novel and better design methods to enable engineers cope with the ever increasing demands of modern communication systems. The design of diplexers has always presented the design engineers with ever growing stringent requirements such as: selectivity, bands isolation, high performance, smaller size, lighter weight, lower cost, etc. RF and microwave diplexers could be designed as lumped elements or distributed elements circuits, but this will depend on requirements and specifications. Diplexers may be achieved with different transmission line techniques including: waveguide, slot-line, strip-line, coaxial line, micro-strip line, coplanar waveguide (CPW), etc. Advancements in computer-aided design (CAD) tools including full-wave electromagnetic (EM) and finite-element method (FEM) simulators have revolutionised the diplexer design and characterisation process

(Hong and Lancaster, 2001). The popular fabrication technologies that has been investigated and reported for modern day diplexers include: printed circuit board (PCB) (Hao et al., 2005; Tang et al., 2007; Nwajana and Yeo, 2016), micro-electro-mechanic systems (MEMS) also referred to as micromachining (Hill et al., 2001; Reid et al., 2008; Skaik et al., 2011), high-temperature superconductors (HTS) (Heng et al., 2013; Zheng et al., 2014; Zheng et al., 2015; Guan et al., 2016), low temperature co-fired ceramics (LTCC) (Fritz and Wiesbeck, 2006; Kim et al., 2010; Chu et al., 2011), liquid crystal polymers (LCP) (Govind et al., 2006; Ashiq and Khanna, 2015), etc.

A diplexer is the simplest form of multiplexer that is widely used for either splitting a frequency band into two sub-bands of frequencies, or for combining two sub-bands into one wide frequency band (Yun et al., 2005; Zhu et al., 2014). Diplexers are popularly used in satellite communication systems to combine both the transmit (Tx) and the receive (Rx) antennas on space crafts. This can reduce the mass and volume of the space craft to a considerable amount, as only one antenna is required to transmit and also receive signals (Yun et al., 2005). As a frequency selective device, the diplexer connects two different networks with different operating frequencies to a single port. Diplexers are commonly used in Radio Frequency (RF) front end of cellular radio base stations to separate the Tx and the Rx bands as shown in Figure 1.2 (Hunter et al., 2002). The diplexer is an important device in the entire system; it is made up of two channel filters and a power splitter. The Tx / Rx diplexer shown in Figure 1.2 allows for the simultaneous transmission and reception of signals through the single antenna. The Tx filter is designed to have high power handling ability to enable it cope with the relatively high power signals generated at the transmitter. The Rx filter, on the

other hand, is only needed to handle very weak signals from the receiver. Therefore, no power handling consideration is needed at the Rx channel. The isolation between the Tx and the Rx bands is a design parameter that must be in the forefront when the diplexer is being formed. This is because a poor isolation between the transmit and the receive bands would mean that a large amount of signal, could be deflecting towards the wrong direction during the diplexer operation. In summary, microwave diplexers are three-port devices that typically operate over the frequency range of 300 MHz – 300 GHz.

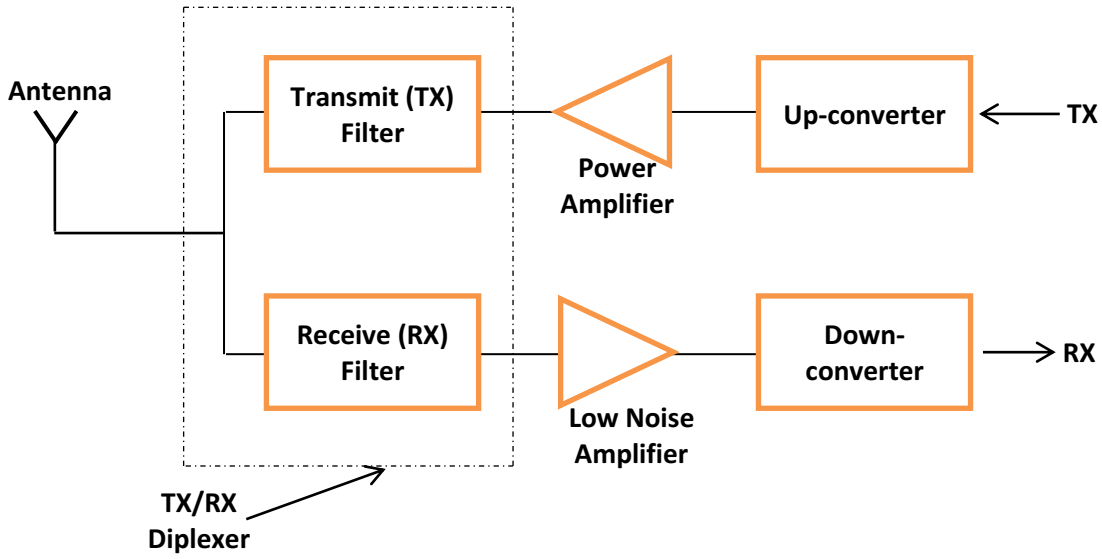

Figure 1.2: RF front end of a cellular base station (Hunter et al., 2002).

The selectivity of the Tx and the Rx bands of diplexers is another very important design criteria that should be put into consideration when designing a diplexer. Several authors have proposed different methods for designing microwave diplexers. The conventional approach to achieving a diplexer is to connect two separately designed filters together using an external non-resonant energy distribution connector. This connecting component could be: a T-junction (Liu et

al., 2013; Yiming and Xing, 2010), a Y-junction (Bastioli et al., 2009; Xu et al., 2007), a circulator (Kodera and Caloz, 2010), a manifold (Heng et al., 2014; Morini et al., 2015) or an out of band common resonator (Yang and Rebeiz, 2013; Tantiviwat et al., 2013). The separate energy distribution connector used in the conventional method of diplexer design had resulted to relatively complex and larger size devices (Nwajana and Yeo, 2016). The complexity of the conventional design approach is as a result of involving the external connecting component or junction, which needs to be continuously adjusted and optimised before an expected result could be realised. The large size problem of the conventional design is as results of the fact that the separate junction component does not contribute to the number of poles contained in the resulting diplexer transmit and receive channels. This means that the external / separate junction has very little or no contribution to the diplexer selectivity, but only there to split the channel and hence, contributing slightly to the relatively larger size of the conventional diplexer.

To overcome the drawbacks associated with the conventional diplexer design method, the work reported in this thesis has successfully eliminated the need for employing the external / separate junction connector in achieving a diplexer and replacing it with resonators that contribute resonant poles to the diplexer responses. This thesis report will show that the design complexity associated with the conventional diplexer design approach, can be averted with a good mastery of the basic principles associated with bandpass filter (BPF) design as reported in Hong and Lancaster (2001), and the dual-band bandpass filter (DBF) design as reported in Yeo and Nwajana (2013). By this novel method, design engineers can achieve diplexers purely based on existing formulations rather than

developing complex optimisation algorithms (Wang et al., 2012; Shang et al., 2013) to achieve the same function. Also, considering the fact that the diplexer reported in this thesis is formed by coupling a section of the Tx and the Rx channel filters resonators, onto a section of the DBF resonators; a reduced sized diplexer is achieved. The reason for the reduced size in the resulting diplexer is because the DBF resonators contribute one resonant pole to the diplexer Tx channel and one resonant pole to the diplexer Rx channel. Parts of the results from this thesis have been published in Nwajana and Yeo (2016) and Nwajana et al. (2017).

The diplexer design method proposed in this thesis involves cascading a section of a dual-band bandpass filter, with a section of two bandpass filters. A dual-band bandpass filter is a filter that passes two bands of frequencies while attenuating frequencies outside the two bands (Deng et al., 2006; Nwajana and Yeo, 2016). A bandpass filter, on the other hand, is a filter that passes frequencies within a single band while rejecting all other frequencies outside the band. The pair of DBF resonators reported here can be viewed as an energy distributor (ED) which distributes energy towards the Tx and the Rx bands of the diplexer. The DBF resonators serve as replacements to the external junction or connector used in other diplexer design methods found in existing literature. The actual function of the DBF resonators employed in this work is to establish the two pass-bands of the microwave diplexer.

1.2 Motivation and Problem Statement

The increasing demand and high interest in size miniaturization, as well as reduction in design complexity of microwave components, have motivated a lot of researchers into seeking solutions and remedies to the ever growing challenges. Microwave diplexer is one of the essential components in the RF front end of most multi-service and multi-band communication systems and sub-systems. This is because the presence of the diplexer reduces the number of antennas required in a system (Deng et al., 2013). The RF front end of any cellular base station is a very good example of a system that has highly benefitted from the merits of achieving a diplexer with simple design and reduced size. The diplexer present in the RF front end of a cellular base station makes it possible for an input signal with two different frequencies, to split into two different signals at the output ports. It also facilitates the combination of two different input signals into one signal at the output port (Xiao et al., 2015).

The main motivation behind the research work reported in this thesis is to achieve a diplexer where each resonator contributes a resonant pole to the diplexer response for reduced size. This means that the proposed diplexer will not rely on any external non-resonant device for energy distribution as is the case with most diplexers design methods reported in literature. The proposed diplexer will also be based on known mathematical formulations for bandpass filter and dual-band bandpass filter designs for simplicity. Some authors have offered different design techniques to achieving diplexers of reduced size but based on complex polynomial evaluation. Skaik and Lancaster (2011) and Skaik et al. (2011) proposed diplexers without external junctions and using coupling matrix

optimisation. The optimisations of the coupling matrix reported in those papers were based on the minimisation of cost functions that were evaluated in order to derive the diplexers. This is an effective but complex way to achieve a diplexer response, as a good mastery of the polynomial evaluation and reduction / convergence technique is highly required. In a related research paper (Lin and Yeh, 2015), a triplexer based on parallel coupled-line filters using T-shaped short-circuited resonators was reported. The design was based on a connecting junction and matching transmission lines. The design of a quad-channel diplexer using stepped impedance resonators (SIRs) has also been researched and presented (Wu et al., 2013). The quad-channel diplexer is made up of two pairs of coupled SIRs with an impedance ratio that is greater than 1, and the quarter-wavelength source / load coupling lines. The resonant modes of the SIRs were simply determined by tuning their impedance ratio and length ratio. This facilitated the implementation of bandpass filters with very close dual-passbands. The source / load coupling lines were designed to correspond to the quarter-wavelength at the centre frequency of the first passband at each output port. The quad-channel diplexer configuration is a simple and relatively effective design approach when compared to the conventional diplexer design technique. The resultant diplexer is also of relatively small size as opposed to conventional standard.

Wang and Xu (2012) reported a diplexer with relatively reduced size when compared to the conventional diplexers. The design was based on the evaluation of the characteristic polynomial functions and the optimisation of error functions to achieve coupling. It employed a common resonator in place of the external junction for energy distribution. The issue here is that the common resonator used

for energy distribution neither contribute a pole to the transmit band nor the receive band of the resulting diplexer. This is evident in the diplexer response curves presented in the paper (Wang and Xu, 2012). For example, the 10-resonator diplexer presented produced 5 poles on the transmit band and 4 poles on the receive band, while the 7-resonator diplexer produced 3 poles on the transmit band and another 3 poles on the receive band. The additional resonator is an out of band resonator which is used for coupling the transmit and the receive paths. Hence, the addition resonator used to split the bands in each case does not contribute any pole to either bands of the diplexer but will take up additional real estate of the design.

The diplexer reported in this thesis neither uses an external non-resonant junction nor a common resonator for energy distribution. Instead, a pair of dual-band bandpass filter (DBF) resonators were coupled onto the transmit (Tx) and the receive (Rx) channel filters resonators to form the diplexer. This simply means that the pair of DBF resonators replaces the first resonators of both the Tx and the Rx channel filters. The coupling scheme for a 10-pole (10^{th} order) diplexer is shown in Figure 1.3.

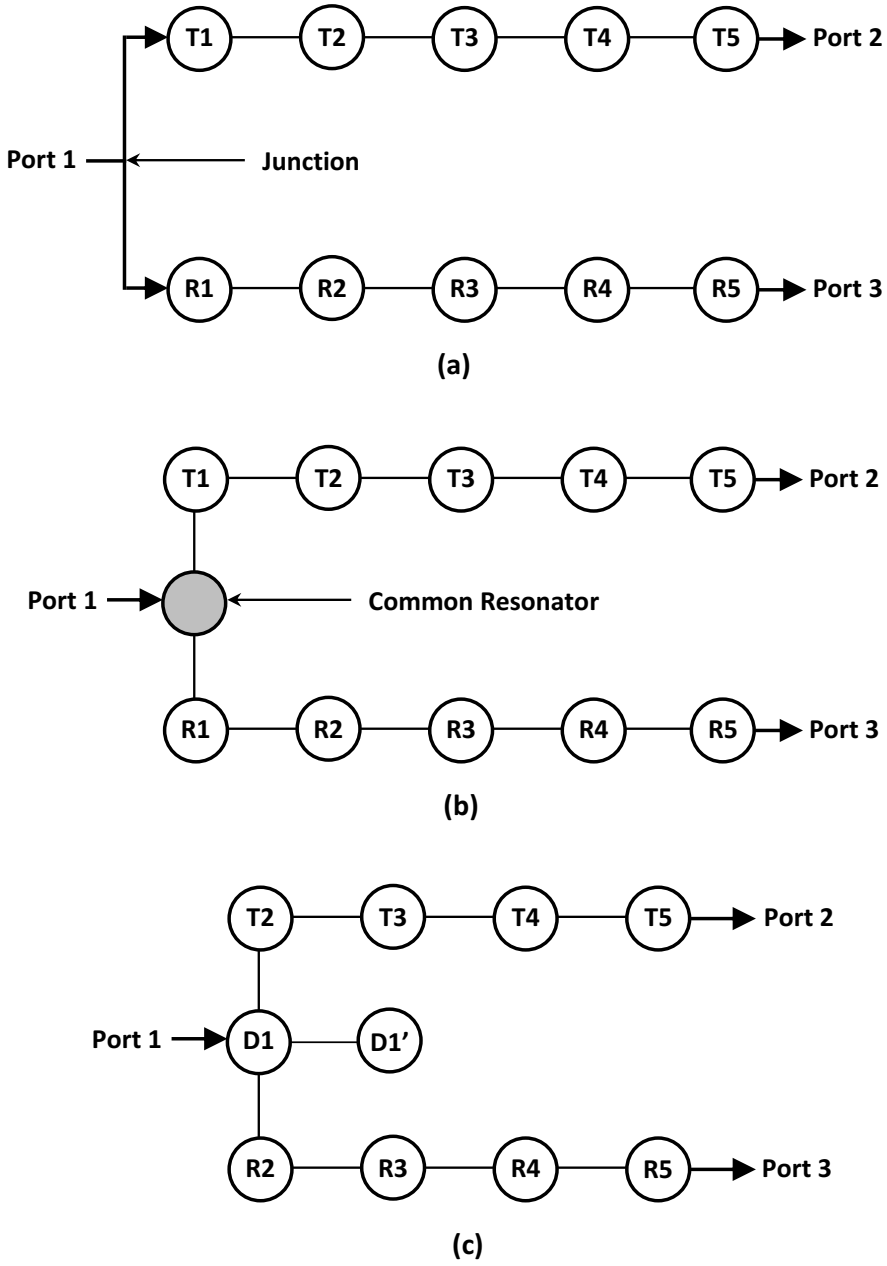

Figure 1.3: 10-pole diplexer coupling scheme. (a) Conventional topology. (b) Common resonator topology. (c) Proposed topology.

The conventional (i.e. junction) diplexer is represented in Figure 1.3 (a), while the common resonator diplexer and the proposed diplexer are shown in Figure 1.3 (b) and Figure 1.3 (c), respectively. D1 and D1' in Figure 1.3 (c) are the pair of dual-band bandpass filter resonators; T1, T2, T3, T4, T5 and R1, R2, R3, R4, R5 are the Tx and the Rx channel filters resonators, respectively. The external

junction indicated in Figure 1.3 (a) could be a T-junction (Chen et al., 2014; Shi et al., 2011), a Y-junction (Shimonov et al., 2010), a circulator (Saavedra, 2008) or a manifold (Taroncher et al., 2006). A diplexer based on a coupling scheme similar to that of the common resonator shown in Figure 1.3 (b) was proposed in Chen et al. (2006).

1.3 Research Method

The most widely employed method when it comes to the design of RF and microwave diplexers is to use two separately designed bandpass filters, having distinct frequencies, with a three-port impedance matching network. The combining network (i.e. the impedance matching network) is normally aimed at producing good transmission in one passband and exhibiting high impedance in the other passband, in order to achieve the necessary channel isolation (Wu et al., 2015). The reality is that designing a matching network that can produce a very good transmission in one passband and a good attenuation in the other passband is a very challenging feat to achieve (Guan et al., 2014). Numerous examples abound in literature were researchers have successfully achieved diplexers using a three-port matching network. T-junctions (Zhang et al., 2010; Hung et al., 2010) are the most popular matching networks used in diplexer design. Other types of junctions that have been employed in achieving diplexers include: the manifold (Rhodes and Levy, 1979; Packiaraj et al., 2005), the Y-junction (King et al., 2011; Harfoush et al., 2009), and the circulator (He et al., 2012). A common resonator (Guan et al., 2016; Chen et al., 2006) has also been used in place of the matching network to successfully achieve multiport devices such as diplexers and triplexers.

The method of diplexer design proposed in this thesis involves cascading a section of a dual-band bandpass filter (DBF), with sections of two separately designed bandpass filters (BPFs) as shown in Figure 1.3 (c). D1 and D1' are the first pair of dual-band resonators obtained by separately designing a DBF, whose fractional bandwidth (FBW) is equal to the combined FBWs of the two BPFs that would form the transmit (Tx) and the receive (Rx) channels of the proposed diplexer. The main function of the pair of dual-band bandpass filter resonators present in the proposed diplexer is to establish the two pass-bands of the diplexer. Like the external junctions used in the conventional diplexer design approach, the dual-band bandpass resonators are responsible for distributing energy towards the Tx and the Rx bands of the diplexer. Unlike the external junctions that do not contribute to the number of poles present in the resultant diplexers, the dual-band bandpass filter resonators do contribute to the number of poles by physically replacing one resonator from the Tx channel and one resonator from the Rx channel as shown in Figure 1.3 (c). This explains why the physical size of the proposed diplexer is relatively smaller when compared to that of the conventional diplexer.

The circuit model of the proposed diplexer was simulated using the Keysight Advanced Design System (ADS) circuit simulator, while the microstrip layout simulation was achieved using the Keysight ADS momentum simulator. The electromagnetic (EM) simulation of the SIW layout of the proposed diplexer was based on the finite-element method (FEM) of the Keysight electromagnetic professional (EMPro) 3D simulator. It is important to note that any other

professional circuit, EM or even FEM simulators could be used to achieve results similar to those presented in this thesis. The microstrip diplexer fabrication was based on the printed circuit board (PCB) milling process, while the SIW diplexer was fabricated using the PCB micro-milling process based on the Leiterplatten-Kopierfrasen (LKPF) Protomat C60.

1.4 Literature Review

A diplexer is the simplest form of multiplexer. It is a three port (3-port) frequency distribution device mostly utilised in communication networks. Microwave diplexers are widely used in splitting input signals from a single port, into two communication channels operating at different frequencies. They can also be used to combine two separate communication channels into a single combined signal for transmission via a shared antenna. The transmitter and the receiver of diplexers are designed to operate at different frequency bands and are duplexed to the transceiver diplexer (Chen et al., 2011). It is important to note the clear difference between a diplexer and a duplexer. Though both devices (i.e. diplexer and duplexer) have similar design procedures, the transmit channel of a duplexer suffer from power handling issues. Hence, this must be considered when duplexers are been designed. The transmit and the receive bands terminologies repeatedly referred to throughout this thesis are for the two channels of the diplexer. Therefore, no power handling issues have been considered in this thesis. In designing a microwave diplexer, an accurate computer aided design (CAD) is required in order to avoid the over reliance on turning screws or any other adjusting component which actually limits the maximum transmittable power, and also increases the cost of the device.

1.4.1 Diplexers Based on Design Approach

Various approaches to the design of diplexers have been reported in literature. The most vastly reported approach to designing diplexers is the conventional method which involves combining two bandpass filters (BPFs) with a three-port impedance matching network (Chan, 2015) such as a manifold (Guglielmi, 1993; Ye and Mansour, 1994), a circulator (Saavedra, 2008; Kodera and Caloz, 2010), a T-junction (Thirupathaiah et al., 2014; Kordiboroujeni et al., 2014), or a Y-junction (Bastioli et al., 2009, Wu and Meng, 2007). Another approach that has been recently reported is the common resonator method, which involves replacing the three-port impedance matching network of the conventional method with a common resonator. The synthesis of coupled resonator diplexers based on linear frequency transformation and optimisation have also been reported (Wang et al., 2012; Macchiarella and Tamiazzo, 2006). This approach is based on the evaluation of suitable characteristic polynomials of the diplexer.

The traditional or conventional approach to achieving a diplexer is to combine two separately designed bandpass filters (BPFs) with a three-port impedance matching network as shown in Figure 1.4. The two BPFs are distinctly designed to operate at different frequencies that correspond to the frequencies of the transmit (Tx) and the receive (Rx) bands of the target diplexer. The combining network, which in this case is the 3-port impedance matching network, is normally designed to produce good transmission in one passband and exhibit high impedance in the other passband (Wu et al., 2015). This stringent design condition of the 3-port impedance matching network is to facilitate the achievement of the desired channel isolation. According to an investigation by

Guan et al. (2014), designing a matching network that can produce a good transmission in one passband and a good attenuation in the other passband is a very challenging feat to achieve. The performance of a conventional diplexer will highly depend on the channel filters, as well as the 3-port matching network (Chan et al., 2015). This is because the overall losses experienced in the diplexer are due to the sum of all the individual losses contributed by the channel filters and the combining network.

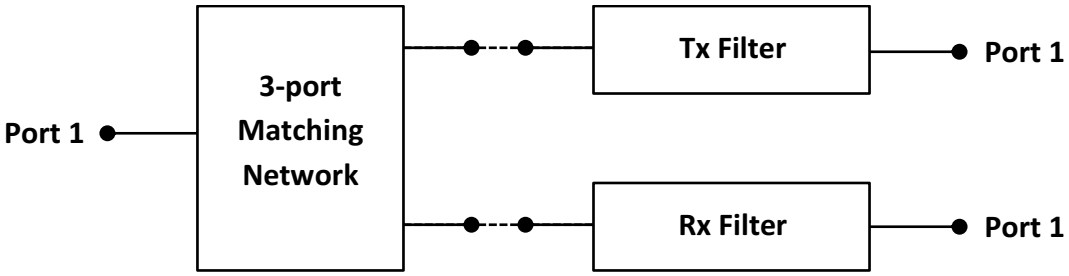

Figure 1.4: Conventional diplexer architecture.

The 3-port matching network shown in Figure 1.4 could be a manifold, a circulator, a Y-junction or a T-junction. In addition to contributing to the size and complexity of a diplexer, each type of matching network has its peculiar disadvantage. For example, tuning of diplexers / multiplexers designed with a manifold as the connecting device can be time-consuming and expensive. Such diplexers are also not open to flexible frequency plan; meaning that changes in any channel frequency will require a totally new diplexer design (Cameron and Yu, 2007). On the other hand, diplexers employing circulators as the connecting device suffer from extra loss per trip as signals must pass in succession through the circulator. According to Cameron and Yu (2007), low-loss, high-power ferrite circulators are expensive. Circulators are also prone to higher level of passive

intermodulation (PIM) products when compared to T- and Y- junctions and manifolds. Various authors have reported different diplexers/multiplexers achieved by means of employing each and every one of the four types of 3-port matching network highlighted in this sub-section.

Rhodes and Levy (1979) reported a multiplexer with immittance compensation. The involvement of the immittance compensation was done in such a way that not only preserved the canonic form of the multiplexer network, but also assisted in the physical construction by spacing the channel filters along the manifold. In another research paper (Guglielmi, 1993), the computer aided design (CAD) procedure for the manufacture of a class of manifold diplexers was described. This approach was based on filters implemented with thick inductive windows in rectangular waveguide. A study by Packiaraj et al. (2005) reported a manifold cavity diplexer based on tapped line interdigital filters topology. The work made provision for tuning screws at the end of each resonator to carter for post fabrication tuning. In a different study, the authors combined finite element electromagnetic based simulators with space mapping optimisation to produce manifold-coupled multiplexers, with dielectric resonator loaded filters (Ismail et al., 2012). A novel X-band diplexer based on overmoded circular waveguides for high-power microwaves was proposed by Li et al. (2013). The research finding relied on mode-matching techniques and numerical optimisation to achieve results. A radial waveguide structure with six rectangular ports was used as the duplexing manifold (Li et al., 2013). The schematic diagram of a 12-pole manifold diplexer is given in Figure 1.5 (Skaik and AbuHussain, 2013).

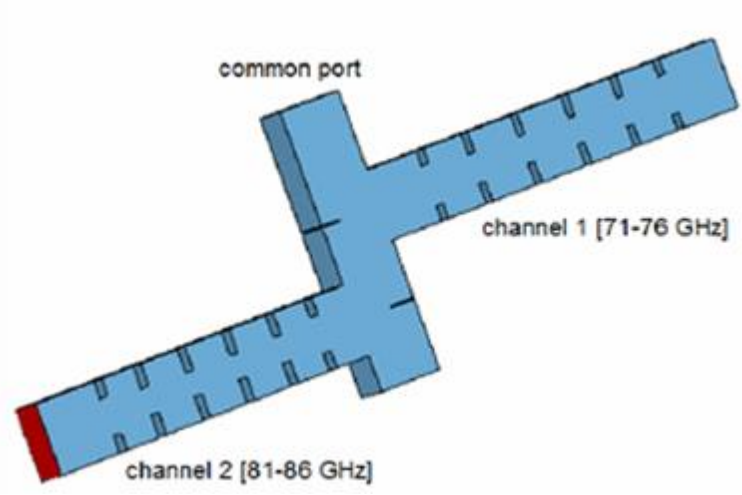

Figure 1.5: 12-pole manifold diplexer schematic (Skaik and AbuHussain, 2013).

In another investigation, a manifold-coupled narrowband superconducting quadruplexer with high isolation was reported (Heng et al., 2014). The work employed a binary matching network in order to minimise the undesired interactions amongst the four channels of the quadruplexer. Carceller et al. (2015) reported on manifold-coupled multiplexers with compact wideband. The method used was based on the sequential connection of filters to the manifold, and then making some adjustments at the point of interconnection. The filters were attached to the manifold without the use of stubs, thereby, minimising the effect of spurious resonance (Carceller et al., 2015). The efficient design of waveguide manifold multiplexers based on low-order electromagnetic (EM) distributed models (Cogollos et al., 2015) has also been reported. The main requirement for the design is that all channel filters and other design elements must be successfully represented by means of distributed models. Even though manifold diplexers / multiplexers are capable of realising optimum performance, both in terms of absolute insertion loss and amplitude and group delay response (Cameron and Yi, 2007); they have the disadvantage of having relatively large

size, complex design, time consuming and expensive tuning, and are not responsive to a flexible frequency plan. This means that a change of a channel frequency will require a new diplexer / multiplexer design.

Circulators are another group of traditional or conventional impedance matching network devices that have been employed in the design of microwave diplexers. When compared to manifolds, diplexers achieved using circulators are simple to tune as channel filters do not interact. They are also responsive to flexible frequency plan (Cameron and Yi, 2007). Like the manifolds, however, circulators contribute to the large size of resultant diplexers / multiplexers. They have higher level of passive intermodulation (PIM) products when compared to manifolds or even the T- and the Y- junctions. It is also expensive to obtain low-loss, high-power ferrite circulators. They have a peculiar disadvantage of making signals pass in succession through the circulator, thereby, incurring extra loss per trip (Cameron and Yi, 2007). A number of research papers have, in the past decade, reported diplexers based on circulators. Saavedra (2008) proposed a diplexer employing a circulator and interchangeable filters. The microwave diplexer employed a passive or active 3-port clockwise circulator device. ‘The use of a circulator in place of a manifold structure in the diplexer means that the filters can be tuned or even exchanged without the need to modify the manifold’ (Saavedra, 2008). In another research paper, a SIW circulator was used in the design of a novel compact Ka-band high-rejection diplexer (He et al., 2012). The SIW circulator employed in the design uses inductive windows to increase bandwidth. The entire design, including both channel filters and circulator as shown in Figure 1.6, were implemented on the SIW technology.

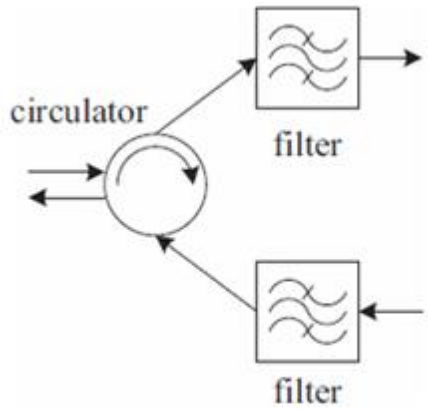

Figure 1.6: A diplexer formed with filters and a circulator (He et al., 2012).

Diplexers achieved by employing Y- and T- junctions are very similar in their design and operation. Like every other external matching network, the Y- and the T- junctions contribute to the size and complexity of the resultant diplexer. When compared to circulators, the Y- and the T- junctions exhibit low level of PIM products. Microwave diplexers formed with a Y- or a T- junction are simple to tune as there exist no interaction between channel filters. They are also amenable to modular concept, i.e. any change of a channel frequency may not necessarily require a new diplexer design.

The Y-junction has been reported in a number of published works found in literature. Xu et al. (2007) used a dual-mode rectangular stripline ring resonator to design two separate filters and then used a Y-junction feed-line to connect the two filters to form a diplexer circuit. Another research paper presented a diplexer designed and implemented in the X-band frequency (Harfoush et al., 2009). The two channels of the diplexer were designed using a waveguide Y-junction to equally split the any received signal. In a different investigation, Bastioloi et al.

(2009) proposed a resonant Y-junction for compact waveguide diplexers. The Y-junction employed in the design contained an elliptic ridge which served as a common dual-mode resonator for both the transmit (Tx) and the receive (Rx) channels of the diplexer. A diplexer which is formed by a combination of two electric plane (E-plane) filters and a magnetic plane (H-plane) Y-junction splitter has been reported (Shimonov et al., 2010). The design was based on the mode matching technique (MMT) and used the diplexer schematic shown in Figure 1.7. In a study by King et al. (2011), a microstrip diplexer using step impedance resonator (SIR) with folded hairpin structure was reported. The diplexer was achieved by separately designing two distinct bandpass filters (BPFs) and then connecting them with a Y-junction.

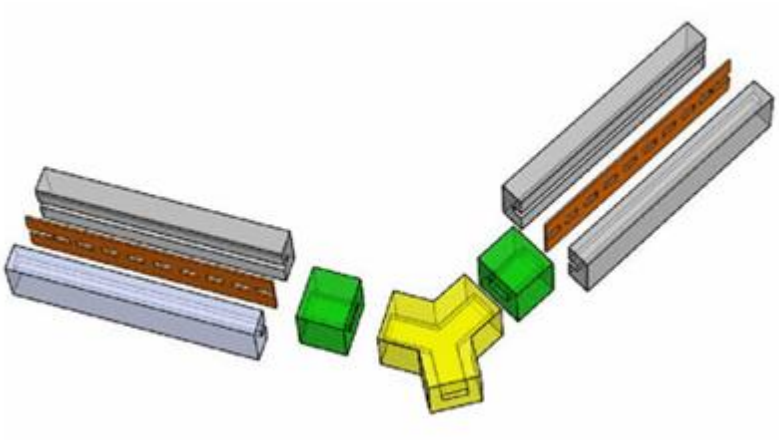

Figure 1.7: Y-junction diplexer schematic (Shimonov et al., 2010).

T-junctions are by far the most widely used 3-port impedance matching network employed in the design of microwave diplexers. This is a fact based on published works available in literature. The schematic diagram of a 2n-pole T-junction diplexer is given in Figure 1.8 (Tsai et al., 2013). Different authors have employed T-junctions in order to successfully achieved diplexers that meet their needs. The

design of a diplexer based on dual composite right-left handed metamaterial (D-CRLH-MTM) have been reported (Mansour et al., 2014). The design was formed by using a T-junction to combine two notch filters having different stop bands. In a different study, Chen et al. (2015) proposed a wide-band T-junction and bifurcated SIW diplexer. The T-junction employed in their work was designed to have short arms. This is to ensure that junction resonance in the wide-band frequencies are kept at the barest minimum (Chen et al., 2015).

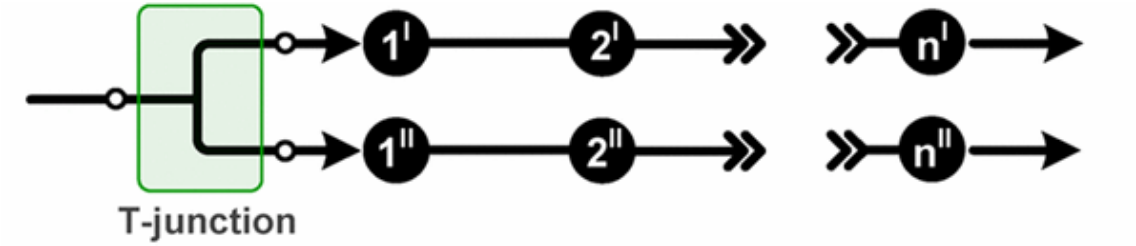

Figure 1.8: 2n-pole T-junction diplexer schematic (Tsai et al., 2013).

Another research paper reported a T-junction SIW diplexer based on circular triplet combline filter sections (Sirci et al., 2015). The design placed the transmission zeros of the diplexer below and above the passband. Positive and negative couplings were conveniently provided to facilitate the control of the location of each transmission zero in the diplexer responses. Rezaee et al. (2015) proposed a V-band diplexer based on the groove gap waveguide technology. The diplexer was formed by combining two channel filters with an H-plane T-junction. The major advantage of the groove gap waveguide diplexer over the traditional waveguide diplexer is that there is no need for an electrical contact between the top and the bottom metal plate. This is vital as it provides an opportunity for the integration of the diplexer to active transceiver circuits. A diplexer with high

isolation employing multi-order resonances (Wang et al., 2015) and a switchable diplexer design employing switchable bandpass filters (Xu, 2016) have both been reported. Both reports used the T-junction as the three-port matching network for energy distribution. A compact broadband waveguide diplexer that covers the Ku-band transmit and receive channels has also been proposed (Teberio et al., 2016). The diplexer was formed by combining a T-junction with a compact Ku-band, high-power lowpass and bandpass filters based on inductive irises. In another interesting research paper by Lee et al. (2016), a balance quad-band diplexer with wide common mode suppression and high differential-mode isolation was proposed. The 6-port balanced diplexer was achieved by connecting two dual-band bandpass filters through two stepped-impedance Resonators (SIRs) inserted T-junctions (Lee et al., 2016). The common disadvantages of all T- junction based diplexers are their increased size and design complexity.

A more recent approach to the design of microwave diplexer is to replace the three-port matching network of the traditional / conventional diplexer with a common resonator (CR) as shown in Figure 1.9. Though this recent method has proved effective in achieving diplexers of relatively small size when compared to the conventional approach, more size reduction can still be achieved using the approach proposed in this thesis. The common resonator method of diplexer design involves connecting two separately designed filters by means of a CR as the connecting device. Like the conventional diplexer, the performance of a CR diplexer will depend on the two channel filters and common resonator performances. This means that the losses experienced in a CR diplexer are due

to the individual losses contributed by each channel filter and the common resonator.

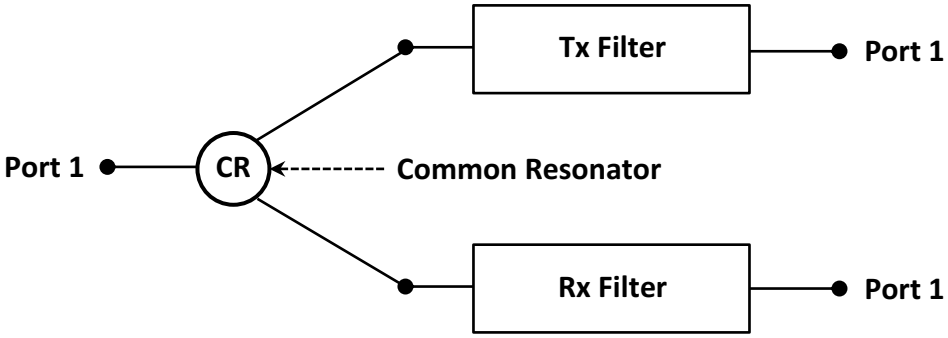

Figure 1.9: Common resonator diplexer architecture.

A number of research papers have, in the past decade, reported diplexers achieved based on the common resonator approach. The variable frequency response of the stepped-impedance resonator (SIR) has been exploited in the design of a common resonator diplexer (Chen et al., 2006). The fundamental and first spurious resonant frequency of the CR was well assigned in such a way as to allow it to be shared by both the transmit (Tx) and the receive (Rx) channels of the diplexer. Chuang and Wu (2011) also reported a microwave diplexer design employing a common T-shaped resonator. The common resonator (i.e. the T-shaped resonator) used in the design was employed as a frequency selective signal splitter that facilitated the design of a diplexer with extremely close frequency bands. A microwave diplexer based on the evaluation of the characteristic polynomials of the common resonator and the Tx and the Rx channel filters has also been reported (Wang and Xu, 2012). The CR used in the paper did not contribute to the number of poles contained in the diplexer response. Hence, the CR plays no role in the selectivity of the diplexer but only

acts as a channel splitter and energy distributor. Tantiviwat et al. (2013) is another research proposal that reported a diplexer with common resonator based on the exploitation of the variable frequency response of the SIR.

A different research paper presented a tuneable diplexer with flexible tuning capabilities and high selectivity (Yang and Rebeiz, 2013). Tsai et al. (2013) developed a novel laminated waveguide diplexer based on the modal orthogonality of multiple cavity modes. To replace the matching network of the conventional diplexer, they correctly located the feeding probes and coupling slots to successfully achieve the required coupling coefficients and external quality factors at both passbands. A SIW diplexer using dual-mode common resonator has been reported (Cheng et al., 2013). The resonant frequencies of the dual-mode square cavity were assigned to the relevant frequencies by improving on the strength of the perturbation distance. Other authors that have recently published their research findings in relation to CR diplexers include Guan et al. (2016) and Zhao and Wu (2016). A diplexer employing a square ring resonator as the CR has been proposed (Guan et al., 2016). The square ring resonator was perturbed by means of a square patch which excites the two degenerated mode of the common resonator. The two modes of the CR were designed to correspond to the two channels of the Tx and the Rx bands of the diplexer.

Within the last decade, a number of researchers have proposed and reported diplexers based on the evaluation of suitable characteristic polynomials. This method is predominantly appropriate when a very small band separation is

required between the Tx and Rx channels of the diplexer. The approach normally begins with an iterative algorithm which evaluates the characteristic polynomials of the two channel filters and the connecting three-port device used in forming the diplexer (Macchiarella and Tamiazzo, 2006; Loras-Gonzalez et al., 2010; Macchiarella and Tamiazzo, 2010; Skaik, 2012). The coupling matrices are then obtained by optimisation and then simplified in order to converge and give rise to the desired diplexer (Loras-Gonzalez et al., 2010; Skaik and Tubail, 2015). A direct synthesis approach has also been used to design two Chebyshev filters which were then combined using a Y-junction, in order to realise a diplexer (Wu and Meng, 2007). The direct synthesis approach is based on the notion that the polynomial functions for filter synthesis are composed of matched loads. The polynomial functions can be normalised with assumed complex load impedance and by real reference load impedance, using power wave's normalisation. Some other authors have also reported diplexers and multiplexer of reduced size but based on complex polynomial evaluation (Meng and Wu, 2010; Wang and Lancaster, 2013; Araujo and Oliveira, 2013). These investigations are based on optimisations performed by minimising cost functions or error functions related to the component parts of the diplexer/multiplexer. According to Tubail and Skaik (2015), the cost functions employed in the optimisation are expressed in terms of the determinants and the cofactors of a given matrix.

Moreover, the synthesis of microwave resonator diplexers based on linear frequency transformation and optimisation has also been researched (Wang et al., 2012). The investigation is based on the evaluation of the characteristic polynomials of the diplexer using the proposed linear frequency transformation. The coupling matrix of the entire diplexer was then determined using hybrid

optimisation methods. In another study, a coupled resonator diplexer was researched and designed based on the synthesis of coupling matrix of a three-port coupled resonator circuit using optimisation (Skaik and Lancaster, 2011). Though the diplexer configuration, unlike conventional diplexer designs, did not use any external junctions for energy distribution, it involved polynomial evaluation and optimisation which is a complex method of diplexer realisation. The challenge in this approach of diplexer synthesis is that the designer needs to have a sound knowledge and good mastery of the techniques involved in polynomial evaluation and optimisation to achieve convergence.

1.4.2 Diplexers Based on Implementation

A wide range of planar and non-planar transmission line technologies have been utilised in the implementation of microwave diplexers. Some of the popular technologies that have been well researched and reported for diplexer implementation include slotline, stripline, coplanar waveguide, microstrip, waveguide, and the SIW. Though diplexers implemented with non-planar (e.g. waveguides) transmission lines have high Q-factor, low loss, and better power handling ability, they become bulky at lower frequencies (Packiaraj et al., 2005). Diplexers implemented with planar (e.g. slotline, stripline, coplanar waveguide, and microstrip) transmission lines, on the other hand, are more compact in size but suffer from low power handling abilities. SIW diplexers combine the advantages of both planar and non-planar transmission lines by being of small size, low cost, low loss and high Q-factor (Adabi and Tayarani, 2008).

A number of literatures have reported diplexers implemented with the slotline technique. Liu et al. (2013) used the hair-pin stepped impedance resonator (SIR) in achieving a microwave diplexer. Two sets of slotline SIR were designed to have different dimensions and hence, resonate at different frequencies for the diplexer operation. The design consists of two second order slotline bandpass filters and a microstrip T-junction connecting the individual bandpass filters to a common input port. Microstrip feed-lines were introduced to feed the slotline SIRs through a microstrio-to-slotline coupling. The study also involved two separate filters and a T-junction, hence, a complex and bulky design though in a planar (two-dimensional) form. A parallel-coupled line diplexer excited via slotline resonators (SLRs) has also been investigated and presented (Kuan et al., 2009). The basic topology of the diplexer comprises two different parallel-coupled line structures with SLRs which are used for generating the filtering response with high-channel selectivity. Another study by Chen et al. (2015) reported a compact diplexer based on a slotline-loaded microstrip ring resonator. The ring resonators were loaded with four backside slotlines and a few half-wavelength microstrip resonators. Some other research papers that successfully achieved diplexers using the slotline technique include Gouget et al. (2003), Chan et al. (2015), and Wu et al. (2015).

Researchers have successfully investigated and designed microwave diplexers using the stripline technology. A diplexer made up of two parallel oriented rectangular stripline rings and a connecting line between them has been presented (Xu et al., 2007). The degenerated mode resonance was used in forming the transmit, Tx, and the receive, Rx, bands. They used the dual-mode rectangular stripline ring resonator to design two separate filters, and then used

a feed-line (Y-junction) to couple the two filters in order to achieve a diplexer circuit. The Tx and the Rx rings were joined by a connecting strip. A short stub was also tapped to the strip in order to form the diplexer's common port. The tapping position and the length of the connecting strip were carefully designed in order to minimise the mutual loading effect existing between the stripline rings. Just like the T-junction, the Y-junction must be separately and carefully designed before use. It therefore increases the complexity, as well as the size of the resultant diplexer. A study on the realisation of diplexers in suspended stripline using quasi-lumped elements has also been presented (Menzel and Balalem, 2005). They separately designed a lowpass filter (LPF) and a highpass filter (HPF), and then combined both the LPF and the HPF in order to achieve a diplexer.

In another study, a diplexer was designed based on double-sided parallel stripline (Xue and Chen, 2008). The study made use of an inserted conductor plane to provide two separate transmission paths for the radio frequency (RF) signals. It is vital to note that though the stripline is a planar technology, it exhibits high metal losses when compared to the SIW technique. A compact millimeter-wave stripline diplexer with two modified hairpin filters have also been reported (He et al., 2008). To achieve the most miniaturised design, they compared a parallel-coupled half-wavelength resonator filter, a folded staggered resonant array filter, and a hair-pin filter in order to decide which is best for the most compact diplexer. Zhang et al. (2006) and Chen et al. (2008) also proposed diplexers based on the stripline implementation technique.

The coplanar waveguide (CPW) technology is another implementation option available to diplexer designers. This method of diplexer implementation is similar to the slotline and stripline techniques as it is also two-dimensional (i.e. planar). It is a very popular technique when it comes to transitions between planar and non-planar transmission lines. A study by Lin and Chen (2002), reported a lumped element CPW diplexer that utilised a lowpass filter and two bandpass filters in achieving a diplexer. CPW and microstrip transmission lines have also been combined in order to realise diplexer responses (Xu and Ho, 2007; Xu et al., 2009; Setoodeh et al., 2013). In a recent publication, Lai et al. (2014) proposed an on-chip small-sized diplexer implemented on glass-based integrated passive device (GIPD). They employed the dual-mode right- and left-handed CPWs in achieving the diplexer. Another paper by Ahn and Tentzeris (2016) criticised the earlier findings by Lai et al. (2014) by pointing out some wrong assumptions made in the earlier design. The most significant advantage of the CPW over the microstrip is its ability to connect both active and passive circuit components in shunt, from the conducting strip (i.e. the signal line) to the ground plane on the same side of the substrate (Collin, 2001).

Microstrip is by far the most popular transmission line employed in the implementation of microwave passive devices including filters, couplers, antennas, multiplexers and diplexers. Microstrip diplexers, like other planar transmission line devices, are of compact size (Bao et al., 2010; Zhou et al., 2014; Chen et al., 2016; Yang and Rebeiz, 2016) but have low power handling abilities (Packiaraj et al., 2005). Various authors have researched and reported diplexers implemented using the microstrip transmission line technology. A study that implemented a microstrip diplexer using a T-shaped resonator has been

presented (Chuang and Wu, 2011). The T-shaped resonator can be conveniently used as a frequency selective signal splitter, making it possible to design diplexers for systems with extremely close bands. Just like most conventional microwave diplexer design methods, their design involved two separate filters and a T-junction, thus achieving a complex and relatively bulky filter.

In another study, a microstrip diplexer was achieved by a dual-passband filter and two matching circuits (Deng et al., 2006). The dual-passband filter was realised using parallel coupled microstrip structures, while the two matching circuits were developed based on stepped-impedance transmission line sections, along with suitable open stubs. A third order Chebyshev microstrip diplexer with two centre frequencies and good isolation was successfully implemented, as a result of suitably incorporating the open stubs into the matching circuits. Although using a single dual-passband filter in the design resulted in a compact diplexer when compared to the conventional technique of using two single-passband filters, the down side lies on the matching circuits. Achieving consistency in the matching circuits is the tricky part and will surely require a high level of technical know-how. The variable frequency response of microstrip stepped-impedance resonator (SIR) has been exploited in designing a diplexer circuit (Chen et al., 2006). This was achieved by placing a common resonator in the path of two filter channels in other to realise the diplexer circuit. By taking advantage of the variable frequency response of the SIR, resonators can be shared by two filter channels of the desired diplexer provided their fundamental and the first spurious resonant frequencies are properly assigned.

A microstrip diplexer has also been researched and presented based on a design involving quarter-wavelength resonators (Cheng et al., 2012). The diplexer was made up of two filters implemented with quarter-wavelength resonators, and then coupled by metallised vias. Each of the metallised vias is said to be inductive and behaves just like a K-inverter. The T-shaped stepped-impedance resonators (SIRs) has been utilised in the design of microstrip bandpass filters for wide harmonic suppression. The banspass filters were then applied in the achievement of a high performance diplexer (Lerdwanittip et al., 2011). Many other researchers have reported diplexers successfully implemented using the microstrip transmission line technique (Deng and Tsai, 2013; Chen et al., 2014; Tu and Hung, 2014; Feng et al., 2014; Peng and Chiang, 2015). One thing common to all devices implemented on the microstrip transmission line is that they are mostly fabricated by photolithographic processes, and can be simply integrated with other passive and active microwave devices (Pozar, 2005). They are also of compact size and low cost but suffer from low power handling capabilities (Packiaraj et al., 2005). They also lack the high performance of waveguide diplexers.

Waveguide diplexers are well known for their high performance i.e. low loss, high Q-factor, better power handling capabilities, etc. However, integrating them with planar circuits is a very challenging task due to their three-dimensional geometry (Deng et al., 2008). They also have the disadvantage of being bulky, particularly at lower frequencies. Waveguide diplexers have been vastly researched and reported in literature. Some authors reported diplexers employing the conventional rectangular waveguide (Shen et al., 2003), while others have recently proposed diplexers based on circular waveguides (Li et al., 2013). In one

research paper, Rakic et al. (2004) proposed a diplexer design approach in which they first designed two fifth order filters and then used a T-junction in E-plane to combine the individual filters in order to realise a diplexer circuit. The design and performance of a low passive inter-modulation (PIM) and multiplication free Ka-band waveguide diplexer with an E-plane T-junction was also researched and presented (Yun et al., 2005). The waveguide diplexer consists of a transmit filter and a receive filter, combined to the antenna port through an E-plane T-junction. The T-junctions utilised in the above two investigations resulted in a more complex design and also added to the size of the diplexer.

In a different study, a waveguide diplexer was achieved by employing connected bi-omega particles (Palma et al., 2012). The two sets of bi-Omega particle have different dimensions which enabled them to resonate at two different frequencies, hence, enabling the frequency selective transmission required for the diplexer operation. In other to achieve the waveguide diplexer, they first designed two individual sets of connected bi-Omega particles resonating at two different frequencies in the X-band. They assumed that the two bi-Omega particles were printed and characterised on a light substrate, with the only difference between them being in the loop radius. Xia et al. (2014) and Duong et al. (2016) are more recent research papers that have reported diplexers implemented on the waveguide technology. Though waveguide diplexers have high Q-factor, high power handling and low radiation loss, they are very bulky and difficult to integrate onto other microwave and millimetre-wave components due to their three-dimensional (3D) nature.

The SIW technique has been proposed and investigated. This technology is relatively new and promises to be a prime candidate for the implementation of microwave and millimetre-wave (mm-wave) devices or integrated circuits, and systems for the next generation of wireless communication systems. The SIW shows the promise of operating at a higher frequency band (mm-wave) with low losses, which means it is possible to implement power-efficient systems, which is a major requirement of the next generation of wireless systems. The SIW resonator was probably first proposed by Piolote, Flanik and Zaki (Han et al., 2007). They developed the idea of using a series of metallic posts (or via holes) through the substrate, to replace the waveguide walls. The idea did not change the effect of metallic walls, but gave rise to the SIW transmission line resonator. The SIW consists of two parallel rows of via holes embedded in the dielectric substrate (Karim et al., 2011). This technology combines the merits of printed circuits such as low cost, small size, etc., as well as the advantages of being a waveguide such as high quality factor (Q-factor), low insertion loss, etc. (Adabi and Tayarani, 2008).

SIW diplexers have been recently investigated and reported in literature. A microwave diplexer has been designed by using two separate filters and a circulator (He et al., 2012). All component parts of the diplexer (including both filters and the circulator) were implemented based on the SIW technology. Though the SIW has the combined advantages of waveguides and planar circuits (Adabi and Tayarani, 2008), the introduction of a circulator between the two filters makes for a bulky and complex design. A high-performance millimeter-wave planar diplexer, developed based on the complementary characteristics of dual-mode SIW filters with circular and elliptic cavities has also been presented (Tang

et al., 2007). The investigation made some trade-off on isolation, insertion loss, and selectivity in order to achieve the desired result. The triplet topology has also been used in the design of a microwave diplexer (Han et al., 2007). The triplet topology enabled the SIW resonators to be arranged in such a way as to achieve compact size in the diplexer design. The resultant microwave diplexer in their investigation exhibited the generalised chebyshev characteristics, as well as the SIW merits. In another recent study, a planar diplexer was developed based on the SIW with complementary split-ring resonators (CSRRs) etched on the waveguide surface (Dong and Itoh, 2011). The diplexer was implemented based on two cascaded two-pole bandpass filters based on the SIW structure. An SIW diplexer has been investigated, designed, and presented based on dual-mode SIW resonators (Cheng et al., 2013). The study showed that the resonant frequencies of the dual-mode square cavity can be assigned based on specific requirements. This is done by improving on the perturbation strength of the dual-mode square cavity. As a result, the SIW cavity can be used as a common resonator which replaces the T-junction in a conventional design approach. Some other research studies have successfully achieved microwave diplexers using the SIW technique (Hao et al., 2005; Athanasopoulos et al., 2011; Cheng et al., 2014; Garcia-Lamperez et al., 2014; Kordiboroujeni and Bornemann, 2015; Schorer et al., 2016). The SIW has proved to remedy the design issues with waveguide and microstrip passive components, as it largely retains the advantages of both the waveguide and the microstrip transmission lines (Deng et al., 2008). With the SIW technique, both active and passive microwave and millimeter-wave components can be integrated on a single substrate platform (Deslandes and Wu, 2003).

1.5 Aims and Objectives

The main aim / objective of the research work reported in this thesis is to achieve a microwave diplexer without employing any sort of external non-resonant junction. This simply means that the proposed diplexer would be purely based on direct coupling (both synchronous and asynchronous) using multi-coupled resonators. Hence, no cross-coupling would be utilised throughout the design process. The designed microwave diplexer should be able to split a frequency band into two sub-bands or combine two sub-bands into one wide band (Zhu et al., 2014). A highlight of the complete aims and objectives of this research work include: (i) to model a microwave diplexer circuit without an external non-resonant junction using lumped elements and the Keysight advanced design system (ADS) circuit simulator, hence, achieving size miniaturization; (ii) to simplify the diplexer design process, hence, lowering the cost of implementing a microwave diplexer; (iii) to draw up an analytical formulation for diplexer design, hence, greatly reducing design uncertainties; (iv) to implement the diplexer circuit model using the microstrip transmission line technology and the full-wave electromagnetic (EM) 2.5D simulation software such as the ADS; (v) to further improve on the diplexer performance by employing the SIW technology and the full-wave finite element method (FEM), Keysight electromagnetic professional (EMPro) 3D simulator; (vi) to implement a novel microstrip-CPW-SIW input / output coupling that exploits the step impedance between a 50 Ohms input / output feedline and the transition to control the input / output couplings of a device; (vii) to fabricate the designed microwave diplexer using the low cost, commercially available printed circuit board (PCB) technology; (viii) to measure the fabricated diplexer and then use the measurement results in validating the simulation results.

1.6 Thesis Contributions

Microwave diplexers have been vastly investigated and designed using various techniques reported in literature. Most diplexer design methods reported involves the use of one sort of external device or the other for energy distribution towards both channels of the diplexer. Popular matching devices that have been used in achieving diplexers include manifolds (Cameron and Yu, 2007), T-junctions (Yang et al., 2010), Y- junctions (Wu and Meng, 2007), and circulators (He et al., 2012). A common resonator (Wang and Xu, 2012) has also been used in place of the external device, in an attempt to reduce the size of the resultant diplexer. The common resonator approach actually achieved a relatively reduced size diplexer when compared to the conventional diplexers that relied on external junctions. However, a close look at the results presented in Wang and Xu (2012) shows that the common resonator employed in the design did not contribute to the number of poles contained in the diplexer response. This simply means that the common resonator, like any other type of external junction, is primarily concerned with splitting the channels and distributing energy. It plays very little or no role in the selectivity of the diplexer and hence, contribute to the physical size of the diplexer. Apart from the external energy distribution techniques, other diplexers reported in literature are mostly based on the evaluation of complex polynomials and error functions (Skaik and Lancaster, 2011; Wang and Xu, 2012).

The microwave diplexer reported in this thesis has successfully extended the idea of using common resonators to achieve reduced size, by making sure that the energy distributing resonators also contribute to the number of poles present in a

diplexer. This means that the energy distributing resonators are also completely involved in the selectivity of the diplexer and hence, leading to a further reduction in the physical size of the resulting diplexer. Also, instead of relying on the evaluation of polynomials and error functions, the work reported in this thesis has successfully shown that diplexers can be achieved by simply relaying on known equations for bandpass filter and dual-band bandpass filter designs. For the SIW realisation of the proposed diplexer, this investigation used a novel microstrip to coplanar waveguide to SIW (microstrip-CPW-SIW) input / output coupling. The proposed microstrip-CPW-SIW input / output coupling exploits the step impedance between a 50 Ohms input / output feedline and the transition to control the input / output couplings of the diplexer.

1.7 Thesis Structure

This thesis is arranged and presented in seven chapters. Chapter 1 is the introductory chapter which starts with a background into the radio frequency and the microwave spectrums. The chapter also covers the aims and objectives of the thesis, the motivation and problem statement, the research method, the thesis contribution, and the literature review into the various diplexer design approaches that have been investigated and reported by various authors. The chapter also looks at a number of transmission line technologies that have been utilised in the implementation of microwave diplexers including slotline, stripline, coplanar waveguide, microstrip, waveguide, and the SIW. The chapter concludes by highlighting the structure of the thesis.

Chapter 2 gives a brief overview on transmission line technologies. The microstrip and the SIW transmission line technologies are covered in details. The characteristics impedance and losses in microstrip and microstrip resonators are also presented in details. The SIW cavity, modes in SIW cavity, SIW related transition, and losses in SIW are also presented with a majority of the formulations required in making a design based on the SIW technique.

Chapter 3 looks at microwave filters including their frequency responses and transfer functions. Filter design methods including image parameter and insertion loss techniques are also presented. The chapter concludes by reporting a SIW bandpass filter designed with a novel Microstrip-CPW-SIW input/output coupling. The simulation and measurement results of the SIW bandpass filter are in excellent agreement.

Chapter 4 develops a microwave diplexer circuit model that does not require any separate / external junction for energy transmission. Each resonator used in the design contributes a single pole to the diplexer circuit responses. The diplexer circuit model was achieved by cascading a section of a dual-band bandpass filter (DBF), with sections of two separately designed bandpass filters (i.e. BPF1 and BPF2). The DBF was used to establish the transmit and the receive bands of the diplexer. BPF1 and BPF2 corresponds to the diplexer transmit and received bands, respectively, in terms of centre frequencies and bandwidths. The simulation results for the diplexer circuit model were also presented.

Chapter 5 reports on a microtrip implementation of the microwave diplexer circuit model developed in chapter 4. The microstrip square open-loop resonator was employed in the implementation of the diplexer circuit. The microstrip diplexer was fabricated, measured and results used to validate the circuit model of Chapter 4. Compared results show good agreement between the model and fabricated diplexer responses.

Chapter 6 gives the SIW implementation of the same diplexer circuit model developed in chapter 4. The SIW diplexer was fabricated using printed circuit board (PCB) micro-milling process employing the LKPF (i.e. Leiterplatten-Kopier) protomat C60. Simulated and measured results were presented and discussed accordingly.

Chapter 7 presents the thesis conclusion and also made recommendations for possible improvements on the research work reported throughout the thesis. The future work recommendations include the possible techniques for making the SIW diplexer smaller in size, while also improving on the microwave diplexer responses.

Chapter 2: Transmission Line

2.1 Introduction

A transmission line (TL) is simply any medium that is capable of transmitting electrical signals. Transmission lines store electric (***E***) and magnetic (***M***) energy distributed in space and alternating between the two forms. This means that at any point along a TL, energy is stored in a mixture of ***E*** and ***M*** forms and, for an alternating signal at any point on the TL, converted from one form to the other as time progresses (Steer, 2010). The circuit form of a transmission line contains inductors for magnetic energy, capacitors for electric energy, and resistors for modelling losses. According to Collin (2000), the electrical characteristics of a TL such as the propagation constant, the attenuation constant, the characteristic impedance, and the distributed circuit parameters can only be determined from the knowledge of the fields surrounding the transmission line.

Two broad categories of transmission lines are planar and non-planar lines. Popular planar TLs include slotline, stripline, coplanar waveguide and microstrip line; while non-planar transmission lines are mostly waveguides. Planar transmission lines have their entire conducting metal strip lying on a plane. Hence, planar circuit components and devices are designed on the two dimensional (2D) layout, as the engineer / designer has no control over the depth / thickness of the substrate which are always fixed. A common way of representing a planar transmission line is by placing one or more parallel metal strips on a dielectric substrate material, adjacent to a conducting ground plane (Collin, 2000). Non-planar transmission lines such as waveguides allow

engineers to have total 3D control over their design. This means that engineers and other circuit component / device designers can alter every part of their work, including the thickness / depth of materials. Waveguide transmission lines are three dimensional (3D) and have one conductor (Steer, 2009). It has been reported that early microwave circuits, components, devices and systems relied on waveguide and coaxial TLs for electromagnetic (EM) wave propagation (Pozar, 2004). Waveguide transmission line devices are well known for their high quality factor, low loss and better power handling capabilities. However, they are bulky (especially at lower frequencies) and are expensive. Coaxial line devices are very high in bandwidth and are very convenient for test applications, but are very difficult to handle when it comes to fabricating complex microwave components (Pozar, 2004). Planar transmission line devices, on the other hand, are well known for their compact size, low cost, easy to manufacture, and are capable of being easily integrated with active devices such as diodes and transistors to form microwave integrated circuits (Pozar, 2004). The down side to planar TL devices is that they suffer from low power handling capabilities (Packiaraj et al., 2005) and are more susceptible to losses when compared to waveguide devices.

SIW (Chen and Wu, 2014) is a twenty-first century transmission line that has evolved to bridge the gap between planar and waveguide transmission lines. This new type of TL has changed the paradigm relating to the development of circuits, components, devices, sub-systems and systems operating in the microwave and millimetre-wave frequency range. The SIW is actually a planar structure with waveguide performance. This means that the SIW combines the merits of microstrip, i.e. compact size, low cost, easy to manufacture and easy integration

with active devices; with the merits of waveguides, i.e. low radiation loss, high unloaded quality factor, and high power handling capabilities. Cheng (2015) described the SIW as a dielectric-filled waveguide that is synthesized by two rows of metalized vias, embedded in a dielectric substrate with conductor claddings on the top and bottom walls. Some other main merits of the SIW, besides the high quality factor and high power handling capability include: its ability to integrate typical waveguide components in planar form, the flexibility of its design, and the comprehensive shielding of its structure. SIW devices can be manufactured or fabricated using different technologies such as: the printed circuit board, the low-temperature co-fired ceramics, the monolithic semiconductor, etc.

2.2 Waveguide

Waveguide components / devices are well known for their high quality factor, low insertion loss, and high power handling capabilities. However, they are bulky (particularly at lower frequencies) and are expensive. Though a lot of microwave components are recently being fabricated using planar transmission lines due to their size miniaturization and ease of integration, waveguides are still one of the earliest types of transmission line that are still in demand today (Pozar, 2004). Waveguides are still in high demand when it comes to high-power devices and some precision test applications.

Waveguides are hollow pipes that have been implemented using different cross-sections including circular, elliptical, square and rectangular shapes. The first demonstration of waveguide propagation was carried out using hollow pipes in the 1930s (Lee, 2004). However, the most common type of waveguide is the

rectangular case shown in Figure 2.1. This is as a result of the simple nature of modelling the wave propagation in the rectangular waveguide. Hollow rectangular waveguides are unable to support transverse electro-magnetic (TEM) mode propagation since they only contain a single conductor (Pozar, 2004). They can however propagate either transverse electric (TE) or transverse magnetic (TM) modes depending on how they are excited.

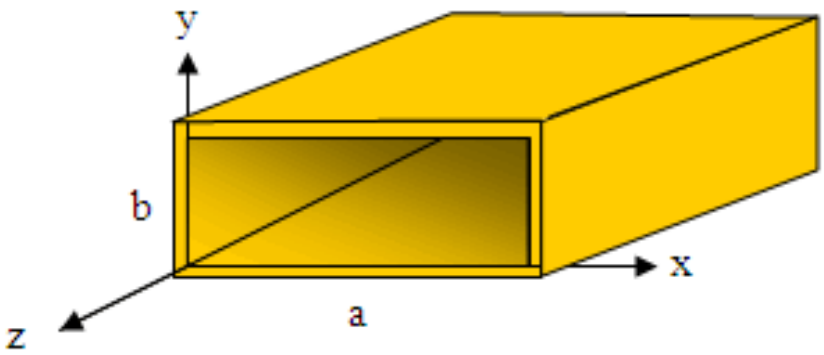

Figure 2.1: Hollow rectangular waveguide geometry.

2.2.1 Mode Naming

When both the electric and the magnetic fields are transverse to the direction of propagation, the mode is said to be *TEM*. If however, only the electric or the magnetic field is transverse to the direction of propagation, the mode is *TE* or *TM* respectively. The excitation of a rectangular waveguide determines if the mode is *TE* or *TM*. In naming the mode, the alphabet following the "*T*" shows which component of the field is transverse to the direction of propagation. Sub-scripts are used to complete the mode specification by showing the number of half-waves at cut-off that fit across the x- and y-directions of a given rectangular waveguide, or along the diametrical and circumferential directions of a given

circular waveguide (Lee 2004). Therefore, $TM_{i,j}$ indicates that there are i half-waves of M-field across the x-direction and j half-waves of M-field across the y-direction for the given rectangular waveguide.

2.3 Microstrip Line

Microstrip transmission line is arguably the most popular type of planar transmission line. This is basically because it can be fabricated by photolithographic processes, and can be simply integrated with other passive and active microwave devices (Pozar, 2004). It is by far the most widely used planar transmission line when it comes to RF and microwave circuit design. The structure of a microstrip line is shown in Figure 2.2. The diagram presents the microstrip line as a conducting strip having a width *w* and a thickness *t*, placed on the top of a dielectric substrate with a relative permittivity (or dielectric constant) ε_r and a substrate thickness *h*. The base of the substrate is a conducting ground plane.

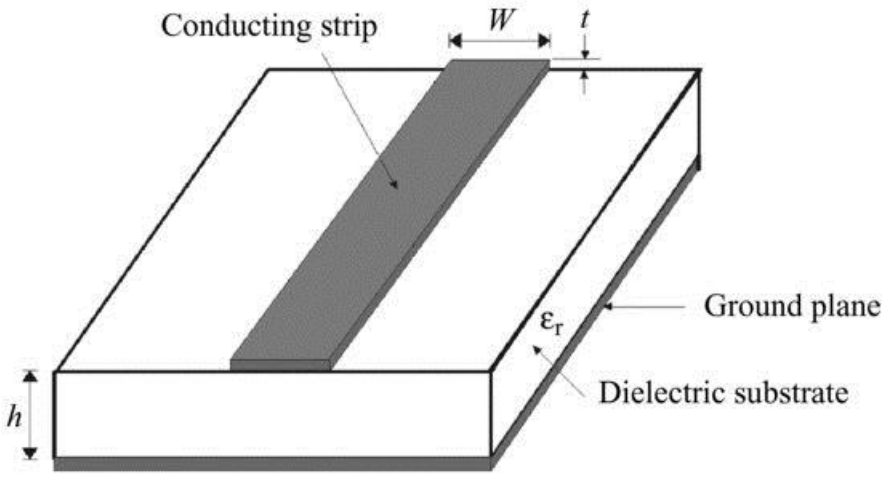

Figure 2.2: Microstrip line geometry (Hong and Lancaster, 2001).

Microstrip line components have the benefits of compact size, ease of design, manufacture, and integration. The flexibility of the microstrip makes it easy to handle during design and fabrication. It propagates alternating current (AC) and direct current (DC). All these advantages make the microstrip a very widely used technology in RF and microwave circuit design. Besides the benefits of the microstrip highlighted above, some challenges or demerits have been associated with this type of transmission line. For example, microstrip components suffer from low power handling capabilities (Packiaraj et al., 2005) and are more susceptible to losses when compared to waveguide components. In designing filters and switches or other devices that normally require high isolation, some external shielding must be considered in order to use microstrip for implementation. Radiation is also a problem with microstrip as it could cause unintended responses in a circuit. Dispersion is also an issue with the microstrip, though a minor one. By dispersion, signals of different frequencies travel at different speed. Though this may not usually be a serious issue, it normally causes the asymmetric frequency in bandpass filters for example. The microstrip structure is also inhomogeneous since its field extend within two media (the air above, and the substrate below). As a result of its inhomogeneous nature, microstrip does not support a pure TEM wave (Hong and Lancaster, 2001). The quasi-TEM mode of the microstrip is an issue worthy of consideration when making a choice of the transmission line to employ for circuit implementation.

The fundamental mode of propagation in a microstrip line is not a pure transverse electromagnetic (TEM) mode; rather it is a quasi-TEM mode. This means that the longitudinal components of the fields for the dominant mode of a microstrip line

may be neglected, since they remain very much smaller than the transverse components (Hong and Lancaster, 2001).

2.3.1 Losses in Microstrip

The microstrip transmission line has three major loss components that include the conductor, the dielectric, and the radiation losses. Other loss components, which may be considered minor, include the conductor surface roughness and the thickness variation of the substrate material. Magnetic substrates such as ferrites are also susceptible to magnetic loss (Denlinger, 1980; Pucel et al., 1968).

According to Pucel et al. (1968), the predominant loss components that affect a microstrip line over a non-magnetic substrate are the conductor losses (also known as ohmic losses) in the strip and the ground plane; and the dielectric losses in the substrate. Imperfections in conductors (including surface roughness) are mostly responsible for microstrip losses at microwave frequencies. This is more so in microstrip lines that are fabricated on a low-loss dielectric substrate. Pucel et al. (1968) argues that the current density in the strip and ground plane conductors of a microstrip line is concentrated in a sheet approximately a skin depth deep inside the conductor surfaces exposed to the electric field. Both Denlinger (1980) and Pucel et al. (1968) summarised the conductor attenuation constant, α_c, with Eqn. (2.1), where R_s denotes the series skin resistance of the microstrip transmission line, and Z_0 is the characteristic impedance of the microstrip line. The current density at radio and microwave frequencies is not evenly distributed throughout the cross-section of the signal line. As a result of the induced eddy current in a signal trace, the signal current

tend to fade at the centre of the conductors but concentrate about the edges. This efficiently condenses the cross-sectional area of the signal at microwave frequencies, increases the signal resistance and hence, the attenuation of the microstrip line.

$$\alpha_c = \frac{R_s}{2Z_0} \tag{2.1}$$

The dielectric loss in microstrip is another major component as it tends to increase with increase in frequency. This makes it a serious concern at microwave and millimeter-wave frequencies. Denlinger (1980) and Pucel et al. (1968) analysed the attenuation due to the dielectric loss in microstrip and represented it using Eqn. (2.2); where tan δ indicates the loss tangent of the dielectric substrate, $\mathcal{E}_{eff}$ denotes the effective dielectric constant of the microstrip line, λ_g is the guided wavelength along the microstrip line, $\mathcal{E}_r$ is the relative dielectric constant of the substrate, and α_d is the attenuation due to the dielectric loss in the microstrip line.

$$\alpha_d = 8.686\pi \left(\frac{\varepsilon_{eff}-1}{\varepsilon_r-1}\right)\frac{\varepsilon_r}{\varepsilon_{eff}}\frac{\tan\delta}{\lambda_g} \quad dB/unit\ length \tag{2.2}$$

The microstrip line, being a semi-open geometry, allows any radiation to either propagate freely away or to induce currents on the metallic enclosure, giving rise to radiation loss which is sometimes known as housing loss (Hong and Lancaster, 2011). This simply means that the radiation losses in a microstrip line are caused by radiating fields which induce currents on surrounding conducting bodies, in the neighbourhood of the signal line.

2.3.2 Characteristic Impedance of Microstrip

The characteristic impedance Z_0 and the effective dielectric constant $\mathcal{E}_{eff}$ of the microstrip are the two parameters used in describing the transmission characteristics of the microstrip line. Given the substrate thickness *h*, the microstrip width *w*, the relative dielectric constant of the substrate $\mathcal{E}_r$, and the $\mathcal{E}_{eff}$, Z_0 can be determined using Eqn. (2.3) (Pozar, 2004).

$$Z_0 = \begin{cases} \frac{60}{\sqrt{\varepsilon_{eff}}} In\left(\frac{8h}{w} + \frac{w}{4h}\right) & for\ \frac{w}{h} \leq 1 \\ \frac{120\pi}{\sqrt{\varepsilon_{eff}}\left[\frac{w}{h} + 1.393 + 0.667\ In\left(\frac{w}{h} + 1.444\right)\right]} & for\ \frac{w}{h} \geq 1 \end{cases} \quad \text{(2.3 a)}$$

$$\varepsilon_{eff} = \frac{\varepsilon_r + 1}{2} + \frac{\varepsilon_r - 1}{2} \frac{1}{\sqrt{1 + 12^{h}/_{w}}} \quad \text{(2.3 b)}$$

2.3.3 Width of Microstrip

The width, *w*, of the microstrip can be determined for a given characteristic impedance Z_0 and dielectric constant $\mathcal{E}_r$ by first calculating the ratio w/h using Eqn. (2.4) as found in Pozar (2004).

$$\frac{w}{h} = \begin{cases} \frac{8e^A}{e^{2A} - 2} & for\ \frac{w}{h} < 2 \\ \frac{2}{\pi}\left[B - 1 - In(2B - 1) + \frac{\varepsilon_r - 1}{2\varepsilon_r}\left\{In(B - 1) + 0.39 - \frac{0.61}{\varepsilon_r}\right\}\right] & for\ \frac{w}{h} > 2 \end{cases} \quad \text{(2.4 a)}$$

$$A = \frac{Z_0}{60}\sqrt{\frac{\varepsilon_r + 1}{2}} + \frac{\varepsilon_r - 1}{\varepsilon_r + 1}\left(0.23 + \frac{0.11}{\varepsilon_r}\right) \quad \text{(2.4 b)}$$

$$B = \frac{377\pi}{2Z_0\sqrt{\varepsilon_r}} \quad \text{(2.4 c)}$$

2.3.4 Microstrip Resonators

A microstrip resonator is defined as any structure that is able to contain at least one oscillating electromagnetic (EM) field (Hong and Lancaster, 2001). Like all other forms of microwave resonators, they can be employed in various applications including filters, diplexers / multiplexers, couplers, oscillators, frequency meters, and tuned amplifiers (Pozar, 2004). They exchange energy spatially stored in electric and magnetic forms just like in lumped-element resonant circuits, where stored energy is periodically transferred between an inductor which stores magnetic energy and a capacitor which stores electric energy (Steer, 2009).

Microwave resonators are mostly described in terms of their quality factor, Q, as given in Eqn. (2.5) derived from Steer (2009), where f_r is the resonant frequency of the resonator. From Eqn. (2.5), it is obvious that using a low-loss material in constructing a microstrip resonator would definitely increase the Q of the resonator. Note that Q is the characteristic of a resonator on its own i.e. without any loading effect caused by an external circuitry (Pozar, 2004). Hence, Q is actually known as the unloaded quality factor of a resonator. In practice, however, resonators are regularly coupled to other circuitry which will effectively reduce the total loaded quality factor, Q_L, of the entire circuit (Pozar, 2004). Reducing the Q of a resonator increases its bandwidth due to the power lost to external circuits. Hence, $Q_{L,}$ can be determined using Eqn. (2.6), where Q_{ext} is the external quality factor (Steer, 2009). The external quality factor accounts for the power extracted from a resonant circuit.

$$Q = 2\pi f_r \left(\frac{average\ energy\ stored\ in\ the\ resonator\ at\ f_r}{power\ lost\ in\ the\ resonator}\right) \quad (2.5)$$

$$Q_L = 2\pi f_r \left(\frac{average\ power\ stored\ in\ the\ resonator\ at\ f_r}{power\ lost\ in\ the\ resonator\ and\ the\ external\ circuit}\right) \quad (2.6\ a)$$

$$Q_L = \left(\frac{1}{Q} + \frac{1}{Q_{ext}}\right)^{-1} \quad (2.6\ b)$$

It is generally impossible to determine the unloaded quality factor, Q, of a resonator by direct measurement. This is due to the loading effect of the measurement system (Pozar, 2004). However, Q can be determined from measurement of the frequency response of a loaded resonator when the resonator is connected to a transmission line (Khanna and Garault, 1983; Pozar, 2004). Reflection measurement (i.e. 1-port measurement) or transmission measurement (i.e. 2-port measurement) can be used in determining the unloaded quality factor using Eqn. (2.7) (Behagi, 2015); where *IL* is the insertion loss in decibels (dB).

$$IL = 20\ log_{10}\left(\frac{Q}{Q - Q_L}\right) \quad (2.7)$$

A microstrip patch resonator with a strong coupling to the external circuit is shown in Figure 2.3 (a). It is important to note that the strong coupling of Figure 2.3 (a) is as a result of the narrow gap that exists between the patch resonator and the input strip. The strong coupling of Figure 2.3 (a) can be reduced by increasing the gap as shown in Figure 2.3 (b). Hence, coupling is inversely proportional to the width and size of the gap. This implies that the coupling in Figure 2.3 can be

controlled by simply increasing or decreasing the gap between the patch resonator and the input strip. The wider the gap, the weaker is the existing coupling and vice versa.

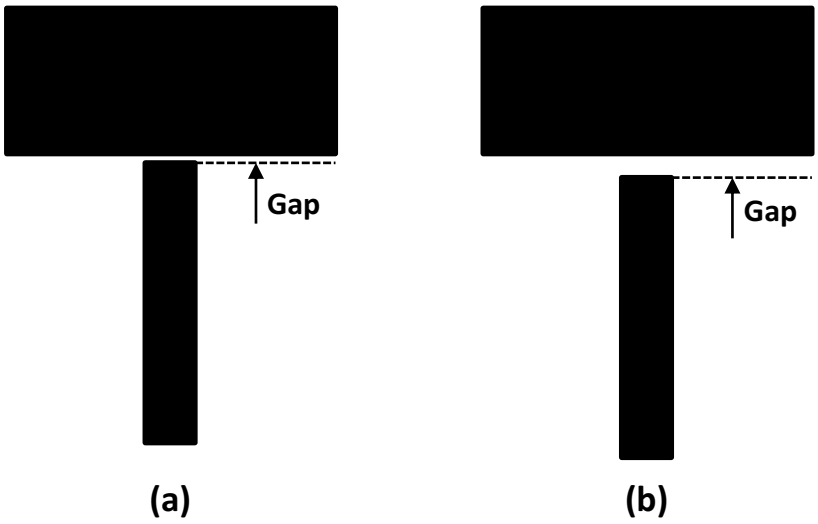

Figure 2.3: Microstrip patch resonators. (a) With strong coupling due to the narrow gap. (b) With weak coupling due to wide gap.

There are several forms of microstrip resonators that have been reported in literature. The popular ones that have been used for the implementation of microwave circuits, components and devices include:

- lumped-element or quasi-lumped-element resonator
- distributed-line resonator
- patch resonator
- dual-mode resonator

The microstrip lumped-element or quasi-lumped-element resonators are formed by lumped or quasi-lumped inductors and capacitors. This class of resonators,

according to Hong and Lancaster (2001), will resonate at an angular frequency, $\omega_r = 2\pi f_r = 1/\sqrt{LC}$, where f_r is the resonant frequency, L is the inductance of the inductor, and C is the capacitance of the capacitor. They may also resonate at other higher frequencies at which their dimensions would no longer be much smaller than their wavelength, as opposed to the definition of lumped-element characteristics (Hong and Lancaster, 2001). Figure 2.4 shows a typical microstrip quasi-lumped-element resonator.

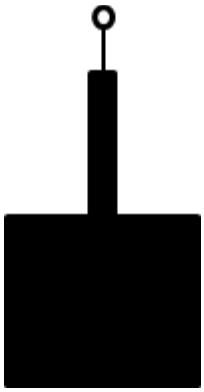

Figure 2.4: Microstrip quasi-lumped-element resonator.

Microstrip Distributed-line resonators are mostly quarter-wavelength and half-wavelength resonators. Some popular types of distributed-line resonators are shown in Figure 2.5. The quarter-wavelength resonators shown in Figure 2.5 (a) and (b) will normally resonate at a resonant length of $\lambda_g/4$, where λ_g is the guided wavelength at the fundamental resonant frequency, f_0. This type of microstrip resonator can also resonate at other frequencies, f, which are higher than f_0, provided $f \approx f_0\ (2n - 1)$ for n = 2, 3, 4,… (Hong and Lancaster, 2001). The microstrip half-wavelength resonator, on the other hand, has a resonant length of $\lambda_g/2$ at its fundamental resonant frequency, f_0. It can also resonate at other higher frequencies, f, when $f \approx nf_0$ for n = 2, 3, 4,… The interesting thing about the half-

wavelength resonator is that the conventional half-wavelength resonator shown in Figure 2.5 (c) can be folded into different shapes and configurations for the implementation of devices such as filters, couplers, diplexers/multiplexers, etc. Some popular resonator shapes and configurations that have been formed from the microstrip half-wavelength resonator include the hair-pin and the square open-loop resonator as shown in Figure 2.5 (d) and (e).

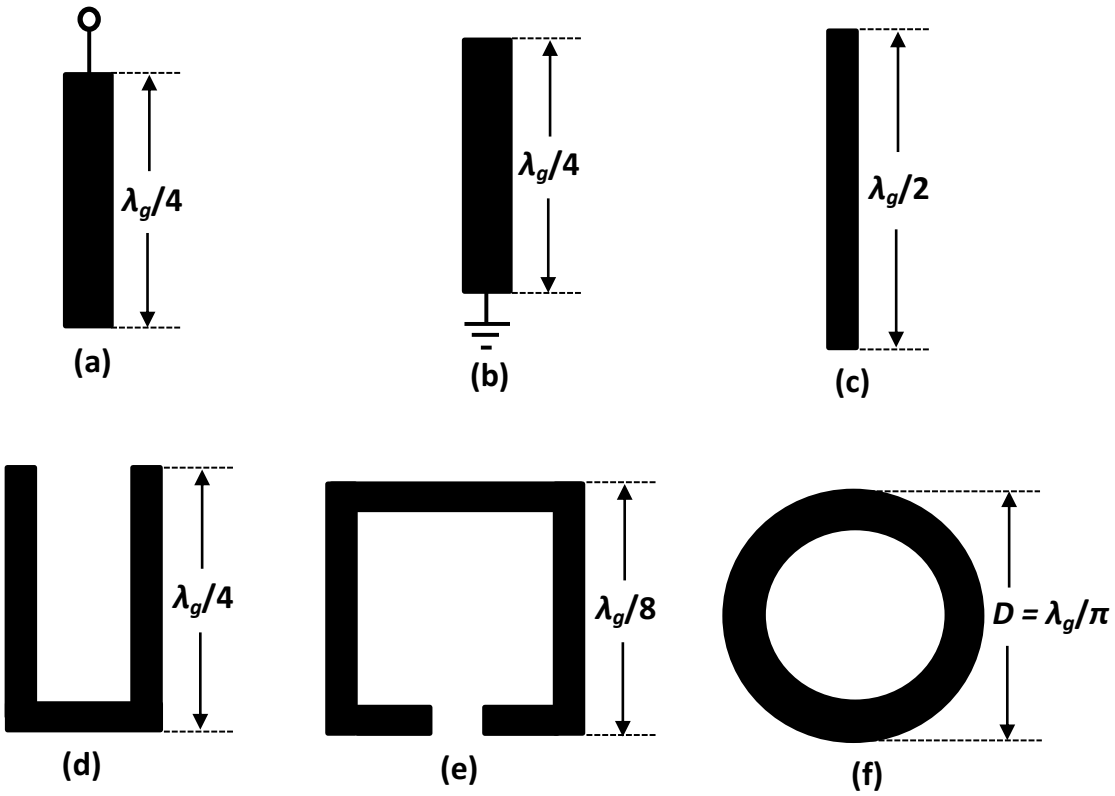

Figure 2.5: Some typical microstrip distributed-line resonators. (a) Quarter-wavelength resonator for shunt-series resonance. (b) Quarter-wavelength resonator for shunt-parallel resonance. (c) Half-wavelength resonator. (d) Hair-pin resonator. (e) Square open-loop resonator. (f) Ring resonator. (Hong and Lancaster, 2001).

The microstrip ring resonator is another type of distributed-line resonator proposed by Wolff and Knoppink (1971). The ring resonator resonates at its fundamental frequency, f_0 when its median diameter, $D \approx \lambda_g/\pi$ or the median

radius, $r \approx \lambda_g/2\pi$. This implies that the median circumference of the ring resonator, at resonance, is approximately equal to λ_g (i.e. $\pi D \approx 2\pi r \approx \lambda_g$). It can also resonate at other higher frequencies, f, when $f \approx nf_0$ for n = 2, 3, 4,… The ring resonator with its dimension is shown in Figure 2.5 (f).

Microstrip patch resonators are increasingly becoming very popular in the design of microwave components and devices. They have proven to be very useful in achieving filters with improved power handling capabilities (Monsour et al., 1996). Many authors have utilised microstrip patch resonators in the implementation of microwave devices. Hong and Lancaster (2000) employed microstrip triangular patch resonator in the implementation of bandpass filters with high power handling capabilities; Yeo and Nwajana (2013) implemented a dual-band bandpass filter using dual-mode square patch resonators; while Watkins (1969) proposed resonant structures based on microstrip circular patch resonators. Microstrip patch resonators are well known for their lower conductor losses when compared to the narrow microstrip distributed-line resonators discussed in the previous paragraph. One issue with patch resonators is their tendency to have stronger radiation, but this can be contained by making provision for a metal housing or enclosure which helps in minimising the radiation loss (Hong and Lancaster (2001). Another issue associated with patch resonators has to do with their large size. Hence, they are mostly employed for the implementation of devices which prioritise power handling or low loss over size. The size of the patch resonator is not really an issue when implementing devices that operate at very high frequencies (Hong and Lancaster, 2001). Microstrip patch resonators can be implemented in different shapes depending on the application. Typical

shapes that have been reported include triangle, square, and circle as shown in Figure 2.6 (a), (b) and (c) respectively.

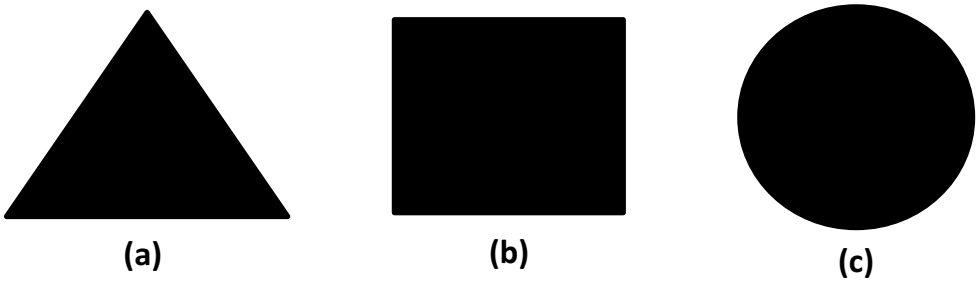

Figure 2.6: Some typical microstrip patch resonators. (a) Triangular patch resonator. (b) Rectangular patch resonator. (c) Circular patch resonator.

Microstrip dual-mode resonator is the class of resonators that are very popular when device miniaturisation is of high importance. This is because each dual-mode resonator can be used as doubly tuned resonant circuit and hence, exhibit two resonant modes which are orthogonal to each other. As a result, the number of resonators required for implementing a circuit is reduced by 50%, leading to device size miniaturisation (i.e. reduction in device size). Microstrip dual-mode resonators have been implemented in various shapes for different applications. Some popular shapes that have been reported for the dual-mode resonator are shown in Figure 2.7 (Hong and Lancaster, 2001). The square loop dual-mode resonator has been used as a common resonator in the implementation of a microwave diplexer (Guan et al., 2016). In another paper, Nwajana and Yeo (2013) utilised the square patch dual-mode resonator in the implementation of a microwave dual-band bandpass filter. One common thing with all the shapes that have been used in implementing dual-mode resonators is that they all have two-dimensional symmetry. The field distributions of the two modes of a dual-mode

resonator are orthogonal to each other; hence, placing a small perturbation to the line of symmetry of the resonator couples the degenerated modes and makes it function as two separate resonators. The small perturbation must be carefully placed at about 45° offset from the resonator's two orthogonal modes.

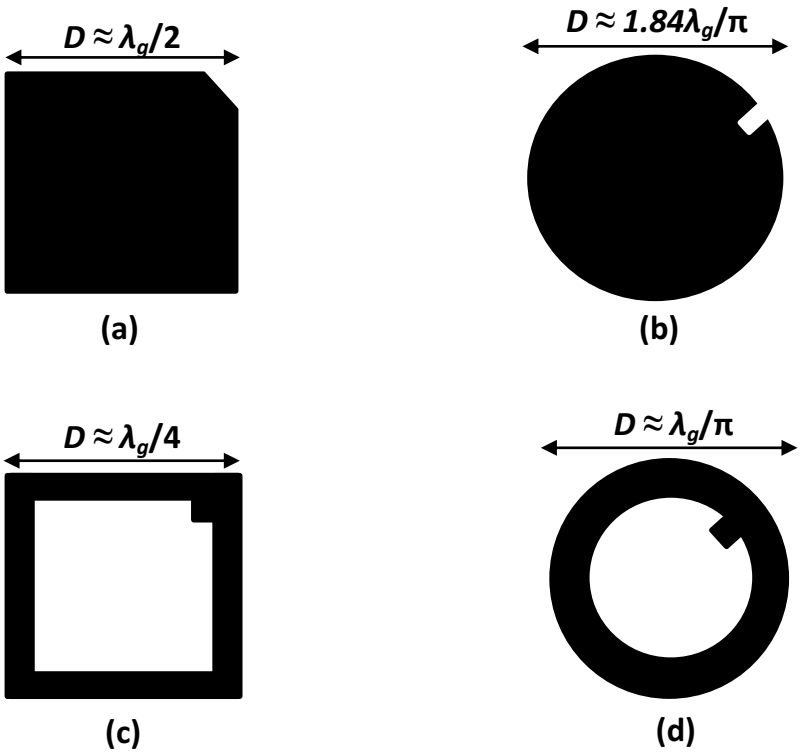

Figure 2.7: Some typical microstrip dual-mode resonators. (a) Square patch. (b) Circular disk. (c) Square loop. (d) Circular ring. (Hong and Lancaster, 2001).

Figure 2.7 (a) and (b) show a square patch and a circular disk dual-mode resonators respectively, with a small cut or notch applied as perturbation at 45° offset from their respective orthogonal modes. A square loop and a circular ring dual-mode resonators are also shown in Figure 2.7 (c) and (d) respectively, with a small patch placed at 45° offset from each resonator's two orthogonal modes, providing the disturbance required for the degenerated modes coupling. The variable *D* indicated above each dual-mode resonator in Figure 2.7 specifies its

symmetrical dimension, and λ_g is the guided-wavelength at the fundamental frequency of the associated dual-mode resonator.

2.4 Substrate Integrated Waveguide

The SIW technology is a twenty-first century transmission line that has evolved since the inception of the century. This new transmission line has become popular in the past decade, as it has changed the paradigm and opened new doors to the development of efficient circuits and devices operating in the microwave and millimetre-wave frequency range (Nwajana et al., 2017). Microstrip circuits and devices are inefficient at high frequency applications and require very stringent manufacturing tolerances when used to implement microwave and millimter-wave components. This is as a result of the fact that wavelengths are small at higher frequencies. Waveguide circuits and devices are preferred for higher frquency applications, but they are expensive and difficult to manfature. It is also very challenging to integrate a waveguide device with palanr devices in it vicinity. The SIW has bridges the gap between the traditional air-filled waveguide shown in Figure 2.8 (a) and planar transmission lines such as microstrip. SIW can be considered to be a dielectric-filled rectangular waveguide (Figure 2.8 (b)), that is synthesized by two rows of metalized vias embedded in a dielectric substrate (Figure 2.8 (c)), with conductor claddings on the top and the bottom walls (Cheng, 2015).

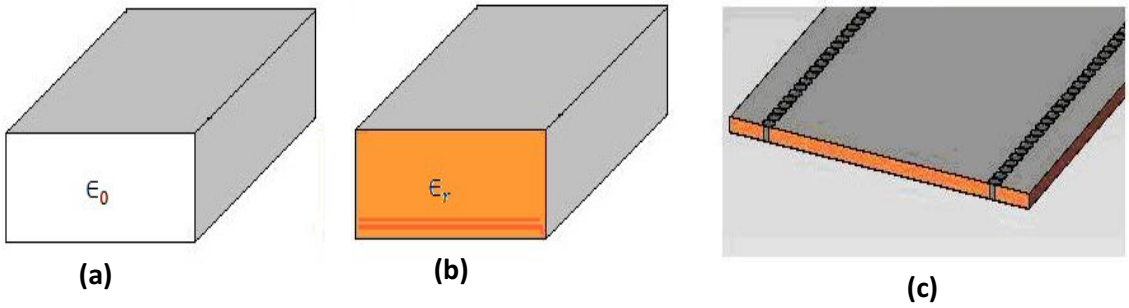

Figure 2.8: Substrate integrated waveguide evolution. (a) Air-filled waveguide. (b) Dielectric-filled waveguide. (c) Substrate integrated waveguide.

This new transmission line technology can simply be summarised as a planar structure with waveguide performance, since it implements a conventional air-filled rectangular waveguide on a piece of printed circuit board (PCB), by replacing the side walls of the waveguide with two rows of metallic posts also known as via holes (Han et al., 2007). The SIW inherits the advantages of the microstrip, i.e. compact size and easy integration, but maintaining some of its waveguide characteristic, i.e. low radiation loss, high unloaded quality factor (Q-factor), as well as the high power handling characteristics (when compared to traditional planar circuits such as microstrip). SIW as a transmission line is well established with details equations governing its physical structures, i.e. propagation mode, width of the transmission line and size of the metallic post, reported in Deslandes and Wu (2006).

2.4.1 SIW Cavity

The physical geometry of the SIW transmission line cavity is shown in Figure 2.9. The structure shows a dielectric substrate material being sandwiched between two metallic plates, with two rows of periodic metallic posts (i.e. metallised via

holes) running along the length of the substrate to mimic the metallic sidewall of a rectangular waveguide.

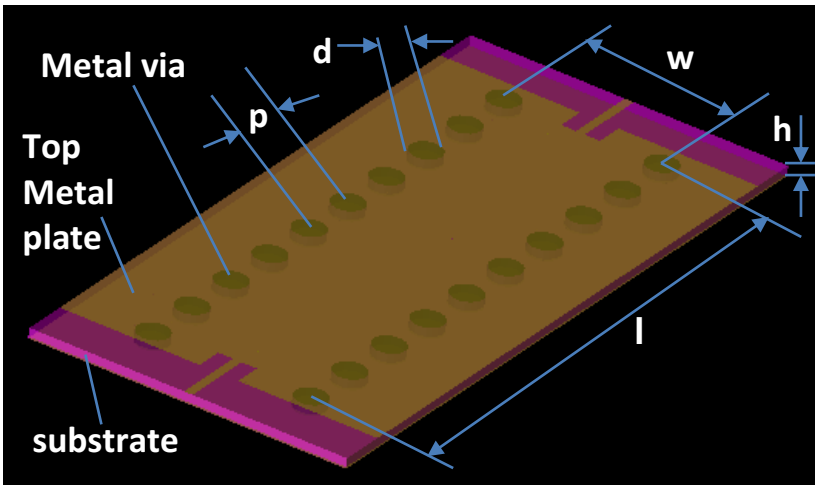

Figure 2.9: Physical geometry of the substrate integrated waveguide cavity.

To design a SIW transmission line to operate at a given frequency, there are three main design parameters that need to be considered. There are namely; the width of the SIW, *w*; the diameter of the metallic post, *d*; and the distance between the metallic posts (also commonly known as the pitch), *p*. The width of the SIW governs the cut-off frequencies of the propagation mode of the SIW transmission line in the same way as it does with width of the rectangular waveguide. The values of the parameters *d* and *p*, determine how well the SIW transmission line mimics the rectangular waveguide. If *p* is reduced to *d/2*, the SIW transmission line is effectively reduced to a dielectric filled rectangular waveguide. The larger *p* becomes the worst it diverges from a rectangular waveguide with electromagnetic energies leaking or radiating out between the metallic posts. According to a study in Deslandes and Wu (2003), for an electrically small metallic post, i.e. $d < 0.2\lambda$ where λ is the wavelength of signal propagating in the

dielectric material, the radiation loss is negligible when the ratio of *d/p* is 0.5. For a constant ratio of *d/p*, the radiation loss decreases as the size of the metallic post get smaller which is conditioned by the fabrication process (Hong, 2011). It is important to note that the ratio *d/p* is considered to be more critical than the values for *p* and *d* alone.

The size of an SIW cavity, for the fundamental TE_{101} mode, can be determined using the corresponding resonance frequency mode, f_{101} given in Eqn. (2.8) (Chen et al., 2005) where w_{eff} and l_{eff} are the effective width and length of the SIW cavity, μ_r is the relative permeability of the substrate (which is "1" for a non-magnetic substrate material), ε_r is the relative permittivity or dielectric constant of the substrate, and c_0 is the speed of light in free space. The empirical formulation for w_{eff} and l_{eff} are given in Eqn. (2.9) (Han et al., 2007).

$$f_{101} = \frac{c_0}{2\pi\sqrt{\mu_r \varepsilon_r}} \sqrt{\left(\frac{\pi}{w_{eff}}\right)^2 + \left(\frac{\pi}{l_{eff}}\right)^2} \tag{2.8}$$

$$w_{eff} = w - 1.08\,\frac{d^2}{p} + 0.1\,\frac{d^2}{w}\;; \quad l_{eff} = l - 1.08\,\frac{d^2}{p} + 0.1\,\frac{d^2}{l} \tag{2.9}$$

2.4.2 Modes in the SIW Cavity

The modes that exist in SIW have been investigated and reported by Xu and Wu (2005). The paper explains that the SIW and the conventional rectangular waveguide have similar guided wave characteristics. The two transmission lines are able to support $TE_{i,0}$ modes with $TE_{1,0}$ being the dominate mode. However, unlike the conventional rectangular waveguide which can support *TM* and $TE_{i,j}$ (*j*

$\neq 0$) modes, the SIW is not able to support these modes due to the discontinuity in its side walls. Hence, only the $TE_{i,0}$ modes can be excited and extracted in the SIW structure (Xu and Wu, 2005). Since surface currents are established in some guided wave structures as a result of mode establishment, Xu and Wu used the surface current distribution of a rectangular waveguide with vias (or slots) on the narrow walls, to explain the phenomenon of the existence of the $TE_{1,0}$ mode in the SIW. This is illustrated in Figure 2.10.

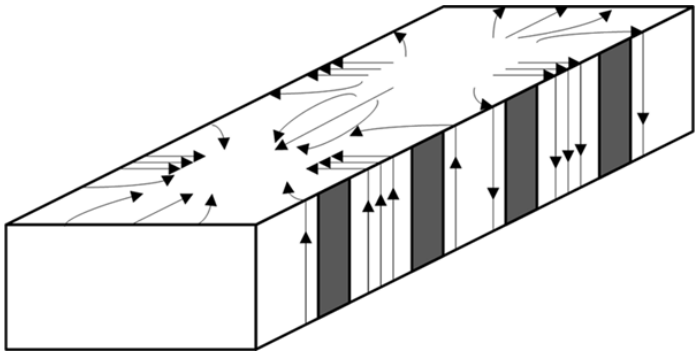

Figure 2.10: $TE_{1,0}$ mode surface current distribution of a rectangular waveguide with vias (or slots) on the narrow side walls (Xu and Wu, 2005).

According to Xu and Wu (2005), an enormous radiation may occur if slots cut the currents in a transverse direction. On the other hand, only a very little radiation may occur if the slots are cut along the direction of the current flow. Now, looking at Figure 2.10, it is clear that the slots do not cut the surface current on the narrow wall. Hence, the $TE_{1,0}$ mode is preserved in the structure. This explains why the $TE_{i,0}$ modes can exist in the SIW structure (Xu and Wu, 2005).

2.4.3 SIW Related Transition

The transition between planar transmission lines and SIW structures is a vital element related to SIW devices (Bozzi et al., 2011). A number of publications have presented SIW research findings with various types of input/output transitions. Microstrip-to-SIW transitions based on a simple taper have been presented (Deslandes and Wu, 2001; Deslandes, 2010). The tapered section connects a 50 Ohms microstrip line and the SIW. The taper is used for transforming the quasi-TEM mode in the microstrip line into the TE_{10} mode in the SIW. Coplanar waveguide (CPW)-to-SIW transition based on a 90^{o} bend has also been proposed (Deslandes and Wu, 2001). Another form of transition between a grounded coplanar waveguide (GCPW) and the SIW based on a current probe was proposed in Deslandes and Wu (2005). The current flowing through the probe generates a magnetic field that matches with the magnetic field inside the SIW structure. Transitions between air-filled waveguide and SIW structure have also been proposed (Huang and Wu, 2003; Xia et al., 2006). Microstrip-to-SIW transition in a multi-layer substrate have also been investigated and presented in Ding and Wu (2007).

The SIW devices presented in this thesis employ a novel Microstirp-CPW-SIW transition as the input / output coupling to the component's cavity resonator. The proposed transition model makes it easy for *RF* and microwave designers to achieve controllable external Q-factor in circuit components and devices design. The proposed transition uses the step impedance from a 50 Ohms microstrip line, to the low impedance GCPW before coupling into the device (filter or diplexer) using the short low impedance GCPW transmission line. This proposed transition,

as an input / output coupling for the device is sure to be very efficient as it allows two degrees of freedom in controlling the input / output coupling, i.e. the input / output coupling or the external Q-factor can be varied by either changing the step impedance of the CPW or the length of the short CPW transmission line.

2.4.4 Losses in the SIW

The main losses that exist in SIW devices can be linked to three loss mechanisms that include: conductor loss, dielectric loss, and radiation loss (Bozzi et al., 2008; Ranjkesh and Shahabadi, 2008; Bozzi et al., 2009). The conductor loss (also known as Ohmic loss) is the loss due to the finite conductivity of the metal walls; the dielectric loss, on the other hand, is the loss due to the loss tangent of the substrate material; while the radiation loss is the loss due to the leakage of electromagnetic energy through the periodic gaps in the two rows of metalized via holes (Xu and Wu, 2005; Bozzi et al., 2007). The conductor and dielectric losses that occur in SIW devices are similar to those that exist in rectangular waveguides. The radiation loss, on the other hand, is specifically linked to the SIW and is due to the periodic gaps present in the two rows of metalized via holes which are embedded in the dielectric substrate. One of the major challenges in the design of SIW devices is the ability to effectively minimise the loss mechanisms particularly when the device is to operate over the millimeter-wave frequency range (Bozzi et al., 2007; Bozzi et al., 2008).

The conductor loss in SIW devices is very similar to that of rectangular waveguide devices, and is as a result of the finite conductivity of the metallic walls. According to a study by Bozzi et al. (2009), a significant reduction in conductor loss can be

achieved by increasing the thickness of the dielectric substrate while keeping other dimensions of the SIW cavity constant. The conductor loss also decreases with a reduction in the pitch *p* (i.e. the spacing between adjacent via holes) due to the increased metal surface (Bozzi et al., 2009). An increase in the diameter *d* of the metalized via holes is also a way of slightly decreasing the conductor loss. The analytical formula for the calculation of the attenuation constant α_c due to the conductor loss in the SIW, at a particular frequency *f*, is given in Eqn. (2.10) (Bozzi et al., 2014); where *h* is the thickness of the dielectric substrate, σ_c is the conductivity of the metal surface, f_0 is the cut-off frequency of the SIW cavity, ε_0 is the permittivity of free space, ε_r is the relative permittivity of the dielectric substrate material, and w_{eff} is the effective width of the SIW cavity. Eqn. (2.10) was originally derived for calculating the attenuation constant due to the conductor loss in rectangular waveguide. It is only valid for calculating α_c if the width of the rectangular waveguide is directly replaced with the w_{eff} (Bozzi et al., 2014).

$$\alpha_c(f) = \frac{\sqrt{\pi f \varepsilon_0 \varepsilon_r}}{h\sqrt{\sigma_c}} \; \frac{1 + 2\,(f_0/f)^2\, h/w_{eff}}{\sqrt{1-(f_0/f)^2}} \tag{2.10}$$

The dielectric loss in SIW components, like the conductor loss, is similar to that of rectangular waveguide components. This loss mechanism is exclusively dependent on the loss tangent of the dielectric substrate material, and has nothing to do with the geometry of the SIW cavity (Bozzi et al., 2011). So long as the substrate thickness *h* of the SIW cavity is smaller than a half-wavelength, *h* will not affect the dielectric loss (Bozzi et al., 2009). The dielectric loss mechanism is typically the most substantial contributor of losses in devices that are designed

to operate at the millimeter-wave frequency range, hence, a careful selection of the dielectric substrate material for such devices is of extreme importance. The analytical formula derived for the calculation of the attenuation constant due to the dielectric loss in the rectangular waveguide, can be adopted for the calculation of the attenuation constant α_d due to the dielectric loss in the SIW. The formula, according to Bozzi et al. (2014) is given by Eqn. (2.11), where c_0 is the speed of light in free space and $tan\ \delta$ is the loss tangent from the dielectric substrate material.

$$\alpha_d = \frac{\pi f \sqrt{\varepsilon_r}}{c_0 \sqrt{1-(f_0/f)^2}}\ tan\ \delta \tag{2.11}$$

The radiation loss mechanism, unlike the conductor and the dielectric losses, is explicitly linked to the SIW and is as a result of the periodic gaps existing in the two rows of metalized via holes, which are embedded in the dielectric substrate material (Bozzi et al., 2014). The radiation loss in SIW devices is due to the energy leakage through the gaps. According to Deslandes and Wu (2002), the radiation loss in SIW can be neglected if the metal via diameter d and the pitch p are chosen based on Eqn. (2.12), where λ_g is the guided wavelength in the SIW. Eqn. (2.12) guarantees that the radiation loss is kept at a very low level and makes it possible for the SIW to be modelled by a conventional rectangular waveguide (Deslandes and Wu, 2002).

$$d < \lambda_g/5 \qquad and \qquad p \leq 2d \tag{2.12}$$

Though Eqn. (2.12) is a sufficient condition for SIW design, it is not always necessary as a value of $d \geq \lambda_g / 5$ and / or a value of $p > 2d$ can be used but with great care (Deslandes and Wu, 2002). Another article by Bozzi et al. (2011) explains that the radiation loss can be kept at a minimum if $p / d < 2.5$. The paper recommended that the value of p should be kept equal to $2d$ for best results. The formula for calculating the attenuation constant α_r due to the radiation loss in SIW was recently proposed by Pasian et al. (2013). This formula is given in Eqn. (2.13), where w is the width of the SIW cavity and λ is the propagation wavelength. Eqn. (2.13) is based on the analytical decomposition of the fundamental (quasi TE_{10}) mode of the SIW into two plane waves. It is also based on the numerical calculation of the transmission coefficient of an infinite grid of metal cylinders (Pasian et al., 2013; Bozzi et al., 2014).

$$\alpha_r = \frac{\frac{1}{w}\left(\frac{d}{w}\right)^{2.84}\left(\frac{s}{d}-1\right)^{6.28}}{4.85\sqrt{\left(\frac{2w}{\lambda}\right)^2-1}} \tag{2.13}$$

2.5 Coplanar Waveguide

The term coplanar waveguide (CPW) is popularly used to refer to coplanar transmission line. According to Hong and Lancaster (2001) and Steer (2009), the CPW was first proposed and invented in the year 1969 by Cheng P. Wen (Wen, 1969). The CPW has its signal line of width W, located between two different adjacent segments of ground plane conductors. Both the signal line and the two ground planes all rest on a dielectric substrate of relative dielectric constant $\mathcal{E}_r$ and a thickness h as shown in Figure 2.11. The spacing between the strip line and each ground plane is denoted by S.

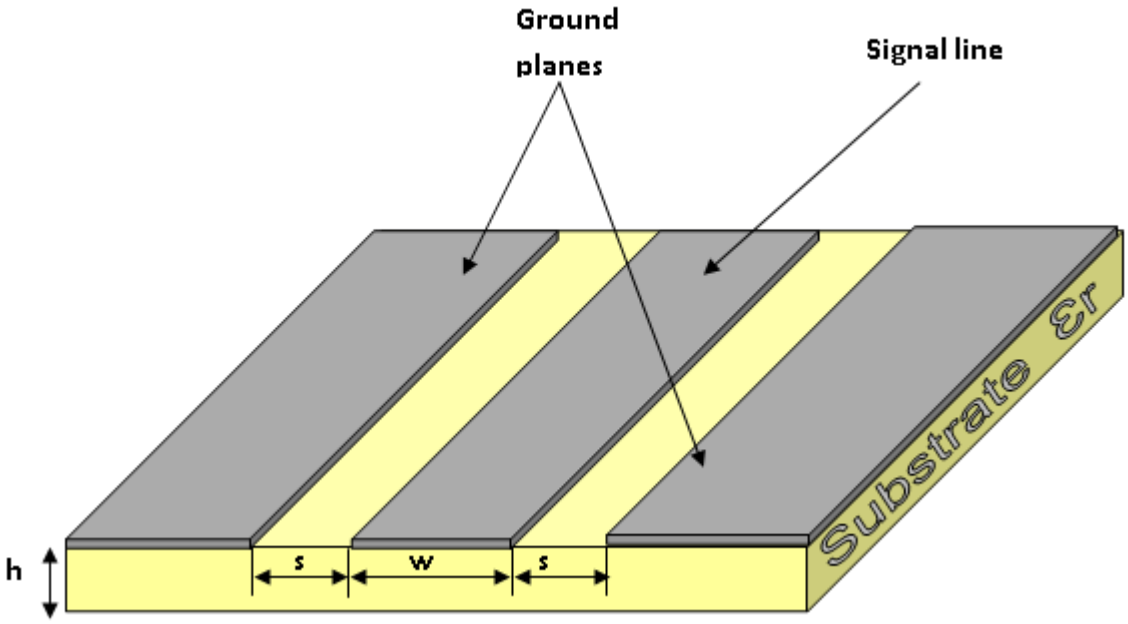

Figure 2.11: Coplanar waveguide geometry.

Like the microstrip, the CPW supports quasi-TEM mode of propagation since a small longitudinal component of the electromagnetic field exists at the dielectric-air interface (Hong and Lancaster, 2001). The most significant merit of CPW over microstrip is its ability to connect both active and passive circuit components/devices in shunt, from the signal line to the grounds plane on the same side of the substrate (Collin, 2000). In microstrip line, one needs to drill via-holes through the substrate in order to connect circuit components or devices in shunt between the signal line and the ground plans. This is due to the fact that the substrate, in the microstrip line structure, separates the signal line from the ground plane. Drilling a via-hole is even more hectic if the design material is ceramic, such as Alumina. CPW is particularly important for fabricating active circuits and devices. This is due to the presence of the signal line and the close proximity of the ground planes (Pozar, 2004).

Chapter 3: Microwave Filter

3.1 Introduction

A microwave filter is a 2-port component usually employed when there is a need to control the frequency response at any given point in a microwave system (Pozar, 2004). Passive microwave filters do not require any active circuit source or energizer in order to operate. They provide transmission at certain frequencies, known as the passband frequencies, or attenuation at certain frequencies referred to as the stopband frequencies. The frequencies outside the passband or the stopband are attenuated or transmitted, respectively. Microwave filters are classified according to their frequency responses as: lowpass, highpass, bandstop and bandpass filters. They are also classified in terms of their transfer functions as: Chebyshev, Butterworth (or maximally flat), and Elliptical filters.

3.2 Filters Based on Frequency Response

In terms of their frequency responses, microwave filters are classified as lowpass, highpass, bandstop, or bandpass filter. This section presents an overview of these four categories of filters and their frequency and elemental design transformations.

3.2.1 Lowpass Filter

A lowpass filter (LPF) is any filter that passes or transmits all signals between zero frequency and its cut-off frequency, and attenuates all signals above its cut-off frequency. The frequency response (including selectivity, roll-off, etc.) of a lowpass filter depends on the filter design. This type of filter can be used in

conjunction with a highpass filter to produce a bandpass filter. A diagram representing the lowpass filter characteristic is shown in Figure 3.1, where *f* is the frequency and f_c is the cut-off frequency.

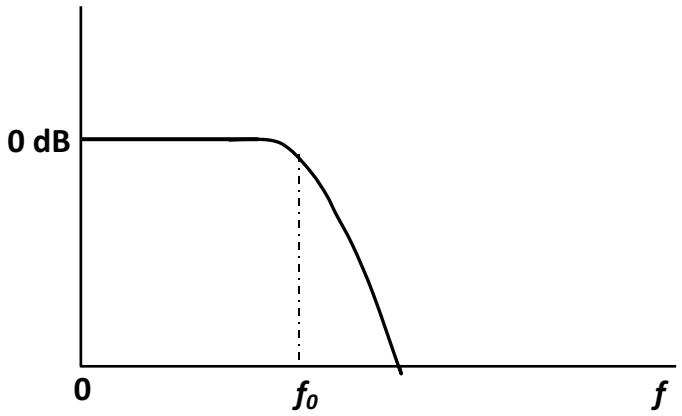

Figure 3.1: Lowpass filter characteristic.

The frequency transformation of a practical lowpass filter can be determined from a normalised lowpass prototype and is given in Eqn. (3.1) (Hong and Lancaster, 2001). Where Ω is the normalised lowpass prototype frequency domain and Ω_c is the normalised lowpass prototype cut-off frequency. The element transformation for the practical lowpass filter can then be determined from Eqn. (3.2), where L_{LPF} and C_{LPF} are the practical lowpass filter inductance and capacitance, respectively. L_p and C_p are the normalised lowpass prototype inductance and capacitance, respectively. The normalised lowpass prototype to practical lowpass element transformation is shown in Figure 3.2 (Hong and Lancaster, 2001).

$$\Omega = \left(\frac{\Omega_c}{f_c}\right) f \tag{3.1}$$

$$L_{LPF} = L_p \frac{\Omega_c}{f_c} \tag{3.2 a}$$

$$C_{LPF} = C_p \frac{\Omega_c}{f_c} \quad \text{(3.2 b)}$$

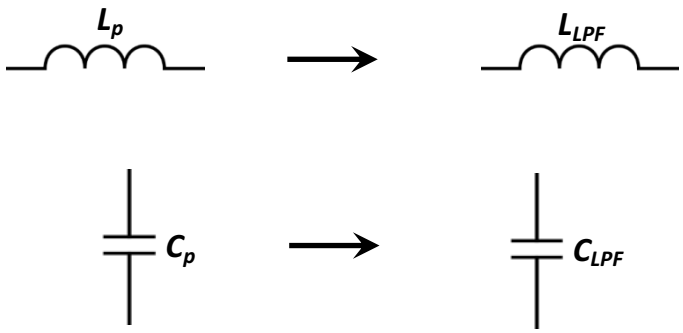

Figure 3.2: Normalised lowpass prototype to practical lowpass element transformation.

3.2.2 Highpass Filter

A highpass filter (HPF) is the direct opposite of a lowpass filter. It attenuates, to a great extent, all low frequency signal components below the cut-off point, while transmitting all signal components above its cut-off frequency. The extent of attenuation depends on the filter design. This type of filter can be used for blocking direct current (DC) from circuits that are sensitive to non-zero average voltages or radio frequency devices. It can also be combined with a LPF to produce a bandpass filter. The HPF characteristic is shown in Figure 3.3.

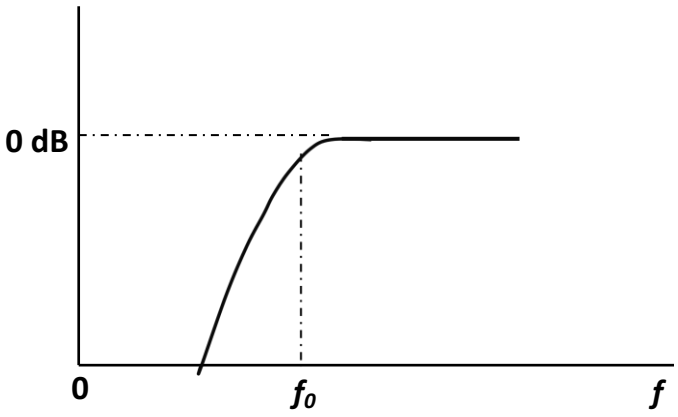

Figure 3.3: Highpass filter characteristic.

The frequency transformation for a highpass filter with cut-off frequency, f_c, is given in Eqn. (3.3) (Hong and Lancaster, 2001). The element transformation for a highpass filter can be achieved by transforming the inductive element of the normalised lowpass prototype to the capacitive element of the highpass filter. Similarly, the capacitive element of the normalised lowpass prototype is then transformed to the inductive element of the highpass filter. The element transformation for a highpass filter is given in Eqn. (3.4), where L_{HPF} and C_{HPF} are the highpass filter inductance and capacitance, respectively. The normalised lowpass prototype to highpass element transformation is shown in Figure 3.4 (Hong and Lancaster, 2001).

$$\Omega = -\frac{\Omega_c}{f} f_c \tag{3.3}$$

$$L_{HPF} = \frac{1}{\Omega_c f_c C_p} \tag{3.4 a}$$

$$C_{HPF} = \frac{1}{\Omega_c f_c L_p} \tag{3.4 b}$$

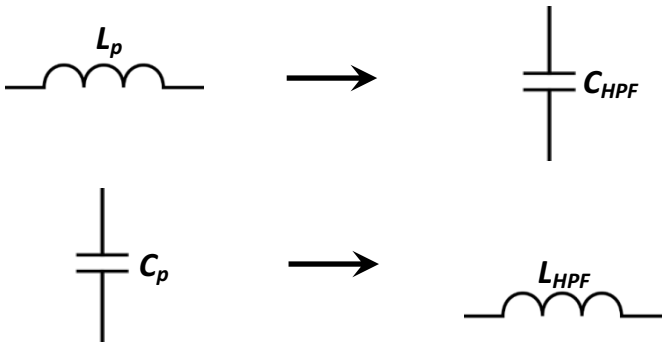

Figure 3.4: Normalised lowpass prototype to highpass element transformation.

3.2.3 Bandpass Filter

A bandpass filter (BPF) passes frequencies within a single band and rejects all other frequencies outside the band (Nwajana et al., 2017). Figure 3.5 shows the response from a bandpass filter that transmits all signal components between a lower frequency boundary, f_L and an upper frequency boundary, f_H, while attenuating and rejecting all other signal components that fall outside the f_L and f_H band. A bandpass filter can be formed by combining a lowpass filter with a highpass filter. Bandpass filters are widely used in radio frequency (RF) front end of cellular radio base station transmitters and receivers. Its main function in the transmitter is to limit the bandwidth of the output signal to the band assigned for the transmission. By this, the transmitter is prevented from interfering with other stations. In the receiver, a bandpass filter permits signals within a certain band of frequencies to be received and decoded, while stopping signals at undesirable frequencies from getting through.

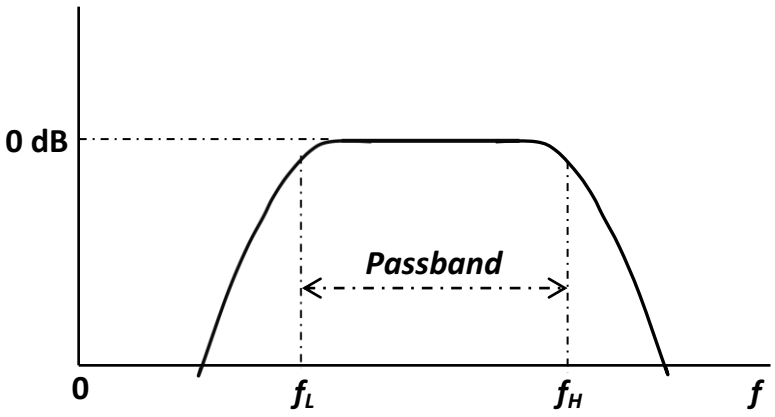

Figure 3.5: Bandpass filter characteristic.

The frequency transformation for a bandpass filter with the passband between f_L and f_H is given in Eqn. (3.5) (Hong and Lancaster, 2001), where f_0 is the centre frequency and FBW is the fractional bandwidth.

$$\Omega = \frac{\Omega_c}{FBW}\left(\frac{f}{f_0} - \frac{f_0}{f}\right) \tag{3.5 a}$$

$$FBW = \frac{f_H - f_L}{f_0} \tag{3.5 b}$$

$$f_0 = \sqrt{f_L f_H} \tag{3.5 c}$$

The element transformation for a bandpass filter can be achieved by transforming the inductive element of the normalised lowpass prototype to a series *LC* resonant circuit in the bandpass filter. The capacitive element of the normalised lowpass prototype, on the other hand, is transformed to parallel *LC* resonant circuit in the bandpass filter. The element transformation for a bandpass filter is given in Eqn. (3.6), where $L_{S\text{-}BPF}$ and $C_{S\text{-}BPF}$ are the series inductance and series capacitance of the bandpass filter, respectively. The parallel inductance and

parallel capacitance of the bandpass filter are denoted by $L_{P\text{-}BPF}$ and $C_{P\text{-}BPF}$ respectively. The normalised lowpass prototype to bandpass element transformation is shown in Figure 3.6 (Hong and Lancaster, 2001).

$$L_{S-BPF} = \frac{\Omega_c L_p}{f_0 FBW} \quad \text{(3.6 a)}$$

$$C_{S-BPF} = \frac{FBW}{\Omega_c f_0 L_p} \quad \text{(3.6 b)}$$

$$C_{P-BPF} = \frac{\Omega_c C_p}{f_0 FBW} \quad \text{(3.6 c)}$$

$$L_{P-BPF} = \frac{FBW}{\Omega_c f_0 C_p} \quad \text{(3.6 d)}$$

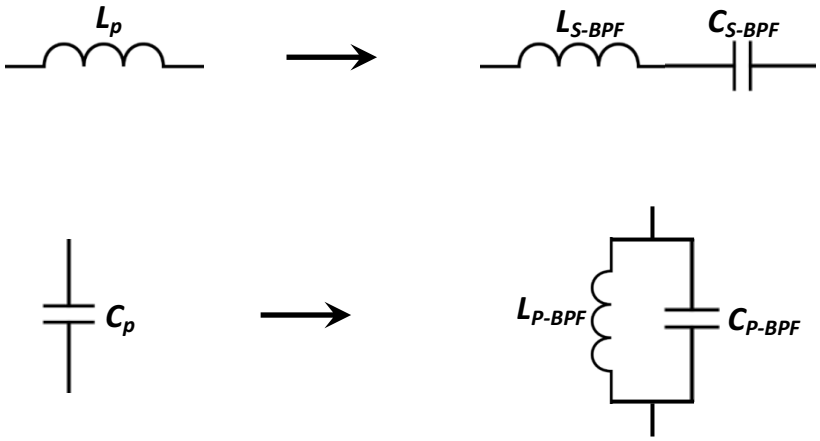

Figure 3.6: Normalised lowpass prototype to bandpass element transformation.

3.2.4 Bandstop Filter

A bandstop filter (BSF) is the direct opposite of a bandpass filter. It is sometimes known as a band-reject filter. This type of filter stops / rejects or attenuates signal

components that fall within a specified frequency band, but passes or transmits all other signal components that fall outside the specified frequency band. For example, a bandstop filter with f_L as the lower frequency boundary and f_H as the higher frequency boundary as shown in Figure 3.7, will stop signal components that fall within the stopband (f_L - f_H), while transmitting all other signal components. A bandstop filter with a narrow stopband (with high quality factor) is referred to as a notch filter.

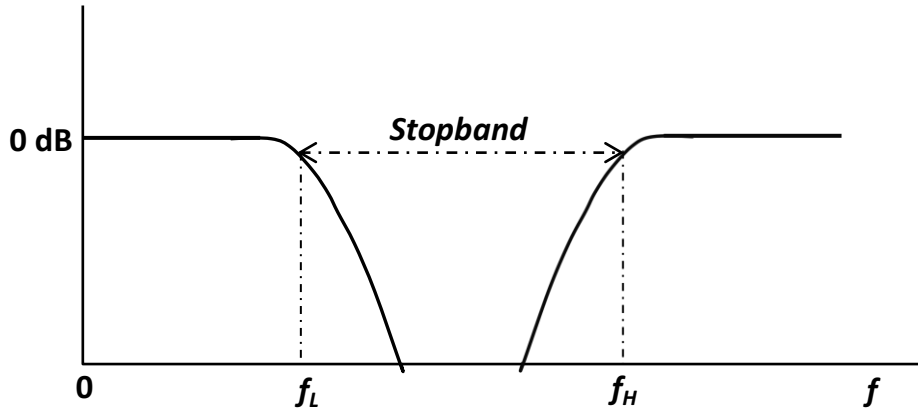

Figure 3.7: Bandstop filter characteristic.

The frequency transformation from normalised lowpass prototype to a bandstop filter with stopband between f_L and f_H can be achieved using Eqn. (3.7) (Hong and Lancaster, 2001), where f_0 is the centre frequency and FBW is the fractional bandwidth.

$$\Omega = \frac{\Omega_c \, FBW}{\left({}^{f_0}/_{f} - {}^{f}/_{f_0}\right)} \tag{3.7 a}$$

$$FBW = \frac{f_H - f_L}{f_0} \tag{3.7 b}$$

$$f_0 = \sqrt{f_L f_H} \tag{3.7 c}$$

The element transformation for a bandstop filter is a direct opposite to that of a bandpass filter. This can be achieved by transforming the inductive element of the normalised lowpass prototype to a parallel *LC* resonant circuit in the bandstop filter. The capacitive element of the normalised lowpass prototype, on the other hand, is transformed to series *LC* resonant circuit in the bandstop filter. The element transformation for a bandstop filter is given in Eqn. (3.8), where $L_{S\text{-}BSF}$ and $C_{S\text{-}BSF}$ are the series inductance and series capacitance of the bandstop filter, respectively. The parallel inductance and parallel capacitance of the bandstop filter are denoted by $L_{P\text{-}BSF}$ and $C_{P\text{-}BSF,}$ respectively. The normalised lowpass prototype to bandstop element transformation is shown in Figure 3.8 (Hong and Lancaster, 2001).

$$C_{P-BSF} = \frac{1}{L_p \, \Omega_c \, f_0 \, FBW} \tag{3.8 a}$$

$$L_{P-BSF} = \frac{\Omega_c \, L_p \, FBW}{f_0} \tag{3.8 b}$$

$$L_{S-BSF} = \frac{1}{C_p \, \Omega_c \, f_0 \, FBW} \tag{3.8 c}$$

$$C_{S-BSF} = \frac{\Omega_c \, C_p \, FBW}{f_0} \tag{3.8 d}$$

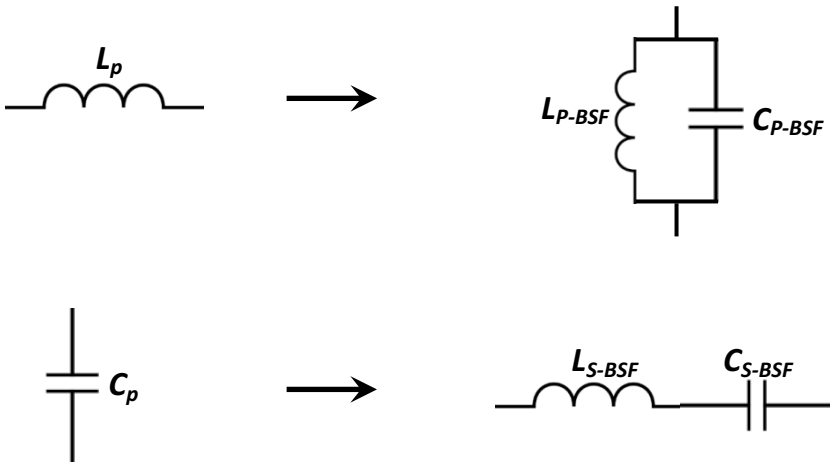

Figure 3.8: Normalised lowpass prototype to bandstop element transformation.

3.3 Filters Based on Transfer Function

The transfer function of a 2-port filter network is a mathematical explanation of the filter response characteristic. Put in another way, it is a polynomial that describes the characteristics of a filter based on mathematical expressions. Mathematically, the transfer function, $T(\omega)$, of a filter is given as the ratio of the output voltage, $V_{out}(\omega)$, to the input voltage $V_{in}(\omega)$ as given in Eqn. (3.9); where (ω) is a radian frequency variable of a lowpass prototype filter (Hong and Lancaster, 2001). Transfer function is usually expressed in decibel (dB). Three common categories of filters in terms of their transfer function are Butterworth, Chebyshev, and Elliptic filters. This section presents an overview on these three categories of filters and the lowpass filter response of each category.

$$T(\omega) = \frac{V_{out}(\omega)}{V_{in}(\omega)} \tag{3.9}$$

3.3.1 Butterworth Filter

A Butterworth filter response is also referred to as a maximally flat filter response due to its passband being maximally flat as shown in Figure 3.9 (Hong and Lancaster, 2001), where *IL* is the insertion loss, ω is the angular frequency, and ω_c is the cut-off frequency. This category of filter has a roll-off that is slower than that of both the Chebyshev and the Elliptic filter responses. The transfer function of a Butterworth or maximally flat filter response is given in Eqn. (3.10) (Matthaei et al., 1980), where *n* is the order of the polynomial which is also referred to as the degree or the order of the filter. The transfer function of the Butterworth or maximally flat filter response can also be expressed in decibel (dB) as given in Eqn. (3.11).

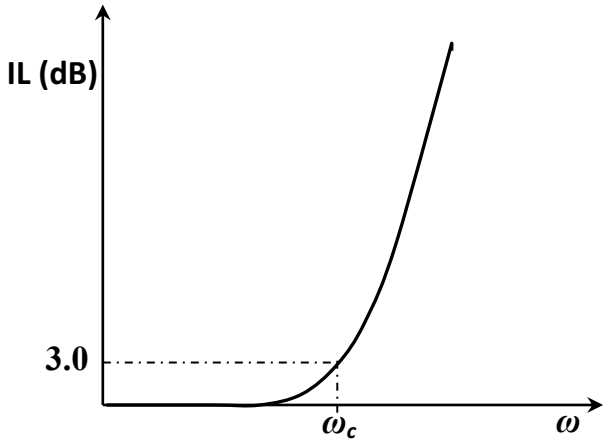

Figure 3.9: Butterworth (maximally flat) lowpass filter response.

$$|T\,(\omega)|\;=\frac{1}{\sqrt{1+\left(\omega/\omega_c\right)^{2\,n}}} \tag{3.10}$$

$$|S_{21}\,(\omega)|\;=\;20\,log_{10}\,|T\,(\omega)|=\;-10\,log_{10}\,\left|1+\;\left(\omega/\omega_c\right)^{2\,n}\right| \tag{3.11}$$

3.3.2 Chebyshev Filter

A Chebyshev filter response exhibits a passband with equal ripple and a stopband that is maximally flat as shown in Figure 3.10 (Hong and Lancaster, 2001), where *IL* is the insertion loss, ω is the angular frequency, and ω_c is the cut-off frequency. This category of filter has a roll-off that is relatively medium when compared to the Butterworth and the Elliptic filter responses. The transfer function of a Butterworth filter response is given in Eqn. (3.12) (Matthaei et al., 1980), where ε is the ripple factor, C_n is the Chebyshev polynomial, P_r is the passband ripple, and *RL* is the return loss. The transfer function of the Chebyshev filter response can also be expressed in decibel (dB) as given in Eqn. (3.13).

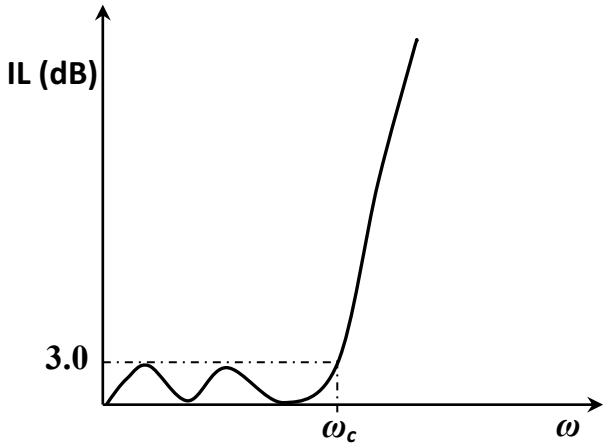

Figure 3.10: Chebyshev lowpass filter response.

$$|T(\omega)| = \frac{1}{\sqrt{1 + \left(\varepsilon\, C_n\left(\omega/\omega_c\right)\right)^2}} \qquad (3.12\text{ a})$$

$$\varepsilon = \sqrt{10^{\frac{P_r}{10}} - 1} = \sqrt{\frac{10^{-\frac{RL}{10}}}{1 - 10^{-\frac{RL}{10}}}} \qquad (3.12\text{ b})$$

$$|S_{21}(\omega)| = 20\,log_{10}|T(\omega)| = -10\,log_{10}\left|1 + \left(\varepsilon\, C_n\left({}^{\omega}/_{\omega_c}\right)\right)^2\right| \quad (3.13)$$

3.3.3 Elliptic Filter

An Elliptic filter response exhibits equal ripple in both the passband and the stopband as shown in Figure 3.11 (Hong and Lancaster, 2001), where *IL* is the insertion loss, ω is the angular frequency, ω_c is the cut-off frequency, and ω_s is the frequency at which the equal ripple stopband starts. This category of filter has a roll-off that is relatively sharp when compared to the Butterworth and the Chebyshev filter responses.

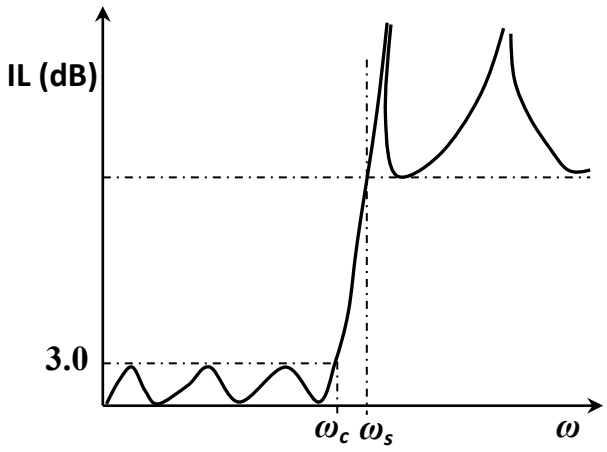

Figure 3.11: Elliptic lowpass filter response.

3.4 Filter Design Methods

Filter design at low frequencies require lumped element parameters such as inductor (*L*) and capacitor (*C*). These *LC* elements have a very simple and general design steps that have been established for their usage in filter design.

The established design steps are based on their simple frequency characteristics (Collin, 2000). At microwave frequencies, however, filter design faces a lot of difficulties as it involves the use of distributed element parameters in place of the traditional lumped elements parameters used at low frequencies. These distributed element parameters are much more complicated, and no complete theory or filter synthesis steps have been developed (Collin, 2000). Two filter synthesis methods are generally in use these days. These two techniques are the image parameter and the insertion loss methods.

3.4.1 Image Parameter Method

The image parameter method of filter design is a technique whereby the needed passband and / or stopband features, of the desired filter are provided. However, the exact frequency features over each region are not specified. An enormous drawback with this method is that a great deal of iteration must be carried out in order to achieve the desired response (Pozar, 2004). This technique also suffers from another concern that involves frequent cut-and-try processes in order to obtain a reasonable and acceptable result (Collin, 2000). Though an arbitrary frequency response cannot be integrated into a design relying on this method, the technique is relatively simple and very useful in simple filter design. The image parameter method provides a link between infinite periodic structures and practical filter design. This technique of filter design finds application in solid-state traveling-wave amplifier design (Pozar, 2004).

Looking at the arbitrary 2-port network, specified by its *ABCD* parameters, as shown in Figure 3.12, which is required for the analysis and design of filters based

on the image parameter method; the image impedances, Z_{i1} and Z_{i2}, are defined for the network as follows: Z_{i1} is the input impedance at port 1 when port 2 is terminated with Z_{i2}; and Z_{i2} is the input impedance at port 2 when port 1 is terminated with Z_{i1}. Hence, both ports are matched when terminated in their image impedances (Pozar, 2004).

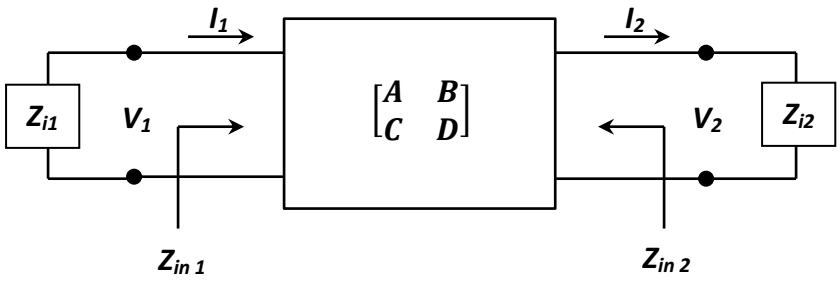

Figure 3.12: An arbitrary 2-port network terminated in its image impedances (Pozar, 2004).

3.4.2 Insertion Loss Method

The insertion loss method of filter design is a technique that begins with a complete specification of attainable features. This specification allows for a suitable filter network synthesis which begins with a normalised lowpass prototype. This filter design method is preferred to the image parameter method considering the huge drawbacks and challenges associated with the image parameter technique (Collin, 2000). The insertion methods of filter design allows for a high degree of control over the filter passband and stopband amplitude, and phase characteristics. All the filter components (i.e. bandpass and dual-band pass filters) achieved and reported throughout this thesis were designed using the insertion loss method. A block diagram highlighting the filter design stages when using the insertion loss method is shown in Figure 3.13.

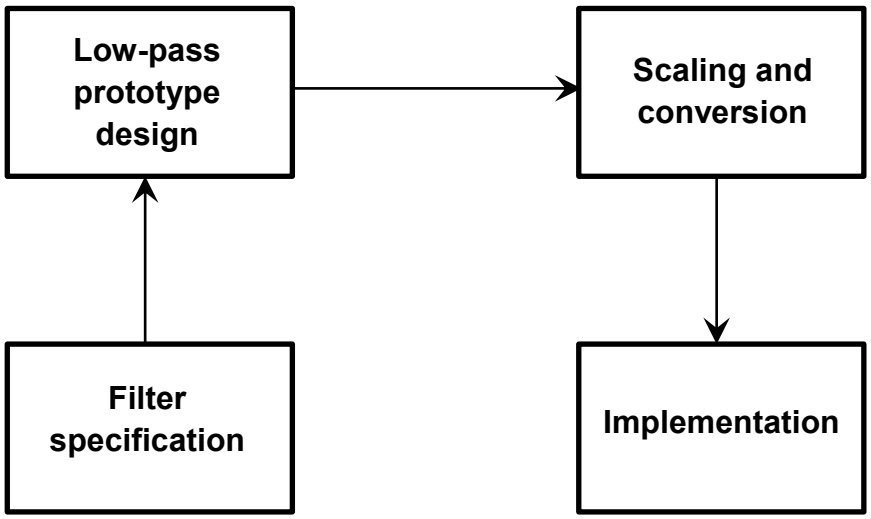

Figure 3.13: The stages of filter design by insertion loss method.

3.5 Immittance Inverters

There are popularly two types of Immittance inverters. One is the impedance inverter (also known as *K*-inverter) while the other is the admittance inverter (also known as J-inverter). Both the *K*- and the *J*- inverters are considered to have unique properties under ideal conditions. In reality, however, the *K* and *J* parameters of practical immittance inverters are frequency dependent (Hong and Lancaster, 2001). In filter design, it is often important and very convenient to use shunt-only or series-only *LC* elements when a particular form of transmission line is to be used for the filter implementation (Pozar, 2004). Combining both series and shunt *LC* elements in the circuit model of a filter, would make the transmission line implementation of the filter a very tedious and challenging task. Using the immittance inverters, series-connected *LC* elements can be transformed to shunt-connected *LC* elements and shunt-connected *LC* elements can be transformed to series-connected elements. By these conversions, a

shunt-only or series-only design can be achieved, making the transmission line realization of the filter more easily attainable.

3.5.1 Impedance Inverter

Impedance inverters are also known as *K*-inverters. An ideal impedance inverter is a 2-port network that has a distinct characteristic at all frequencies (Hong and Lancaster, 2001). This means that when a *K*-inverter is terminated in the load impedance Z_L on one port, as shown in Figure 3.14, the source impedance Z_s seen looking into the other port is as given in Eqn. (4.14), where *K* is a real value which is defined as the characteristic impedance of the *K*-inverter.

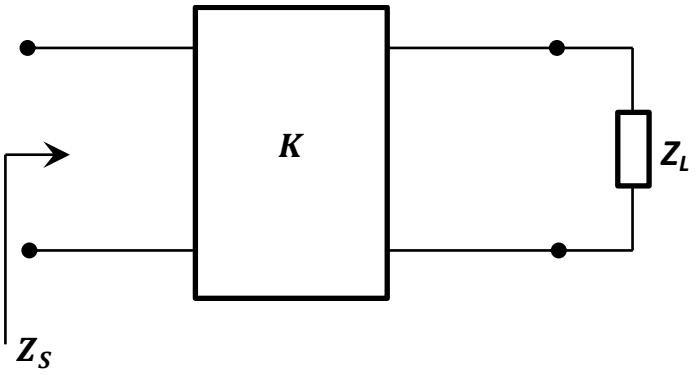

Figure 3.14: Ideal Impedance inverter (*K*-inverter) network.

$$Z_S = \frac{K^2}{Z_L} \tag{4.14}$$

An impedance inverter has a phase shift of $\pm 90^o$ or an odd multiple of $\pm 90^o$ thereof (Hong and Lancaster, 2001). This implies that if Z_L is inductive, in Eqn. (3.14), then Z_s would be conductive. If, on the other hand, Z_L is conductive then Z_s would become inductive (Hong and Lancaster, 2001). According to Matthaei

et al. (1980) and Hong and Lancaster (2001), an ideal impedance inverter may generally be expressed with the ABCD matrix given in Eqn. (3.15).

$$\begin{bmatrix} A & B \\ C & D \end{bmatrix} = \begin{bmatrix} 0 & \pm \frac{K}{j} \\ \pm \frac{1}{j\,K} & 0 \end{bmatrix} \tag{3.15}$$

Impedance inverters can be modelled using quarter wavelength transmission lines, with the *K*-value representing the impedance of the transmission line. They can also be modelled using reactive circuit elements, that is, capacitor or inductor network, or a combination of capacitor and inductor network. Figure 3.15 shows an impedance inverter being modelled as purely capacitive and purely inductive networks.

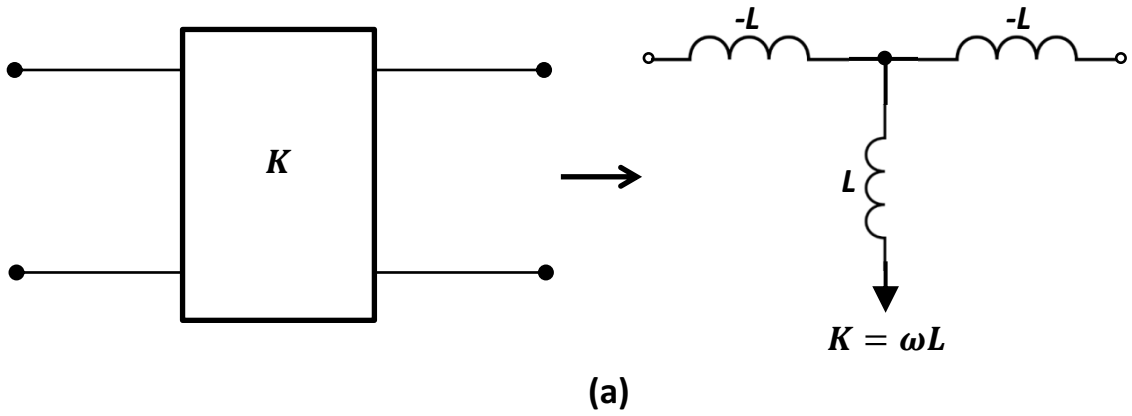

(a)

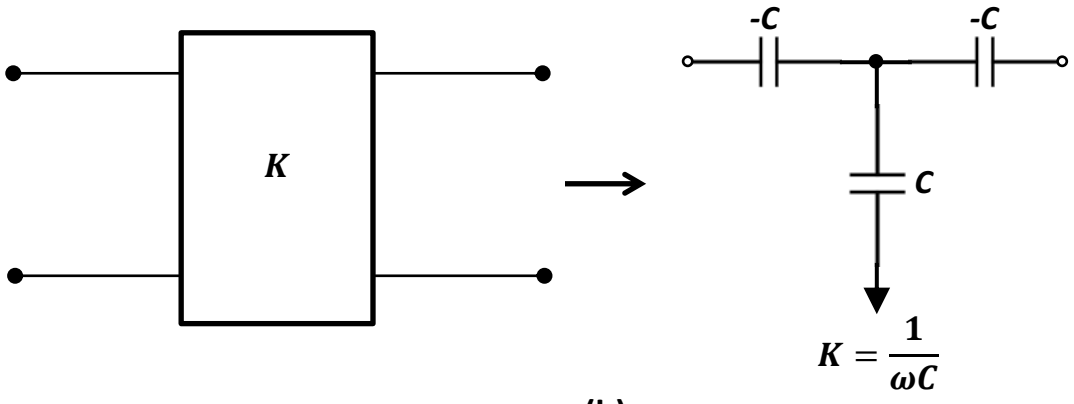

(b)

Figure 3.15: Reactive circuit elements modelling of impedance inverter. (a) *K*-inverter to inductor-only network. (b) *K*-inverter to capacitor-only network. (Matthaei et al.,1980; Hong and Lancaster, 2001).

Impedance inverters are used to obtain series-only network in filter design. This is because they are able to convert shunt reactive components into series reactive components. An example is shown in Figure 3.16 where the impedance inverter is used to convert the shunt capacitor into an equivalent circuit with series inductor. It can be established from Figure 3.16, that for *K* = 1, *L* = C. This is demonstrated in Eqn. 3.16 (Matthaei et al.,1980).

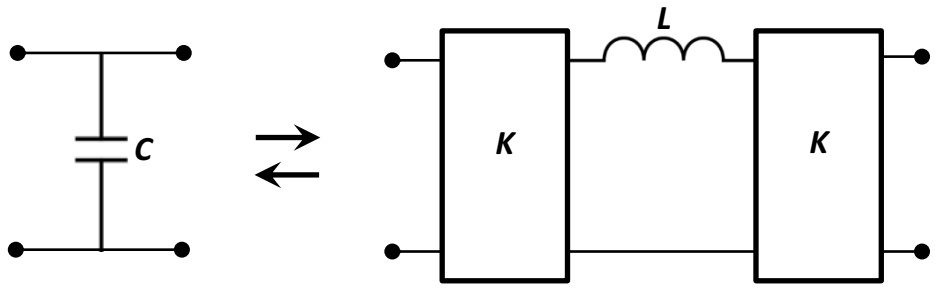

Figure 3.16: Impedance inverter used to convert a shunt capacitance into an equivalent circuit with series inductance (Hong and Lancaster, 2001).

$$\begin{bmatrix} 1 & 0 \\ j\omega C & 1 \end{bmatrix} = \begin{bmatrix} 0 & \frac{K}{j} \\ \frac{1}{j\,K} & 0 \end{bmatrix} \begin{bmatrix} 1 & j\omega L \\ 0 & 1 \end{bmatrix} \begin{bmatrix} 0 & -\frac{K}{j} \\ -\frac{1}{j\,K} & 0 \end{bmatrix} = \begin{bmatrix} 1 & 0 \\ \frac{j\omega L}{K^2} & 1 \end{bmatrix} \qquad (3.16)$$

3.5.2 Admittance Inverter

Admittance inverters are also known as *J*-inverters. Like the impedance inverters, *J*-inverters are 2-port networks that have unique properties at all frequencies

(Hong and Lancaster, 2001). This means that when a *J*-inverter is terminated in the load admittance Y_L on one port, as shown in Figure 3.17, the source admittance Y_S seen looking into the other port is as given in Eqn. (3.17), where *J* is a real value defined as the characteristic admittance of the *J*-inverter.

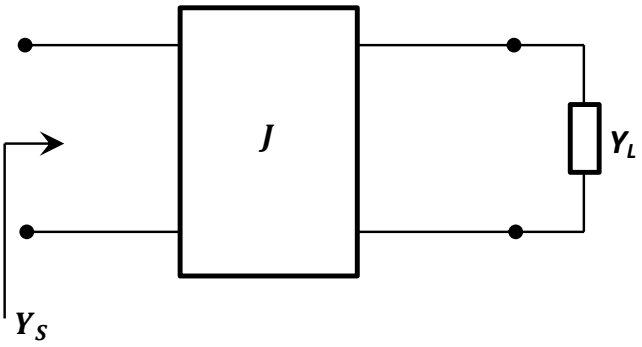

Figure 3.17: Ideal admittance inverter (J-inverter) network.

$$Y_s = \frac{J^2}{Y_L} \tag{3.17}$$

Like the impedance inverters, an admittance inverter has a phase shift of $\pm 90^o$ or an odd multiple of $\pm 90^o$ thereof (Hong and Lancaster, 2001). An ideal admittance inverter may generally be expressed with the ABCD matrix given in Eqn. (3.18). (Matthaei et al., 1980; Hong and Lancaster, 2001).

$$\begin{bmatrix} A & B \\ C & D \end{bmatrix} = \begin{bmatrix} 0 & \pm \frac{j}{J} \\ \pm j \cdot J & 0 \end{bmatrix} \tag{3.18}$$

Admittance inverters can be modelled using quarter wavelength transmission lines, with the *J*-value representing the impedance of the transmission line. They can also be modelled using reactive circuit elements, that is, capacitive or

inductive network, or a combination of capacitive and inductive network. Replacing an admittance inverter with a capacitor-only network is equivalent to modelling an electric coupling between two coupled resonators; while replacing an admittance inverter with an inductor-only network is equivalent to modelling a magnetic field between two coupled resonators. Using a network of both capacitor and inductor to replace an admittance inverter is similar to modelling a mixed coupling between two coupled resonators. Figure 3.18 shows an admittance inverter being modelled as capacitor-only and inductor-only networks.

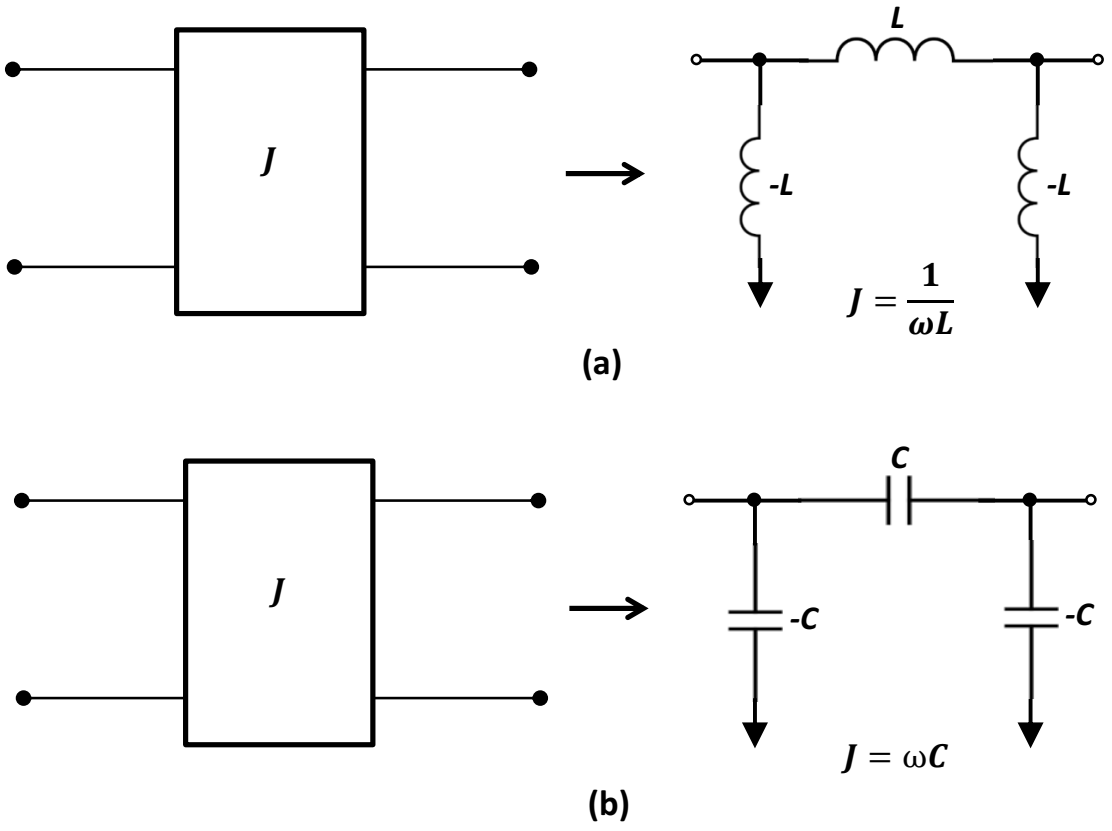

Figure 3.18: Reactive circuit elements modelling of admittance inverter. (a) *J*-inverter to inductor-only network. (b) *J*-inverter to capacitor-only network. (Matthaei et al.,1980; Hong and Lancaster, 2001).

In filter design, admittance inverters are used to obtain shunt-only network. This is because they are able to convert series reactive components to shunt reactive components. An example is shown in Figure 3.19 where the admittance inverter (J-inverter) is used to convert the series inductor into an equivalent circuit with shunt capacitor. It can be established from Figure 3.19, that for $J = 1$, $L = C$. This is demonstrated in Eqn. 3.19 (Matthaei et al.,1980).

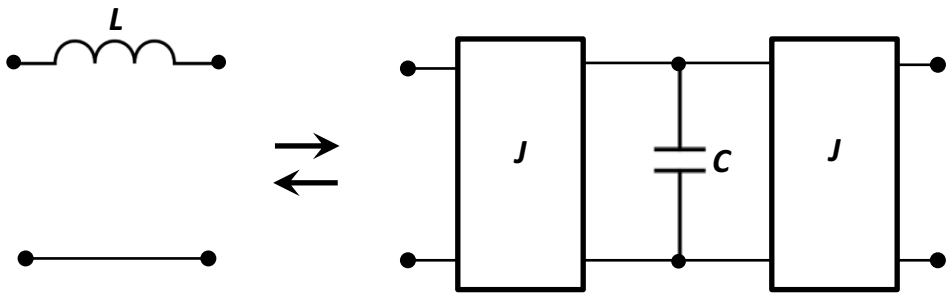

Figure 3.19: Admittance inverter used to convert a series inductance into an equivalent circuit with shunt capacitance (Hong and Lancaster, 2001).

$$\begin{bmatrix} 1 & j\omega L \\ 0 & 1 \end{bmatrix} = \begin{bmatrix} 0 & \frac{j}{J} \\ \frac{1}{j \cdot J} & 0 \end{bmatrix} \begin{bmatrix} 1 & 0 \\ j\omega C & 1 \end{bmatrix} \begin{bmatrix} 0 & -\frac{j}{J} \\ -j \cdot J & 0 \end{bmatrix} = \begin{bmatrix} 1 & \frac{j\omega C}{J^2} \\ 0 & 1 \end{bmatrix} \tag{3.16}$$

3.6 SIW Bandpass Filter Design

An overview on the SIW transmission line technology has been covered in Chapter 2, Section 2.4 of this thesis. Here, the SIW technique is employed in the design of a three-pole (i.e. third order) bandpass filter. The SIW bandpass filter design reported in this section has been presented in a conference organised and sponsored by the Institute of Electrical and Electronic Engineers (IEEE)

(Nwajana et al., 2016), and also published in a peer reviewed journal (Nwajana et al., 2017).

A SIW bandpass filter designed based on the insertion loss methods discussed in sub-section 3.4.2, is presented here with a novel Microstrip-CPW-to-SIW transition at both the input and output (i / o) ports. The input / output transition also serves as the input and output couplings into the filter. The Microstrip-CPW-to-SIW transition structure presented here exploits the step impedance between the 50 Ohms input / output feedline and the transition to control the input / output couplings of the filter. The SIW filter is also shown to have very minimum milling/etching requirement and this reduces the fabrication error. The proposed SIW filter has been validated experimentally and results presented. The simulation and measurement results show excellent agreement on comparison (Nwajana et al., 2017).

Some design factors or parameters of filters such as selectivity, cost, size, sensitivity to environmental effects, power handling capacity, in-band and out-of-band performance metrics, are critical specifications in the development of radio frequency (RF) and microwave communication front end devices. Filter developers are often required to make compromise between several conflicting requirements as it is rather difficult or even physically and/or electrically impossible to simultaneously achieve all design criteria or specifications. For instance, achieving higher channel selectivity usually requires the use of more resonators, which will result in higher insertion loss along the transmission path since insertion loss is approximately proportional to the number of resonators

used in the construction of a filter (Chen and Wu, 2014). Hence, care must be taken when selecting design specifications in order to meet the most critical design targets.

3.6.1 Circuit Model Design and Simulation

The test bandpass filter presented here was designed based on the following specifications: centre frequency f_0, 1684 MHz; fractional bandwidth *FBW*, 4%; and passband return loss *RL*, 20 dB. The bandpass filter circuit model was designed based on the technique reported in Hong and Lancaster (2001). The design method begins with the establishment of the bandpass filter circuit from the normalised lowpass prototype filter shown in Figure 3.20.

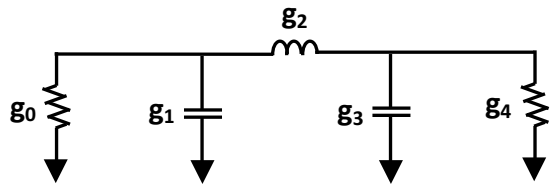

Figure 3.20: Standard 3-pole (third order) normalised lowpass prototype filter (Yeo and Nwajana, 2013).

The normalised Chebyshev lowpass prototype filter parameters *g*, at 0.04321 dB passband ripple, were determined from Hong and Lancaster (2001) and presented in Table 3.1.

Table 3.1: Chebyshev lowpass prototype filter parameters.

g_0	g_1	g_2	g_3	g_4
1.0	0.8516	1.1032	0.8516	1.0

Admittance inverters (also known as *J*-inverters) were utilised in transforming the normalised lowpass prototype filter to a shunt-only network as shown in Figure 3.21. This is based on the technique explained in sub-section 3.5.2 and given in Figure 3.19, where the *J*-inverter was used to convert a series inductance into an equivalent circuit with shunt capacitance. The *J*-inverter values in Figure 3.21 were determined using Eqn. (3.17), where *n* is the order of the filter and *m* = 1, 2, …, *n*. Each of the shunt capacitors in Figure 3.21 was made to be equal to g_1 (Yeo and Nwajana, 2013).

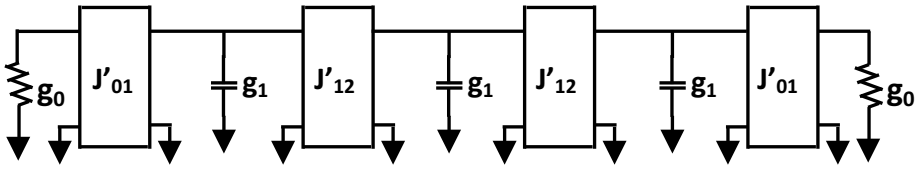

Figure 3.21: Normalised lowpass prototype filter with admittance inverters and shunt-only components (Yeo and Nwajana, 2013).

$$J'_{m,m+1} = \sqrt{\frac{g_1^2}{g_m\, g_{m+1}}} \qquad (3.17\text{ a})$$

$$J'_{01} = J'_{n,n+1} = 1 \qquad (3.17\text{ b})$$

The lossless bandpass filter circuit model with identical parallel *LC* resonators and *J*-inverters is shown in Figure 3.22.

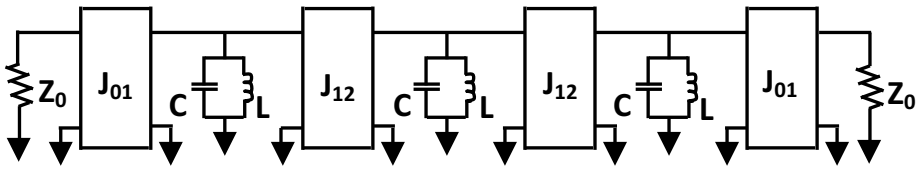

Figure 3.22: Chebyshev bandpass filter circuit model with identical parallel *LC* resonators and admittance inverters (Yeo and Nwajana, 2013).

The shunt inductor *L* and the shunt capacitor *C* of Figure 3.22 were determined using Eqn. (3.18), where Z_0 is the 50 Ohms impedance due to the input and output terminations, and ω_0 is the angular centre frequency of the bandpass filter. The new *J*-inverter values of Figure 3.22 were obtained using Eqn. (3.19).

$$C = \frac{g_1}{\omega_0 Z_0 FBW} \tag{3.18 a}$$

$$L = \frac{Z_0 FBW}{g_1 \omega_0} \tag{3.18 b}$$

The bandpass filter circuit model was simulated using the Keysight Advanced Design System (ADS) circuit simulator. The couplings between resonators were modelled using the method described in sub-section 3.5.2 and given in Figure 3.18 (b). This method involves modelling each *J*-inverter in the circuit model with a pi-network of capacitors. The complete bandpass filter circuit model (in ADS) with admittance inverters (or *J*-inverters) modelled as pi-network of capacitors is shown in Figure 3.23. The numerical design parameters of the bandpass filter are given in Table 3.2.

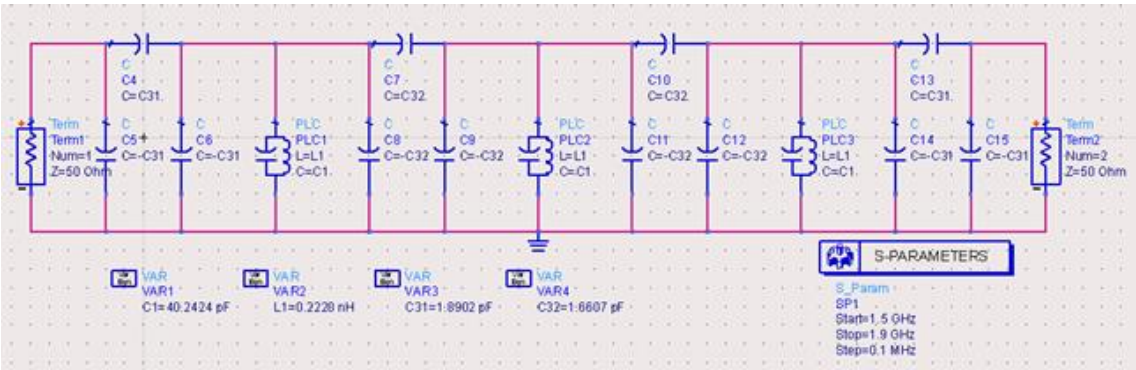

Figure 3.23: Bandpass filter circuit model with *J*-inverters modelled as pi-network of capacitors.

Table 3.2: 3rd order (3-pole) Chebyshev bandpass filter design parameters.

Filter	f_0 (MHz)	L (nH)	C (pF)	$J_{0,1}$	$J_{1,2}$
BPF	1684	0.222	40.2424	0.02	0.0176

The simulation results of the test bandpass filter circuit model are shown in Figure 3.24, where S_{21} is the insertion loss and S_{11} is the return loss. The results clearly show that the filter centre frequency and its minimum return loss are at 1684 MHz and 20 dB as designed. The test filter also has a medium roll-off as shown in Figure 3.24 and equal ripples in the passband as shown in Figure 3.25. Medium roll-off and equal ripples in passband are the two well-known features of Chebyshev filters as explained in sub-section 3.3.2.

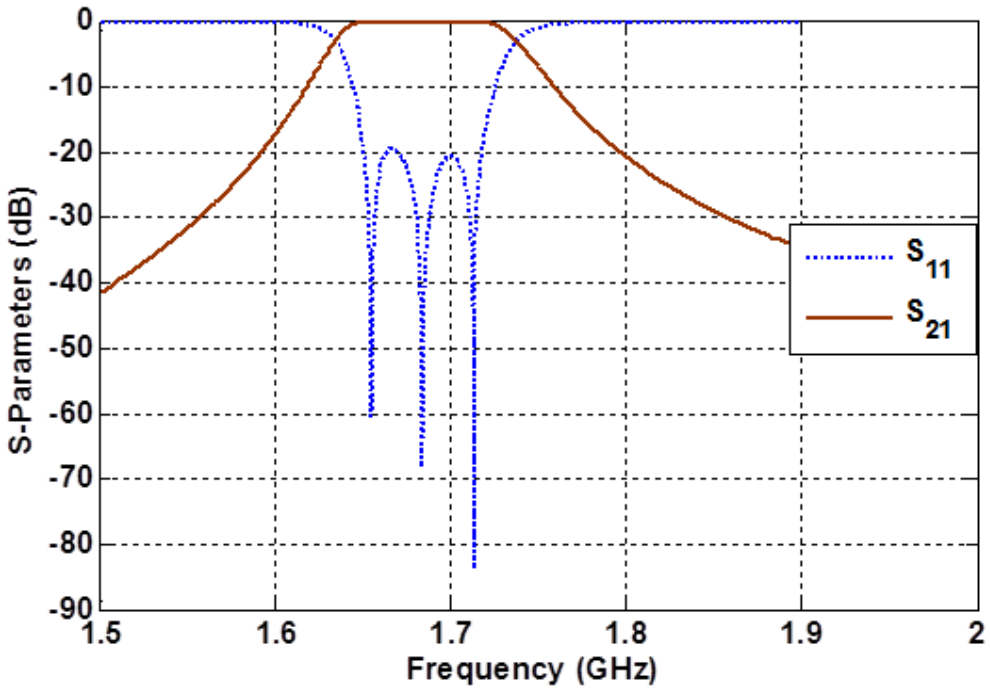

Figure 3.24: Simulation responses of the bandpass filter circuit model.

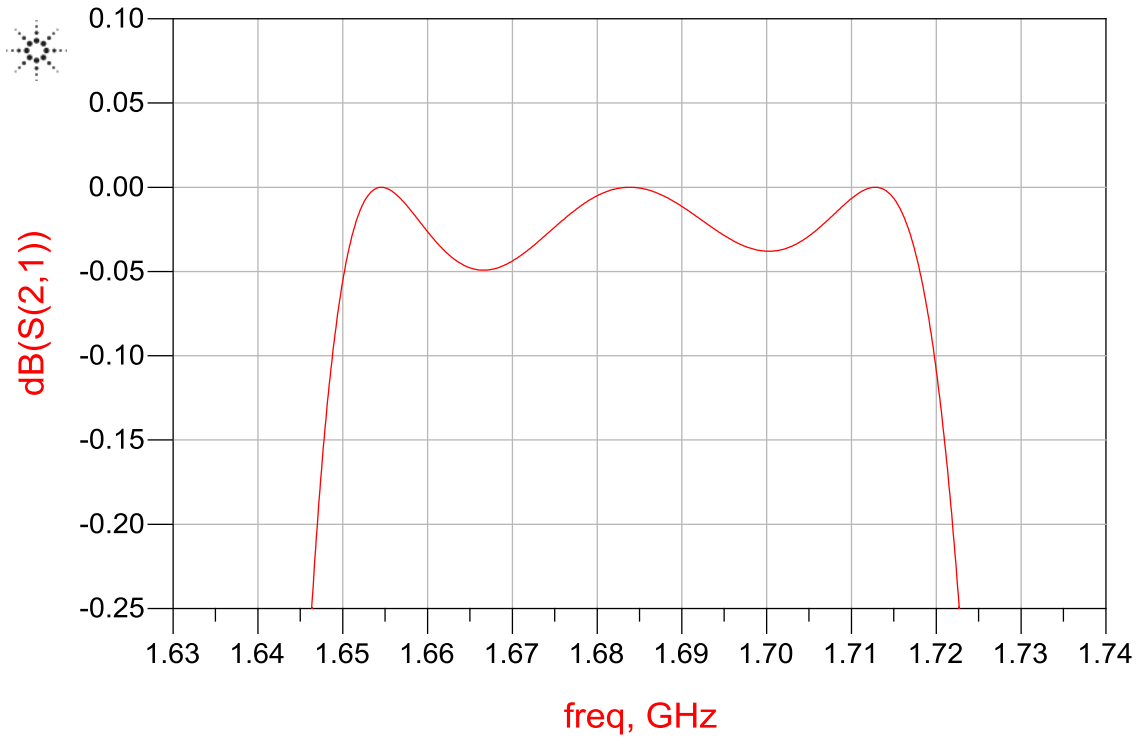

Figure 3.25: Passband ripples of the Chebyshev bandpass filter circuit model.

3.6.2 SIW Design and Simulation

The dimensions of the SIW cavity required in order to realise the bandpass filter, was designed to resonant at the fundamental TE_{101} mode resonant frequency (i.e. the filter centre frequency, f_0) of 1684 MHz using Eqns. (2.7) and (2.8). The design was implemented on the Rogers RT/Duroid 6010LM substrate with relative permittivity or dielectric constant, ε_r = 10.8; thickness, h = 1.27 mm; and relative permeability, μ_r = 1. The design parameters of the SIW cavity were chosen as follows: the diameter of the metallic post, d = 2 mm; the pitch or distance between metallic posts, p = 3.725 mm; the SIW width, w = 37.25 mm; and the length of the SIW, l = 37.25 mm (Nwajana et al., 2017). According to Hong (2011) and Deslandes and Wu (2003), the distance between neighbouring metallic posts, p should be made equal or less than double the diameter of the metallic post, d (i.e. $p \leq 2d$) for best results. Hong (2011) explained that if the values of p and b are made larger, then the electromagnetic leakage through the metallic posts would be higher. This means higher radiation losses which would negatively affect the filter insertion and return losses. The radiation loss becomes negligible at $p = 2d$. This is explained in greater details in Deslandes and Wu (2003).

Electromagnetic (EM) simulations were carried out using the finite-element method (FEM) of the Keysight electromagnetic professional (EMPro) three dimensional simulator. A loss tangent, $tan\ \delta$ = 0.0023 was assumed for the substrate, and a conductivity, σ = 5.8 x 10^7 S/m for the copper metal. The thickness of the copper metal was chosen as 17 microns (μm). To expedite simulation and reduce simulation time, each metallic post was implemented as

an octa-decagon (i.e. 18 sided polygons) (Nwajana et al., 2017). This is as opposed to the standard circular metallic posts that have been widely reported in literature.

The theoretical value of the coupling coefficient, *k*, between two filter resonators was calculated using Eqn. (3.19), where $J_{1,2}$, *L*, and *C* correspond to the values given in Table 3.2. The simulated value of the coupling coefficient, *k*, between each pair of SIW cavities were achieved using the technique shown in Figure 3.26 and using Eqn. (3.20), where f_1 and f_2 are the eigen-modes from simulating a pair of SIW cavities.

$$k = J_{1,2}\sqrt{\frac{L}{C}} \tag{3.19}$$

$$k = \frac{f_2^2 - f_1^2}{f_2^2 + f_1^2} \tag{3.20}$$

The value of *k* that was used to achieve the bandpass filter is $k = 0.041$ at separation distance, $s = 13.05$ mm (Nwajana et al., 2017).

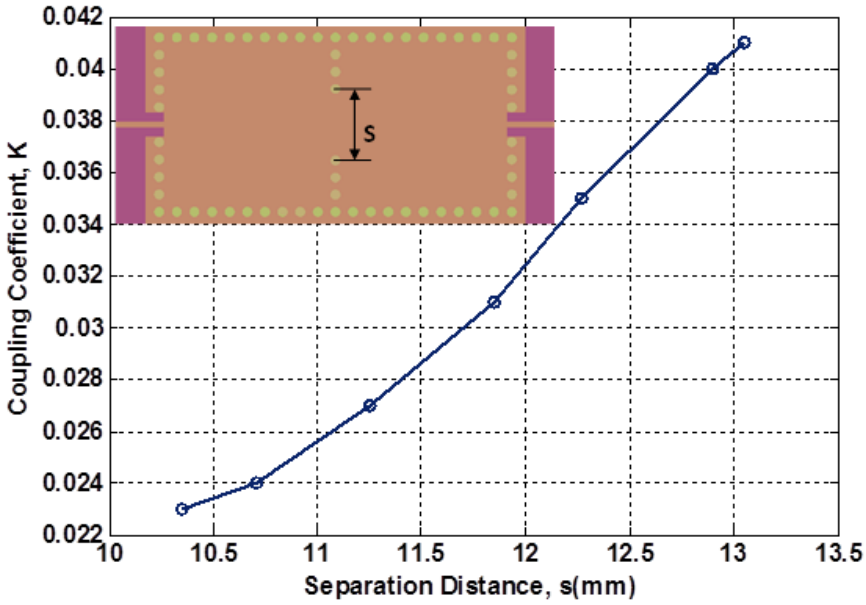

Figure 3.26: Simulated coupling coefficient of a pair of substrate integrated waveguide cavities (Nwajana et al., 2017).

The theoretical value of the external quality factor, Q_{ext} = 21.21 of the bandpass filter was extracted using Eqn. (3.21), where f_0, J_{01}, and C correspond to the parameters given in Table 3.2.

$$Q_{ext} = \frac{2\pi f_0 C}{J_{0,1}} \tag{3.21}$$

The simulated Q_{ext} value was based on the method shown in Figure 3.27, where the Microstrip-CPW-SIW coupling shown in the diagram is a strong coupling necessary for achieving the required Q_{ext}. The CPW-SIW coupling shown in Figure 3.27 is a weak coupling, only used to facilitate the simulation. Hence, the Microstrip-CPW-SIW coupling is the important coupling in Figure 3.27. The length corresponding to the 50 Ohms impedance (Z_0) of the microstrip transmission line was determined using the extensively reported formulations given in Huang and Wu (2003). The impedance (Z_1), at the SIW end of the transition was achieved

by altering the lengths, "*a*" and "*b*", until the required filter Q_{ext} value of 21.21 was attained. A graph showing the variation of Q_{ext} with "*a*", at *b* = 8.13 mm is presented in Figure 3.28 (a). Similar graph showing the variation of Q_{ext} with "*b*", at *a* = 0.7 mm is also presented in Figure 3.28 (b). The value of Z_1 that corresponds to the required Q_{ext} value of 21.21 is 24 Ohms. This characteristic impedance value was determined using the generally known formulations reported in Hong and Lancaster (2001). It is essential to note that an increase in the length, "*a*", would lead to a corresponding increase in the characteristic impedance, Z_1, and vice versa.

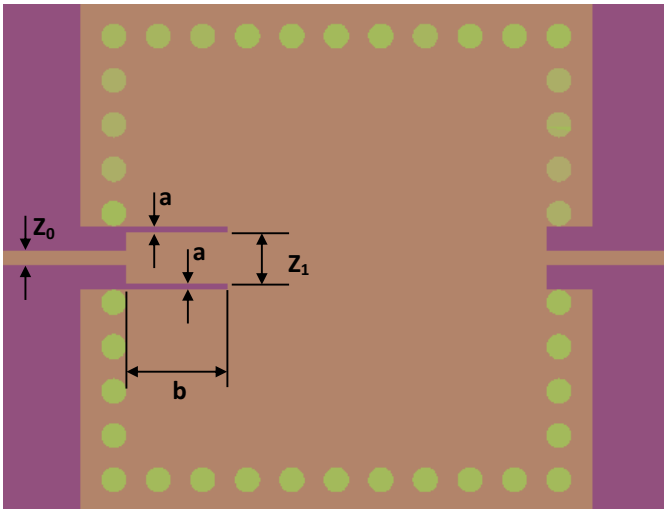

Figure 3.27: Microstrip-CPW-SIW input/output coupling structure for extracting the external Q-factor (Nwajana et al., 2017).

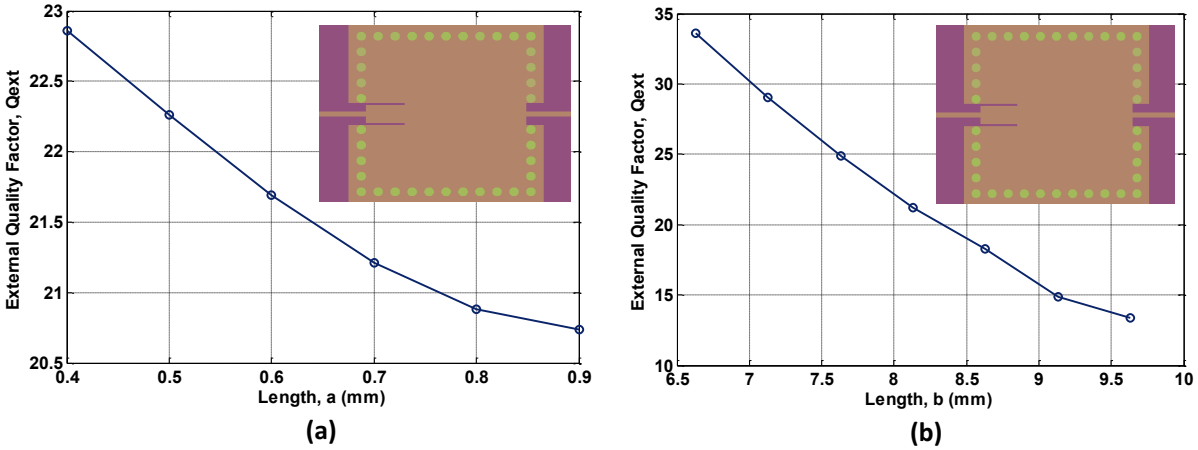

Figure 3.28: Diagram for extracting external Q-factor, Q_{ext}. (a) Variation of Q_{ext}, with length, a, at b = 8.13 mm. (b) Variation of Q_{ext}, with length, b, at a = 0.7 mm (Nwajana et al., 2017).

The coupling structure of the 3-pole (i.e. third order) bandpass filter is shown in Figure 3.29. Each circle in coupling structure represents a resonator (or a cavity). The line linking each pair of resonators represents the coupling between them, while the line linking the first or the last resonator to the input or output port represents the external quality factor Q_{ext}. The matrix of k for the bandpass filter is given in Eqn. (3.22).

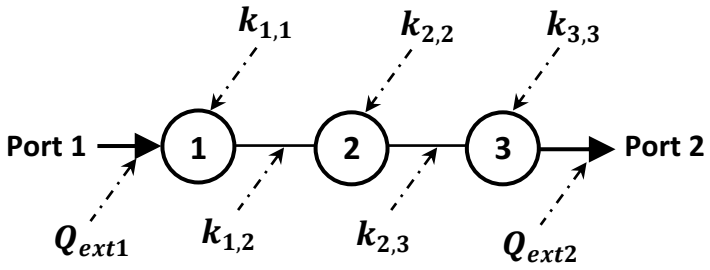

Figure 3.29: 3-pole (third order) bandpass filter coupling structure (Q_{ext1} = Q_{ext2} = 21.21).

$$k = \begin{bmatrix} k_{1,1} & 0.041 & k_{1,3} \\ 0.041 & k_{2,2} & 0.041 \\ k_{3,1} & 0.041 & k_{3,3} \end{bmatrix} \quad (4.22)$$

The layout of the SIW bandpass filter was simulated using the FEM simulator of the Keysight EMPro 3D simulator. The SIW layout of the filter is shown in Figure 3.30, with all the physical dimensions and numerical parameters for the filter given in Table 3.3. The full-wave simulation performances of the proposed filter

are shown in Figure 3.31. It is clear from the simulation performances that the centre frequency of the filter is just about 1684 MHz as designed. The results show medium roll-off which is expected of a Chebyshev filter. A simulated minimum insertion loss, S_{21} of 1.3 dB was achieved across the passband. The simulated return loss, S_{11} is better than 18.5 dB across the passband. The filter passband is based on the fractional bandwidth specification and can be controlled by the input/output coupling and the couplings between each pair of the SIW cavities (Nwajana et al., 2017).

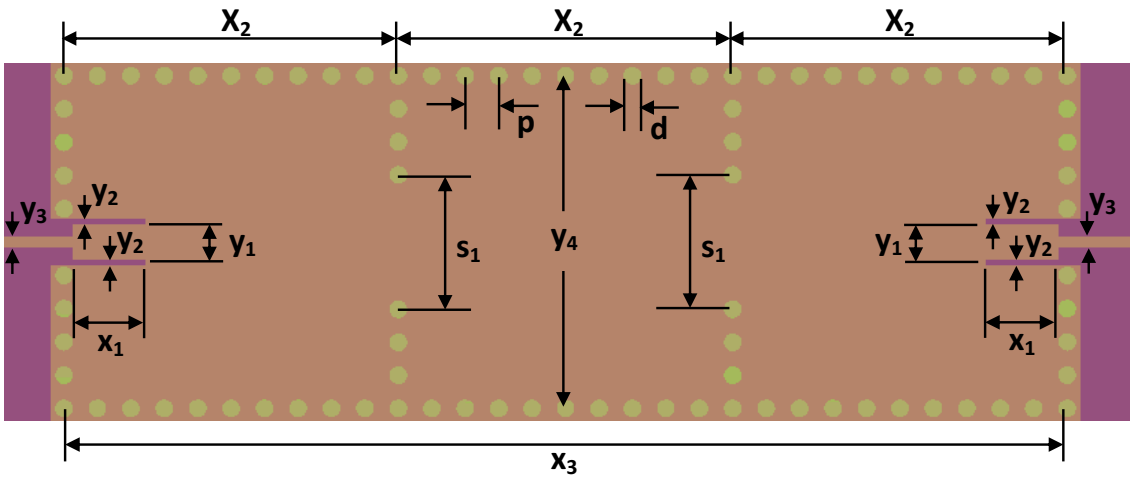

Figure 3.30: Layout of the 3-pole (third order) substrate integrated waveguide bandpass filter on a 1.27 mm thick substrate with a relative permittivity of 10.8 (Nwajana et al., 2017).

Table 3.3: Physical dimensions and numerical parameters of the substrate integrated waveguide bandpass filter (Nwajana et al., 2017).

Dimension	Value (mm)	Dimension	Value (mm)
x_1	8.125	y_1	3.9
x_2	37.25	y_2	0.7
x_3	111.75	y_3	1.1

d	2.0	y_4	37.25
p	3.725	s_1	13.05

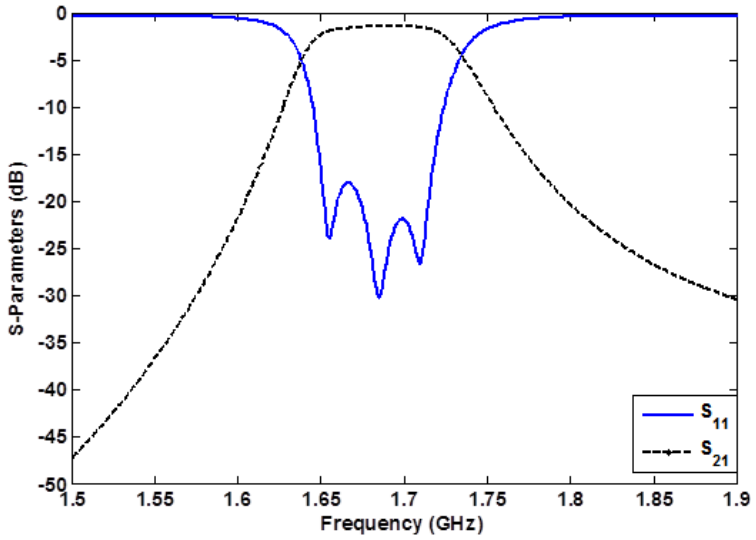

Figure 3.31: Full-wave simulation performances of the 3-pole (third order) substrate integrated waveguide bandpass filter.

3.6.3 Fabrication and Measurement

The filter fabrication was based on the printed circuit board (PCB) micro-milling process using the "Leiterplatten-Kopierfräsen" (LKPF) Protomat C60. A photograph of the fabricated SIW bandpass filter is shown in Figure 3.32. To facilitate filter measurement, two SMA (Sub-Miniature version A) connectors were fitted onto the input and output ports as shown in Figure 3.32. The fabricated filter was measured using the Agilent Vector Network Analyzer and results presented in Figure 3.33. The measured results show that a minimum insertion loss, S_{21} of 1.3 dB was achieved across the passband. The minimum measured return

losses, S_{11} achieved across the passband is better than 20 dB as indicated in Figure 3.33.

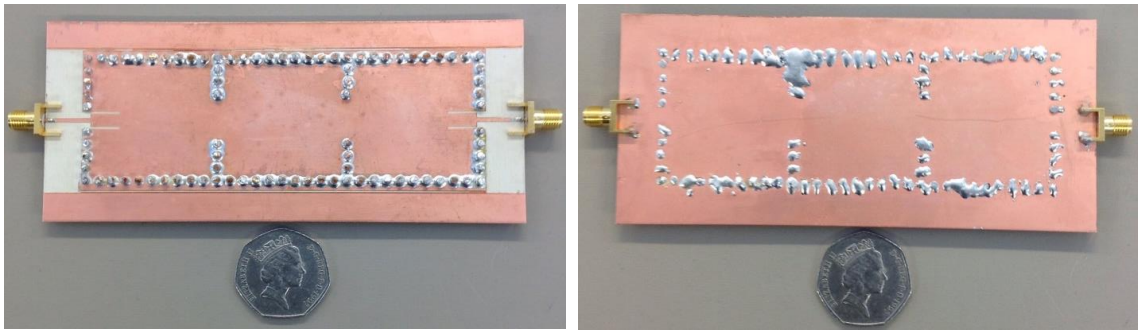

(a) (b)

Figure 3.32: Photograph of the fabricated 3-pole substrate integrated waveguide bandpass filter. (a) Top view. (b) Bottom view. (Nwajana et al., 2017).

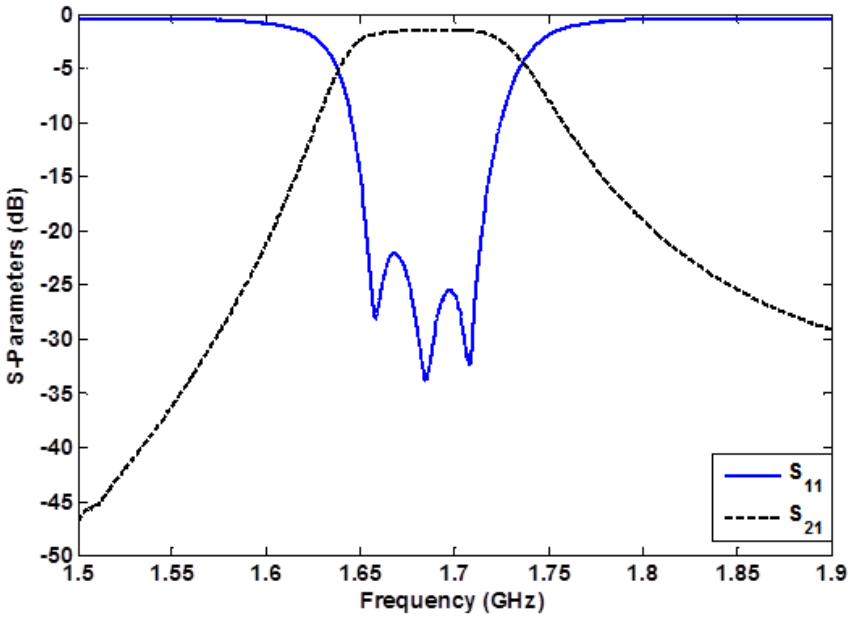

Figure 3.33: Measurement responses of the 3-pole (third order) substrate integrated waveguide bandpass filter.

The measurement and the full-wave simulation responses are mutually presented in Figure 3.34 to facilitate easy comparison. It is obvious from Figure 3.34 that the measurement and the full-wave simulation filter performances are in very good agreement.

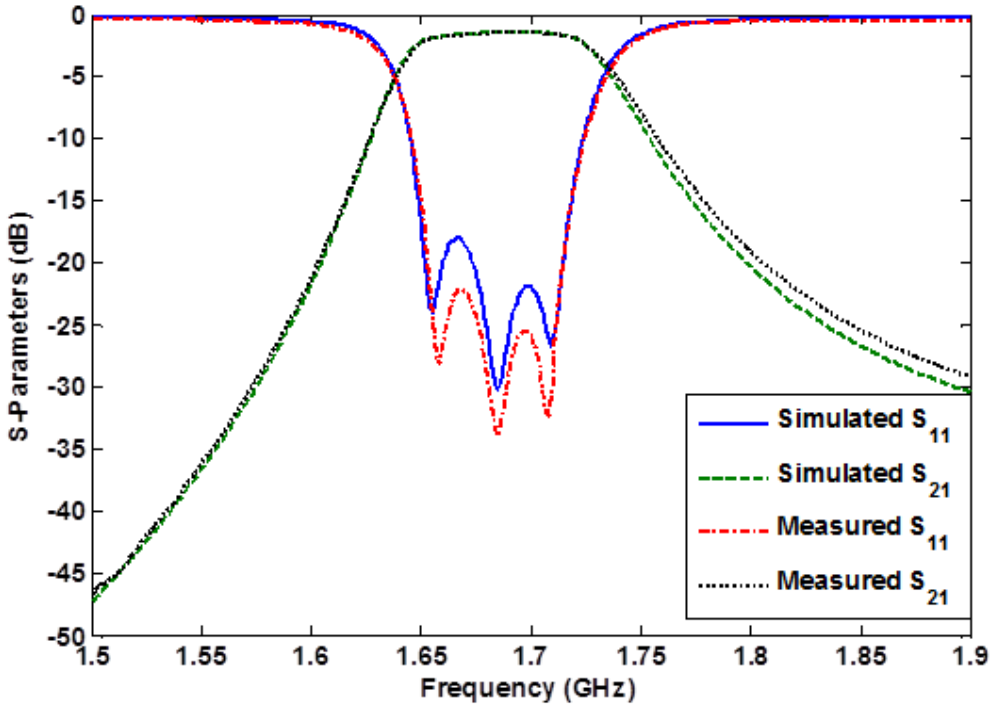

Figure 3.34: Comparison of the measured and full-wave simulated 3-pole (third order) bandpass filter responses.

The electrical size of the SIW bandpass filter reported here is $0.21\lambda_g$ x $0.63\lambda_g$, which is more compact than the conventional waveguide filters reported in literature (Mohottige et al., 2016). The filter is however, less compact when compared to microstrip filters (Nwajana etal., 2017). In general, SIW filters are normally smaller in size when compared to waveguide filters, but are relatively larger in size when compared to microstrip filters. The roll-off factor and the band rejection of the simulated and measured filter results are very good. The filter has

a medium roll-off as expected considedring the design was based on the Chebyshev filter function.

3.6.4 Discussion

A SIW bandpass filter with a new type of Microstrip-CPW- SIW input/output coupling has been designed, simulated, manufactured measured and presented. The Microstrip-CPW-SIW transition employed as the input/output coupling in the design allows for two degrees of freedom in controlling the external Q-factor (Nwajana et al., 2017). Stepping the impedance of the 50 Ohms feed-line to a lower impedance at the SIW end of the transition, makes it easier to realise the required filter external quality factor, Q_{ext}. Varying the impedance at the SIW end of the transition, changes the Q_{ext}.

Both the full-wave EM simulation and the experimental results show that a minimum insertion loss, S_{21} of 1.3 dB was achieved across the passband. The full-wave EM simulation minimum return loss, S_{11} across the passband is better that 18.5 dB, while the measured minimum return loss, S_{11} achieved across the passband is better than 20 dB. The simulation and the measurement centre frequency of the filter are both at 1684 MHz as designed. The unloaded quality factor, Q, based on Eqn. (2.7), was calculated to be 272.9 (with Q_L = 177.5). The results presented show that there is a very good agreement between the full-wave EM simulation and the measurement filter performances. The good comparison between the simulated and measured results can be attributed to the minimum milling / etching requirements of this particular filter design technique (Nwajana et al., 2017).

18-sided polygons were used in place of the conventional circular metallic posts during the full-wave EM simulation. This is a way of reducing the simulation time to about 300%, but this will depend on the number of sides chosen for the polygon. The fewer the number of sides chosen for the polygon, the lesser the time it will take for the simulation complete and vice versa. Care must be taken when choosing the number of sides to use on the polygon. This is because using fewer sided polygons will result in a poor comparison between simulated and measured results, as the simulated result will appear to shift towards the left. The fewer the sides of the polygon used in the EM simulation, the higher the frequency shift observed as can be seen from Figure 3.35. It is also clear from Figure 3.35 that the filter return loss also degrades with fewer sided polygon as metallic posts. Figure 3.36 shows a graph of centre frequency against the number of sides on the polygon used for the metallic posts during the full-wave EM simulation of the SIW bandpass filter. Based Figure 3.36, it is recommended that the polygon to be used in place of the circular metallic posts should have 10 or more sides for better comparison with the conventional circular vias reported in literature, while also improving on the simulation time.

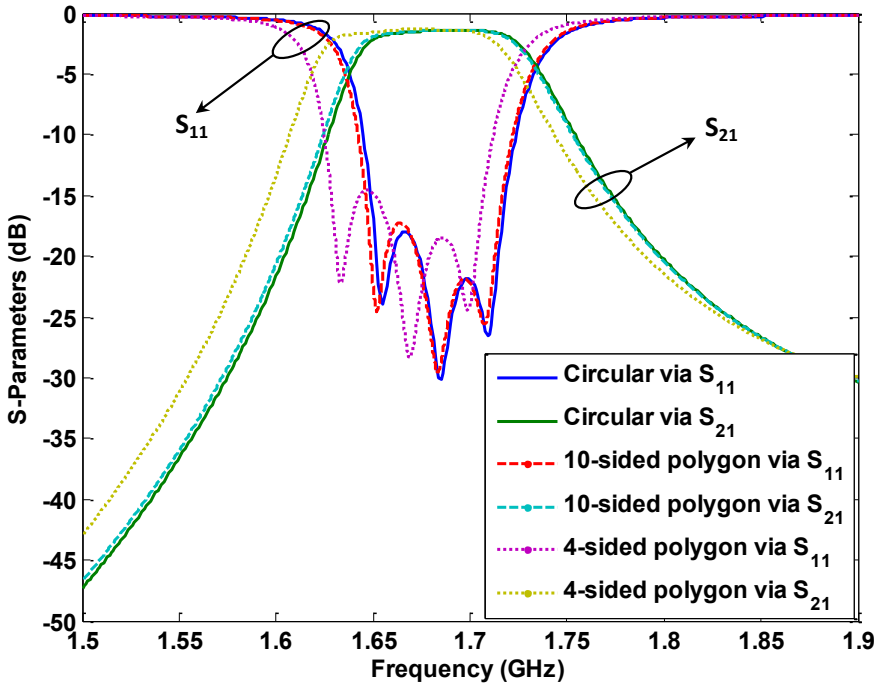

Figure 3.35: 3-pole substrate integrated waveguide filter simulated with circular, 10-sided polygon, and 4-sided polygon as metallic posts.

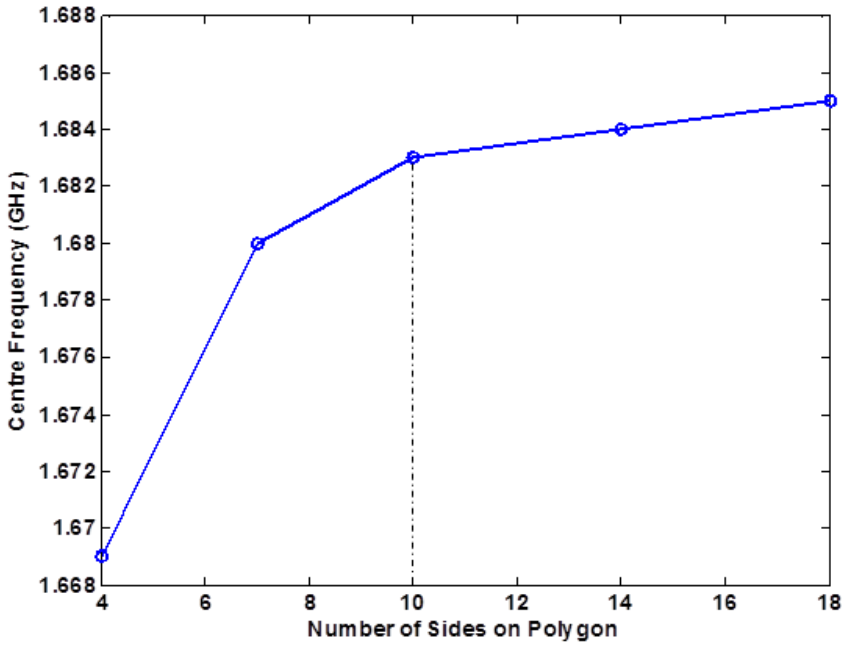

Figure 3.36: Graph of centre frequency against number of sides on the polygon used as metallic posts during the 3-pole SIW filter EM simulation.

Chapter 4: Diplexer Circuit Analysis and Design

4.1 Introduction

Some of the different techniques employed in the design of diplexer circuit have been covered in chapter 1. In this chapter, a novel method of designing a microwave diplexer circuit is presented. This technique involves merging a section of a dual-band bandpass filter (DBF) with a section of two separately designed bandpass filters (BPFs).

Conventional diplexer circuit design techniques usually involve the use of a non-resonant external junction to distribute energy to and from the transmit and the receive bands. The non-resonant external junction is sometimes a T-junction (Liu et al., 2013), or a Y-junction (Bastioli et al., 2009), or a circulator (Kodera and Caloz, 2010), or a manifold (Guglielmi, 1993), or even a common resonator (Yang and Rebeiz, 2013). The diplexer circuit reported in this chapter does not involve any non-resonant external junction, as each resonator contributes a pole to the diplexer circuit response. Figure 4.1 shows three diplexer circuit arrangements. Looking and Figure 4.1 (a) and (b), it is obvious that the non-resonant T-junction and the common out of band resonator would certainly add to the size of the diplexer. However, looking at Figure 4.1 (c), it is clear that the absence of neither the non-resonant external junction nor the common out of band resonator means reduced size and even simpler circuit. The diplexer circuit arrangement of Figure 4.1 (c) is less complex, as the continues adjustment requirements of the external junction is absent.

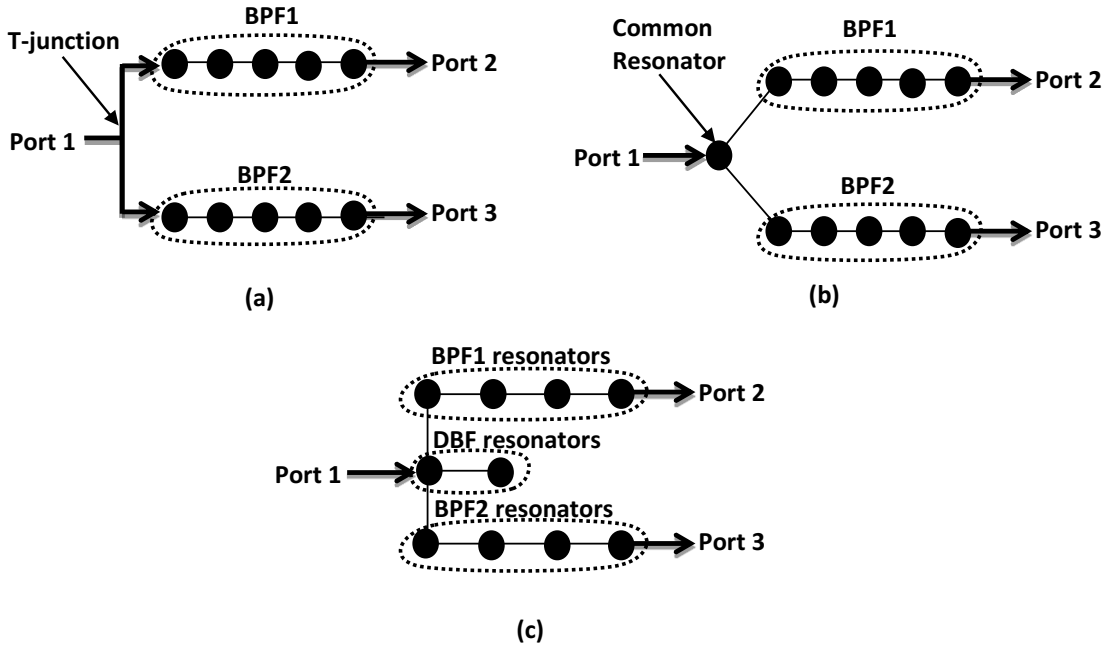

Figure 4.1: Diplexer circuit arrangements. (a) With a non-resonant external T-junction. (b) With a non-resonant external common resonator. (c) Without any non-resonant external junction (Nwajana and Yeo, 2016).

4.2 Circuit Model Design

The proposed diplexer circuit model was designed using the following specifications: centre frequency, f_o, 1849 MHz; centre frequency of the transmit band, $f_{o,Tx}$, 1800 MHz; centre frequency of the receive band, $f_{o,Rx}$, 1900 MHz; fractional bandwidth of the transmit band, FBW_{Tx}, 4%; fractional bandwidth of the receive band, FBW_{Rx}, 4%; passband return loss, RL, 20 dB. The diplexer circuit model design is started off by designing two individual 5-pole bandpass filters (i.e. BPF1 and BPF2) using the conventional method reported in Hong and Lancaster (2001) and covered in the section 3.6. BPF1 has a centre frequency that corresponds to that of the proposed diplexer transmit (Tx) band while BPF2 has a centre frequency that corresponds to that of the proposed diplexer received

(*Rx*) band. Both the *Tx* and *Rx* channel filters were designed with a 20 dB return loss and 50 Ohms termination. Each channel filter has a fractional bandwidth (*FBW*) of 4% to match the proposed diplexer *Tx* and *Rx* bands. The design parameters for both BPF1 and BPF2 are presented in Table 4.1. As explained in Hong and Lancaster (2001), *L*, *C* and *J* are the inductance, the capacitance and the *J*-inverter values, respectively. *F* is the filter centre frequency. The theoretical coupling coefficient $k_{m,m+1}$, and the theoretical external quality factor Q_{ext}, values for both the *Tx* (i.e. BPF1) and the *Rx* (i.e. BPF2) channel filters were calculated using Eqns. (4.1) and (4.2), respectively, where m = 1, 2, 3, 4 (Yeo and Nwajana, 2013). The calculated $k_{m,m+1}$ and Q_{ext} values for both channel filters are presented in Table 4.2 while the coupling arrangements are shown in Figure 4.2; where T1, T2, T3, T4, T5 and R1, R2, R3, R4, R5 are the BPF1 and BPF2 resonators, respectively.

Table 4.1: 5th order (5-pole) Chebyshev bandpass filter design parameters.

BPF n	***F* (MHz)**	***L* (nH)**	***C* (pF)**	$J_{0,1}$	$J_{1,2}$	$J_{2,3}$
1	1800	0.183	43.23	0.02	0.017	0.012
2	1900	0.171	40.32	0.02	0.017	0.012

$$k_{m,m+1} = J_{m,m+1}\sqrt{\frac{L}{C}} \tag{4.1}$$

$$Q_{ext} = \frac{2\pi F C}{J_{0,1}} \tag{4.2}$$

Table 4.2: 5th order (5-pole) Chebyshev bandpass filter coupling coefficient and external quality factor values.

BPF n	$k_{1,2}$	$k_{2,3}$	$k_{3,4}$	$k_{4,5}$	Q_{ext}
1	0.035	0.025	0.025	0.035	24.285
2	0.035	0.025	0.025	0.035	24.285

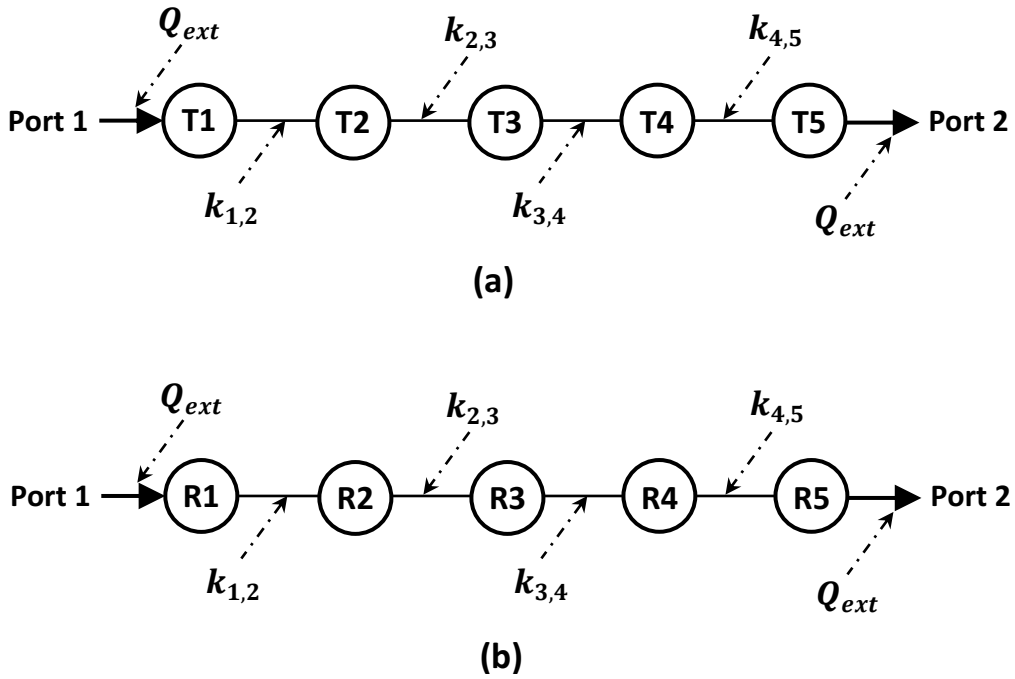

Figure 4.2: Coupling arrangements for the 5th order (5-pole) Chebyshev bandpass filters with the theoretical / calculated coupling coefficients and external quality factor parameters indicated. (a) *Tx* channel. (b) *Rx* channel.

A 10-pole dual-band bandpass filter (DBF) was also designed using the technique reported in Yeo and Nwajana (2013). The DBF was designed to operate at the centre frequency of the proposed diplexer, with a combined *FBW* of 8% (with equal split of 4% each, for the upper and the lower passbands). The upper and lower passbands of the DBF, respectively, agrees with BPF1 and BPF2 in terms of number of poles, *FBW* and centre frequency. The DBF is also designed to

have a 20 dB return loss and 50 Ohms termination. The design parameters for the DBF are presented in Table 4.3 (Nwajana and Yeo, 2016). The k and the Q_{ext} values for the DBF were also calculated using Eqns. (4.1) and (4.2), respectively. The coupling coefficient $k'_{1,1}$ between any pair of DBF resonators was calculated using Eqn. (4.3), where $f_{o,Tx}$ and $f_{o,Rx}$ are the centre frequencies for the diplexer *Tx* and *Rx* bands, respectively. The calculated k, $k'_{1,1}$ and Q_{ext} values for the DBF are presented in Table 4.4. The $J'_{1,1}$ parameter indicated in Table 4.3 is the *J*-inverter that exists between any pair of DBF resonators. The numerical value for $J'_{1,1}$ was determined using Eqn. (4.4) (Yeo and Nwajana, 2013). Figure 4.3 shows the coupling arrangement for the 10th order (10-pole) Chebyshev dual-band bandpass filter; where D1 & D1', D2 & D2', D3 & D3', D4 & D4' and D5 & D5' are the five pairs of the DBF resonators.

Table 4.3: 10th order (10-pole) Chebyshev dual-band bandpass filter design parameters.

Filter	***F*** **(MHz)**	***L*** **(nH)**	***C*** **(pF)**	$J_{0,1}$	$J_{1,2}$	$J_{2,3}$	$J'_{1,1}$
DBF	1849	0.354	20.90	0.02	0.017	0.012	0.013

Table 4.4: 10th order (10-pole) Chebyshev dual-band bandpass filter coupling coefficient and external quality factor values.

Filter	$k_{1,2}$	$k_{2,3}$	$k_{3,4}$	$k_{4,5}$	Q_{ext}	$k'_{1,1}$
DBF	0.069	0.051	0.051	0.069	12.143	0.054

$$k'_{1,1} = \left(\frac{f_{0,Rx}^2 - f_{0,Tx}^2}{f_{0,Rx}^2 + f_{0,Tx}^2}\right) \quad (4.3)$$

$$J'_{1,1} = k'_{1,1}\sqrt{\frac{C}{L}} \tag{4.4}$$

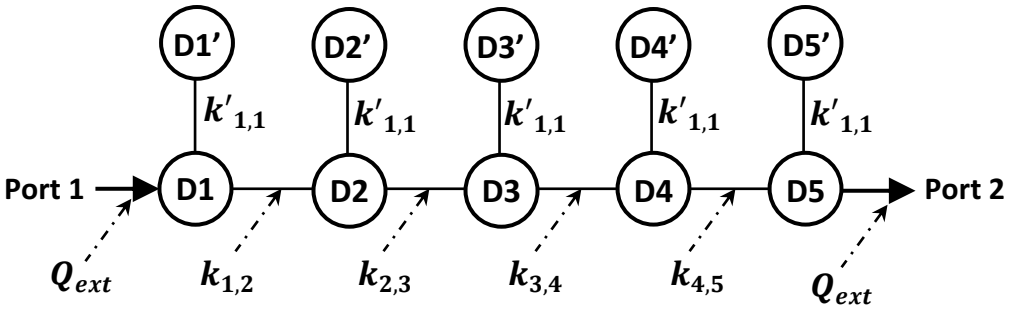

Figure 4.3: Coupling arrangement for the 10th order (10-pole) Chebyshev dual-band bandpass filter with the theoretical / calculated coupling coefficients and external quality factor parameters indicated.

The design parameters for the proposed 10th order (10-pole) microwave diplexer are the same as those indicated in Figures 4.2 and 4.3. The corresponding values are given in Tables 4.2 and 4.4.

4.3 Circuit Model Coupling Arrangement

The proposed 10-pole microwave diplexer circuit is based on the Type-I coupling arrangement shown in Figure 4.4. Before deciding to implement the chosen coupling arrangement, four different possible coupling arrangements were investigated. These four coupling arrangements are shown in Figures 4.4, 4.5, 4.6, and 4.7, as Type-I, Type-II, Type-III, and Type-IV respectively; where D1 & D1', D2 & D2', D3 & D3', and D4 & D4' are the first four pairs of the DBF resonators indicated in Figure 4.3. T2, T3, T4, T5 and R2, R3, R4, R5 are the last four resonators of BPF1 and BPF2 (i.e. *Tx* and *Rx* channel filters of Figure 4.2),

respectively. The line linking each pair of resonators represents the k between them, while the line linking any one resonator to an input or an output port represents the Q_{ext} between them. All the k and the Q_{ext} values have been indicated in Figures 4.2 and 4.3 and their values specified in Tables 4.2 and 4.4.

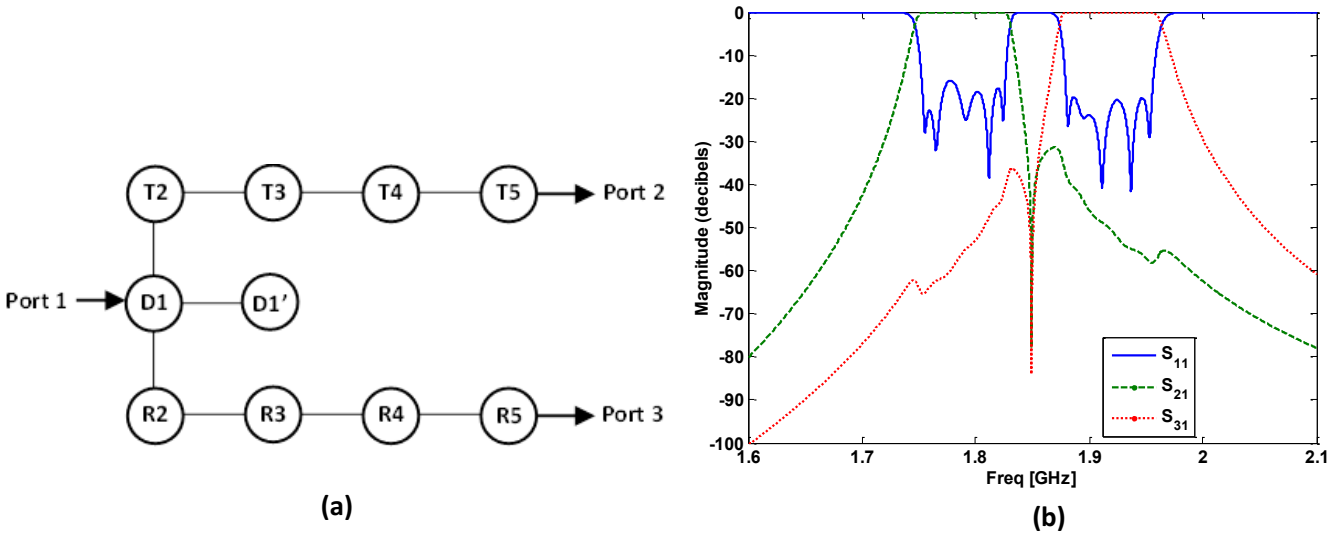

Figure 4.4: Type-I. (a) Coupling arrangement. (b) Simulation responses.

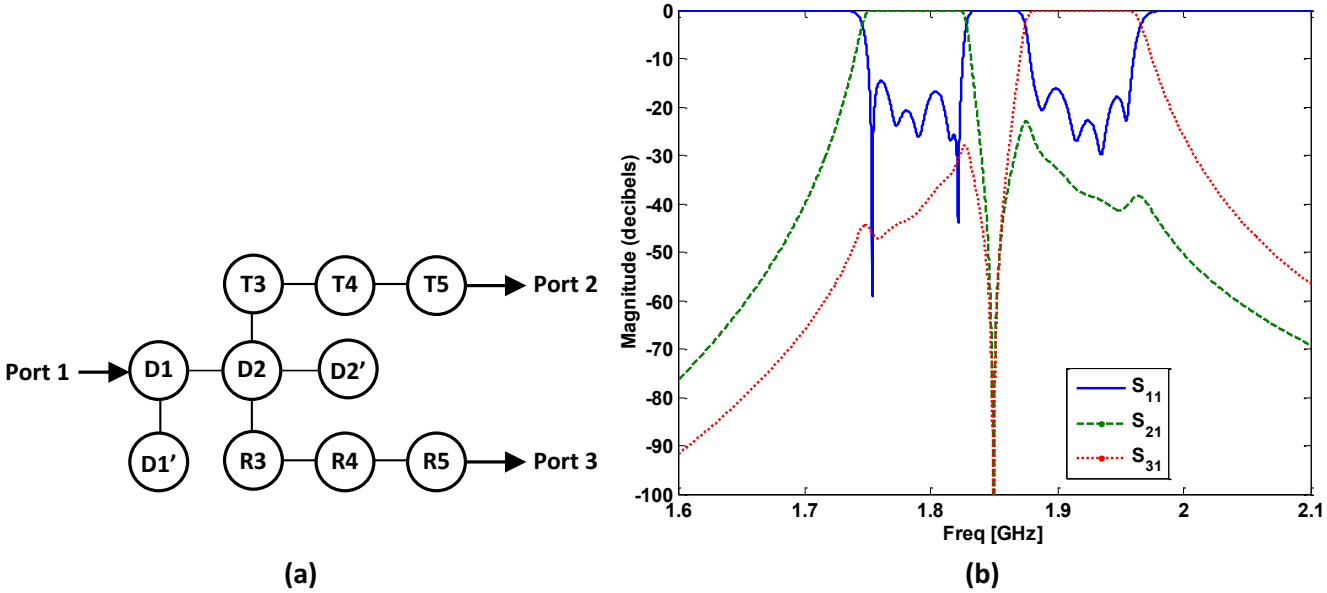

Figure 4.5: Type-II. (a) Coupling arrangement. (b) Simulation responses.

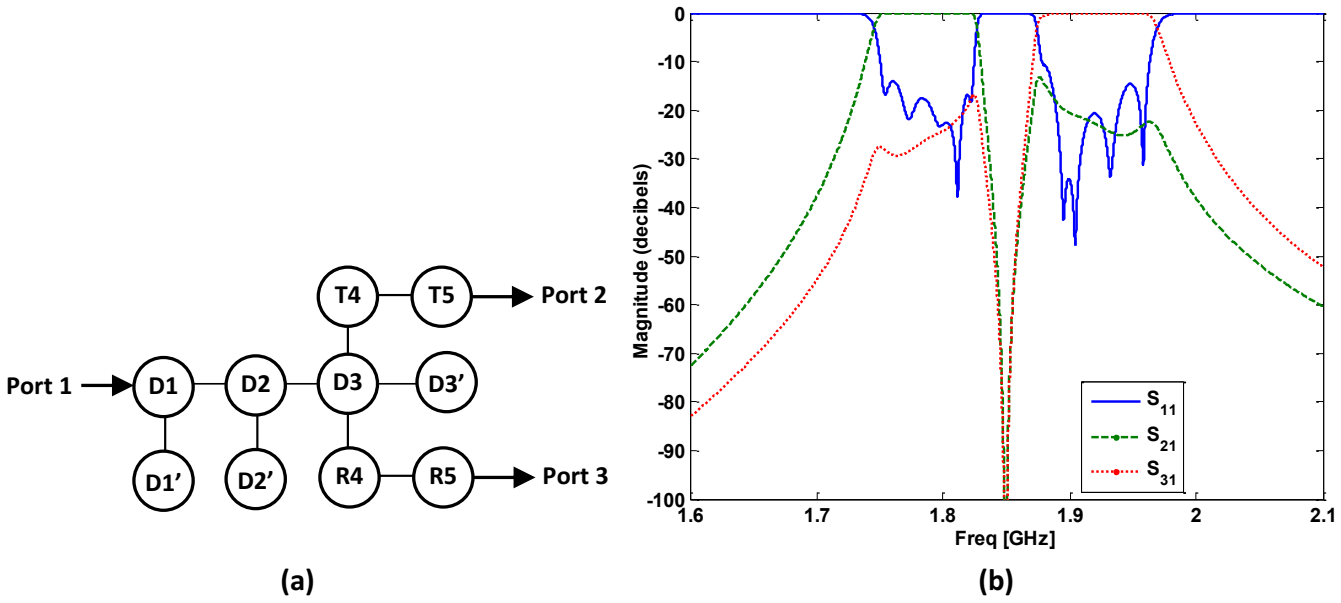

Figure 4.6: Type-III. (a) Coupling arrangement. (b) Simulation responses.

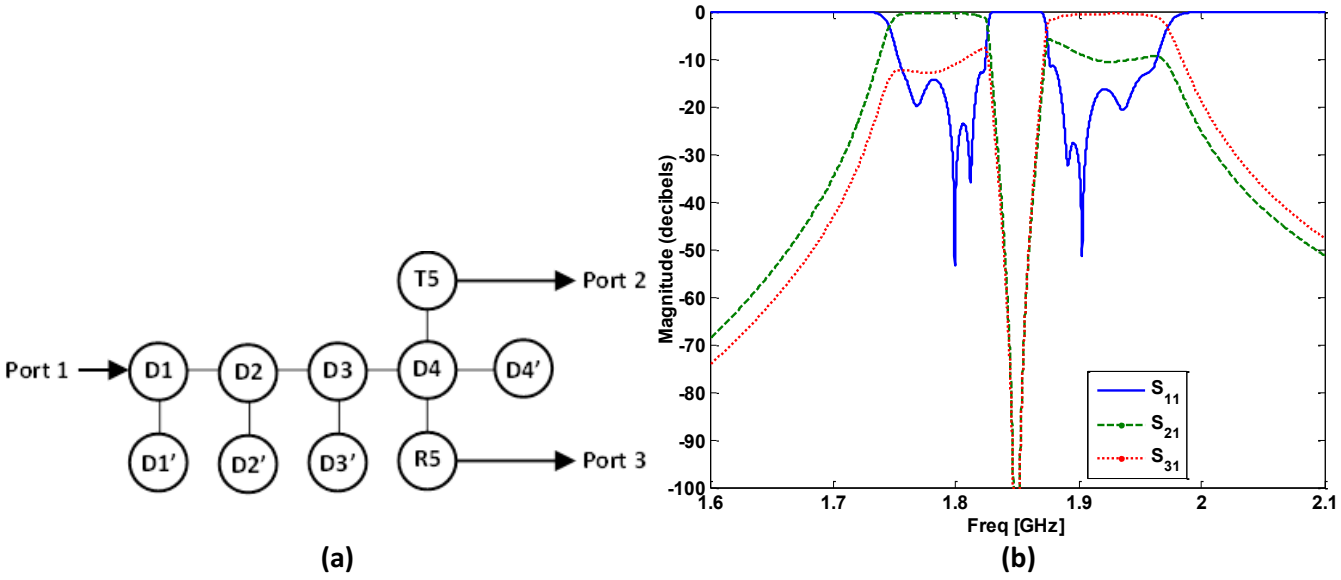

Figure 4.7: Type-IV. (a) Coupling arrangement. (b) Simulation responses.

Considering Figures 4.4, 4.5, 4.6, and 4.7; it is clear that the band matching degrades when more pairs of the DBF resonators are used to replace the *Tx* and the *Rx* channel filters (i.e. BPF1 and BPF2) resonators. The band isolation also gets worse with increasing number of DBF resonators. Hence, the Type-I

coupling arrangement shown in Figure 4.4 is chosen for the 10-pole diplexer circuit model since it has the minimum number of DBF resonators replacing the channel filter resonators. The DBF resonators present in the proposed diplexer circuit can be viewed as the energy distributor which distributes energy towards the *Tx* and the *Rx* bands of the diplexer. This is because they replace the non-resonant external junctions or the common resonator used in most diplexer designs reported in literature. The actual function of the DBF resonators is to establish the two passbands (i.e. the *Tx* and the *Rx* bands) of the diplexer. Apart from establishing the diplexer passbands, the DBF resonators also contribute to the number of poles contained in the diplexer. This is an advantage as it means that the proposed diplexer should be relatively more compact when compared to conventional diplexers were non-resonant external junctions are used for energy distribution.

4.4 Circuit Model Simulation and Results

This section presents more details on Figure 4.4 (i.e. the Type-I coupling arrangement and simulation responses) which has been chosen for the implementation of the proposed diplexer circuit model.

The proposed diplexer circuit model was assembled by merging sections of Figures 4.2 and 4.3 as shown in Figure 4.8; that is, coupling the first pair of the DBF resonators (i.e. D1 and D1'), onto the last four resonators of the transmit channel filter or BPF1 (i.e. T2, T3, T4, and T5) and the last four resonators of the receive channel filter or BPF2 (i.e. R2, R3, R4, and R5). Note that, the first resonator of each of the 5^{th} order (5-pole) Chebyshev BPFs of Table 4.1 is

replaced with a DBF resonator of Table 4.3 as shown in Figure 4.8. The theoretical / calculated coupling coefficients and external quality factor values of Tables 4.2 and 4.4 are also indicated in Figure 4.8.

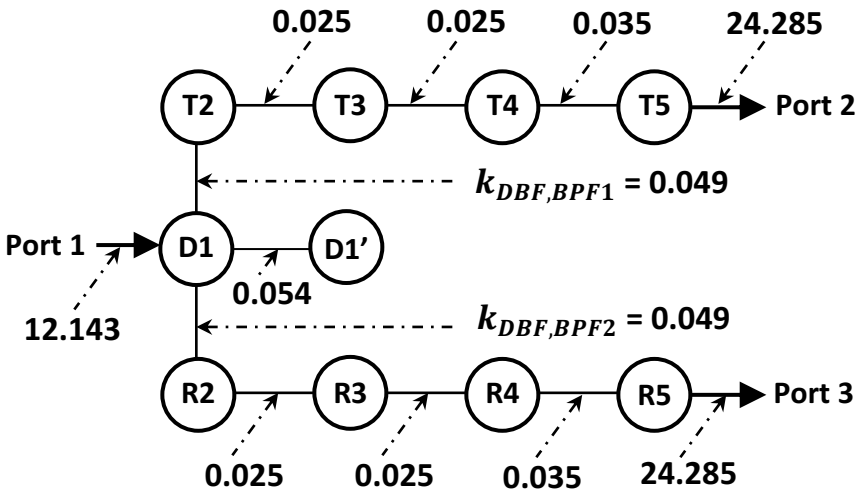

Figure 4.8: Proposed diplexer circuit model with the theoretical / calculated coupling coefficients and external quality factor values indicated.

The theoretical / calculated asynchronous couplings between T2 and D1, and that between R2 and D1 were calculated using Eqns. (4.5) and (4.6), respectively (Yeo and Lancaster, 2001); where L_{BPF1}, L_{BPF2}, C_{BPF1} and C_{BPF2} are the *L* and *C* values indicated in Table 4.1. Similarly, L_{DBF} and C_{DBF} are the *L* and *C* values indicated in Table 4.3.

$$k_{DBF,BPF1} = J_{1,2}\left[\frac{L_{DBF}\,L_{BPF_1}}{C_{DBF}\,C_{BPF_1}}\right]^{0.25} \tag{4.5}$$

$$k_{DBF,BPF2} = J_{1,2}\left[\frac{L_{DBF}\,L_{BPF_2}}{C_{DBF}\,C_{BPF_2}}\right]^{0.25} \tag{4.6}$$

The proposed diplexer circuit model with identical *LC* resonators and admittance inverters (or *J*-inverters) is shown in Figure 4.9. The Agilent Keysight Advanced Design System (ADS) circuit simulator was used for the circuit simulation.

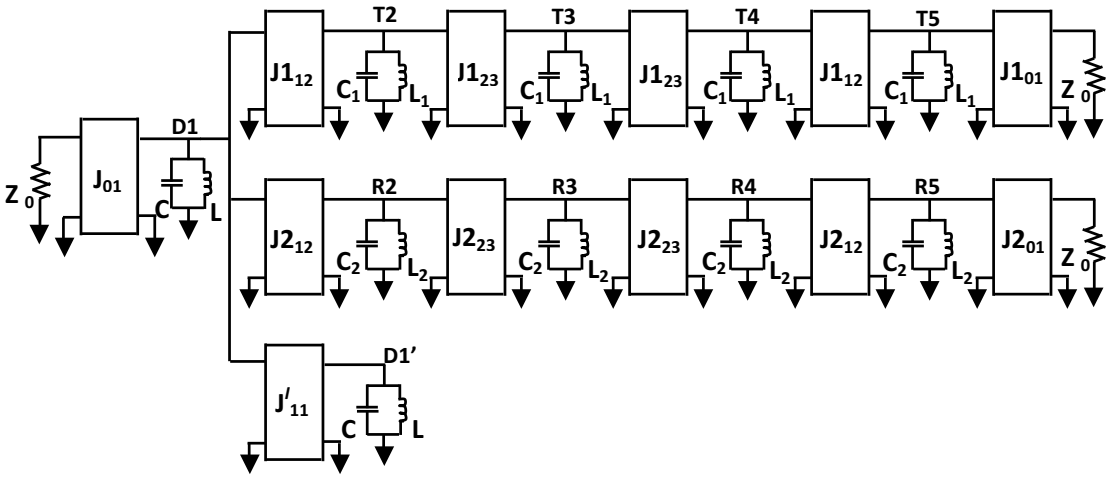

Figure 4.9: Proposed diplexer circuit model with identical *LC* resonators and admittance inverters (Nwajana and Yeo, 2016).

The theoretical coupling coefficients between resonators were modelled using the method described in sub-section 3.5.2 and given in Figure 3.18 (b). This method involves modelling each admittance inverter (or *J*-inverter) in the circuit model with a pi-network of capacitors. The diplexer circuit model (in ADS) with *J*-inverters modelled as pi-network of capacitors is shown in Figure 4.10. The simulation results of the diplexer circuit model are shown in Figure 4.11. From the results, it is clear that the diplexer has a centre frequency of 1849 MHz as designed. A small degradation in the band matching of the intended 20 dB return loss is shown. However, a very good band matching is still maintained. A good pass-bands isolation (i.e. S_{32}) of about 39 dB is achieved between the *Tx* and the *Rx* bands. The very good isolation achieved means that only a minimal amount of signal is expected to deflect towards the incorrect direction. As expected, the

insertion losses on the *Tx* and the *Rx* channels, i.e. S_{21} and S_{31}, respectively are on the 0 dB line. This is due to the fact that the diplexer circuit is in its ideal (i.e. lossless) state. The results presented in Figure 5.9 show very good agreement with the chosen design specifications.

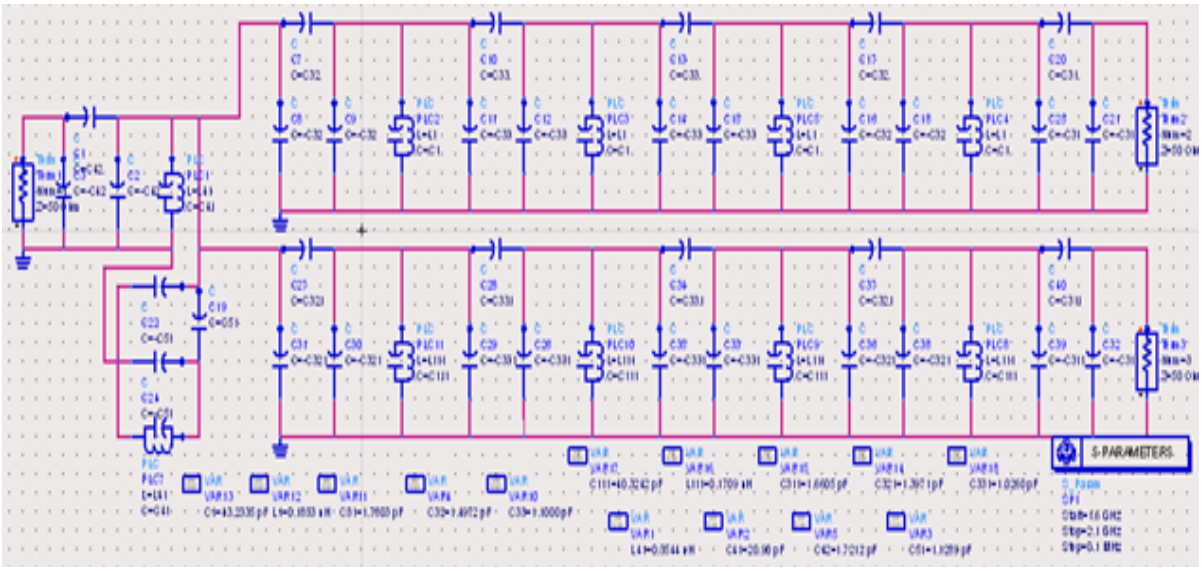

Figure 4.10: Diplexer circuit model with admittance inverters (or *J*-inverters) modelled as pi-network of capacitors.

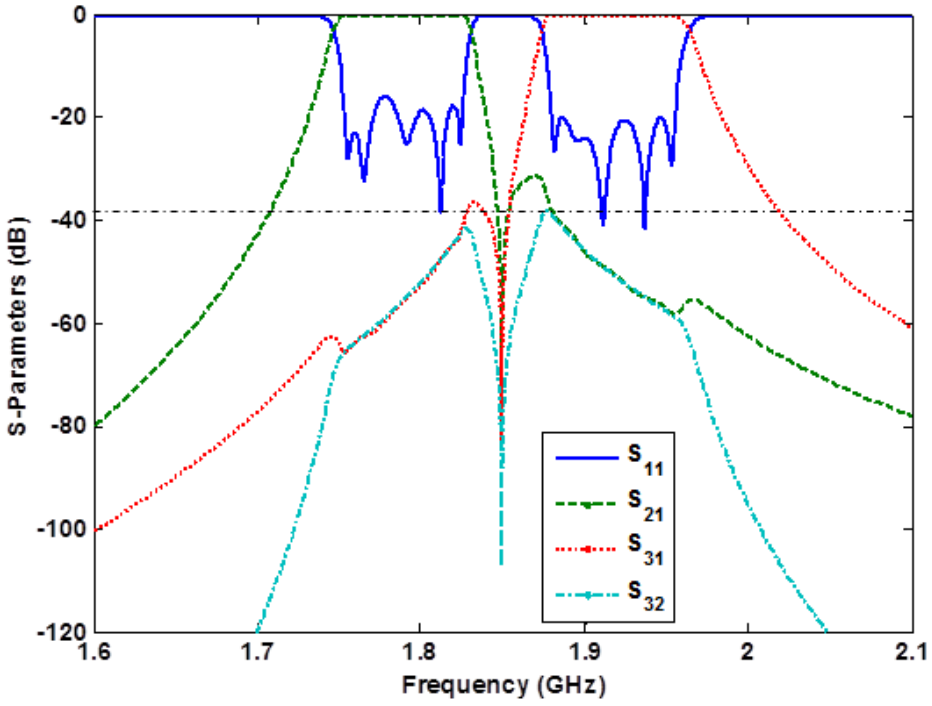

Figure 4.11: ADS simulation results of the proposed diplexer circuit model (Nwajana and Yeo, 2016).

4.5 Conclusion

A microwave diplexer circuit model has been designed, simulated, and results presented. The design technique involves coupling a section of a dual-band bandpass filter, with a section of two different bandpass filters. The design is purely based on direct coupling (i.e. no cross-coupling was involved). The design does not depend on any non-resonant external junction circuit components for energy distribution. This implies that the diplexer circuit, when fabricated, would be of relatively reduced size when compared to conventional diplexer circuits. The design results show good agreement with the original design specifications.

Chapter 5: Microstrip Diplexer Design

5.1 Introduction

This chapter presents a microstrip implementation of the diplexer circuit model established in Chapter 4. The microstrip square open-loop resonator (SOLR) method reported in Hong and Lancaster (1996) has been utilised in the implementation of the microwave diplexer.

5.2 Microstrip Square Open-Loop Resonator

The microstrip square open-loop resonator (SOLR) components have compact size, simpler structure, and are flexible to construct when compared to waveguide cavity components (Hong and Lancaster, 1996). The compact size of the microstrip SOLR has led to its popularity in filter design. The microstrip SOLR is achieved by simply folding a half-wavelength resonator into a square-shaped resonator, having an open gap on one of its four sides as shown in Figure 5.1.

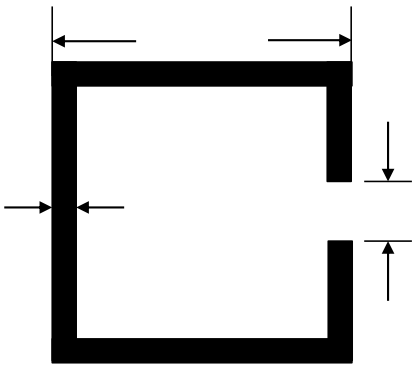

Figure 5.1: Microstrip square open-loop resonator structure.

The length of one side of the resonator is approximately equal to one-eighth of a wavelength (λ/8). When two of the SOLR structures are placed side-by-side, with a separation distance, *s*; proximity coupling due to fringe fields results. The nature and the strength of the existing coupling depend on the nature and the extent of the fringe fields. It has been shown that at resonance of the fundamental mode, each of the microstrip SOLR possess the maximum electric field density at the side with the open gap. Similarly, the side opposite the open gap has the maximum magnetic field density (Hong and Lancaster, 1996). The coupling coefficient between any two microstrip SOLRs depends on the separation distance, *s*. An increase in the value of *s*, leads to a corresponding decrease in the coupling coefficient and vice versa. Figure 5.2 shows the different possible kinds of couplings that can be achieved with the microstrio SOLR.

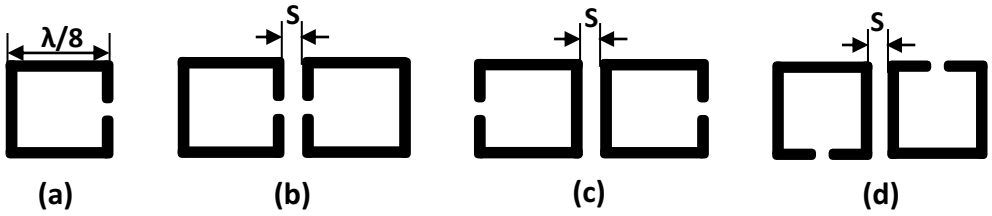

Figure 5.2: Microstrip square open-loop resonator. (a) Uncoupled. (b) Electric coupling. (c) Magnetic coupling. (d) Mix coupling.

The microstrip SOLRs utilised in realising the microwave diplexer presented in this chapter, were designed to have the dimensions shown in Figure 5.3. The transmit band resonator (*Tx*), the receive band resonator (*Rx*), and the energy distributor resonator (*ED*), all correspond to the BPF1, the BPF2, and the DBF component filters, respectively as explained in Chapter 4.

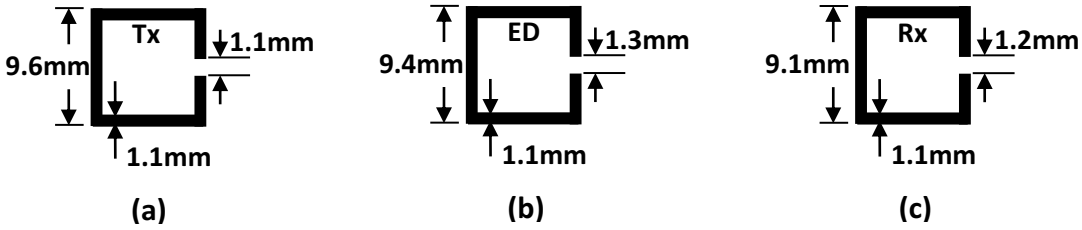

Figure 5.3: Microstrip square open-loop resonator dimensions. (a) Transmit band dimension. (b) Energy distributor dimension. (c) Receive band dimension. (Nwajana and Yeo, 2016).

All dimensions were achieved based on the design specifications (that is, the centre frequencies of the respective component filters). The full-wave simulation layout and responses, in ADS Momentum, for achieving the *Tx*, *Rx* and *ED* resonators dimensions is shown in Figure 5.4, where f_{Tx}, f_{Rx} and f_{ED} are the fundamental resonant frequencies for the *Tx*, *Rx* and *ED* resonators, respectively.

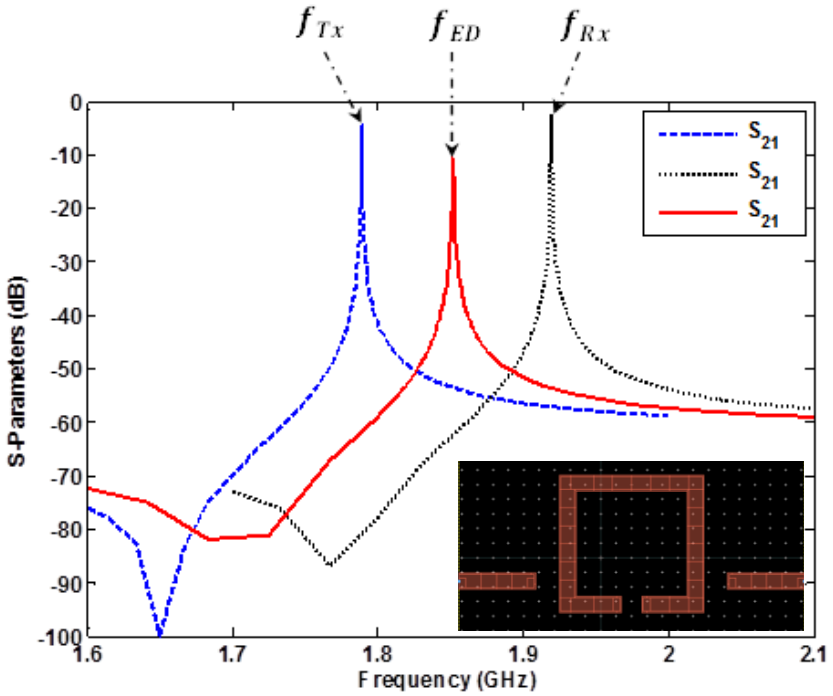

Figure 5.4: Full-wave simulation layout and responses for the *Tx*, the *Rx*, and the *ED* resonators at their respective fundamental resonant frequencies.

5.3 Coupling Coefficient Extraction

Using the Keysight ADS Momentum simulator, the coupling coefficients required for achieving the proposed microwave diplexer were extracted and presented in Figure 5.5. It is clear from Figure 5.5 that an increase in the separation distance *s*, leads to a decrease in the coupling coefficient and vice versa.

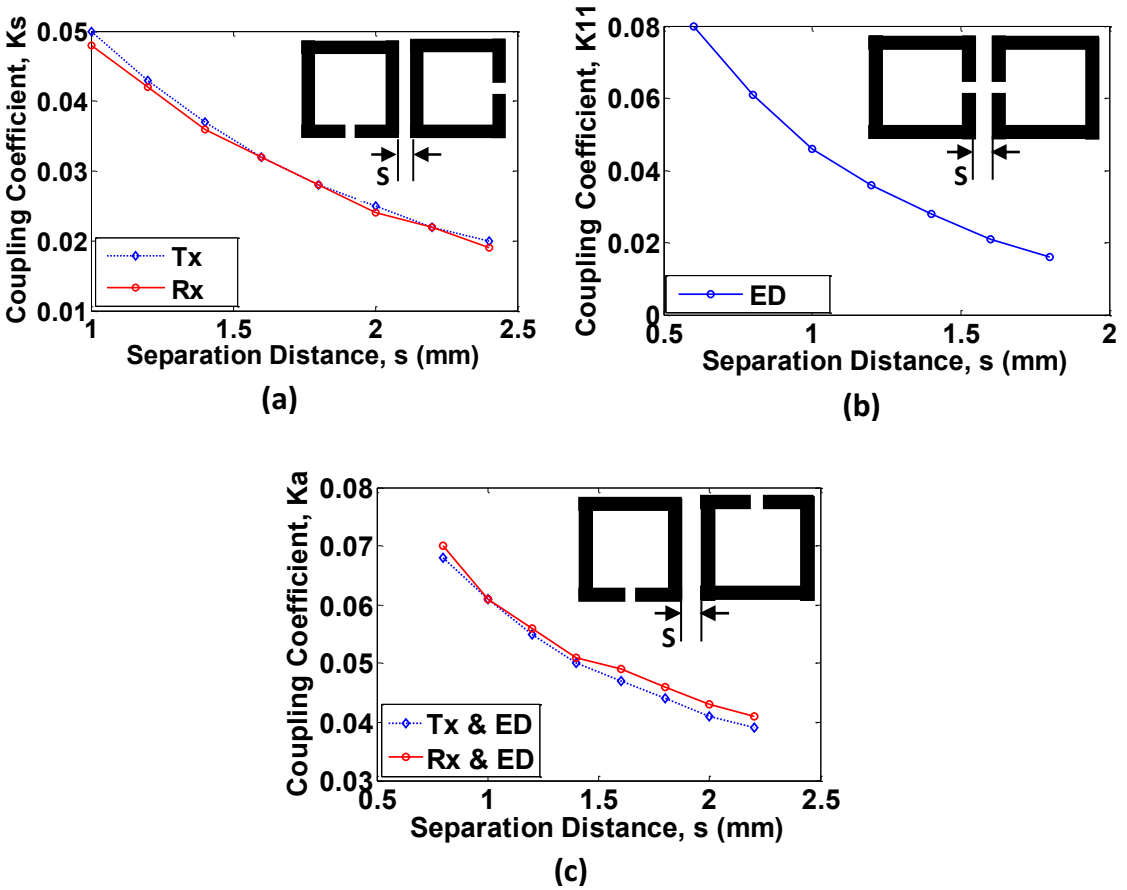

Figure 5.5: Coupling coefficient extraction technique using the microstrip resonators. (a) *Tx* & *Tx* and *Rx* & *Rx* couplings. (b) *ED* & *ED* coupling. (c) *Tx* & *ED* and *Rx* & *ED* couplings. (Nwajana and Yeo, 2016).

The coupling between a pair of the *Tx* or the *Rx* resonators, shown in Figure 5.5 (a), where synchronously tuned since they are of equal dimensions. Similarly, the coupling between the *ED* resonators, shown in Figure 5.5 (b), was also tuned synchronously. In contrast, the coupling between the *Tx* and the *ED* resonators or the *Rx* and the *ED* resonators, shown in Figure 5.5 (c), were asynchronously tuned because of the dissimilarities in the resonator dimensions, that is, the resonators were resonating at different fundamental frequencies. The coupling coefficients shown in Figures 5.5 (a), (b), and (c); were determined by simulating a coupling pair of resonators and using Eqn. (5.1) which is derived from Hong and Lancaster (2001). The variables f_1 and f_2 in Eqn. (5.1) are the eigen-modes from simulating a pair of resonators, f_{r1} and f_{r2} are the fundamental resonant frequencies of resonators 1 and 2, respectively, and k_s and k_a are the synchronous and asynchronous couplings, respectively.

$$k_s = \frac{f_2^2 - f_1^2}{f_2^2 + f_1^2} \tag{5.1 a}$$

$$k_a = \frac{1}{2}\left(\frac{f_{r2}}{f_{r1}} + \frac{f_{r1}}{f_{r2}}\right)\sqrt{\left(\frac{f_2^2 - f_1^2}{f_2^2 + f_1^2}\right)^2 - \left(\frac{f_{r2}^2 - f_{r1}^2}{f_{r2}^2 + f_{r1}^2}\right)^2} \tag{5.1 b}$$

Using Eqn. (5.1 a) and the technique shown in Figure 5.5 (a); S_1, S_2, S_3, S_7, S_8 and S_9 were achieved and tabulated. Similarly, S_5 was achieved and tabulated using Eqn. (5.1 a) and the technique shown in Figure 5.5 (b). S_4 and S_6 were also achieved and tabulated using Eqn. (5.1 b) and Figure 5.5 (c). Table 5.1 presents the simulated *S*-values for the proposed microwave diplexer couplings.

Table 5.1: Simulated separation distance values for the proposed diplexer couplings.

Separation, S_n	S_1	S_2	S_3	S_4	S_5	S_6	S_7	S_8	S_9
Value (mm)	1.5	2.0	2.0	1.6	0.9	1.65	1.95	2.0	1.45

5.4 External Quality Factor Extraction

Using the Keysight ADS Momentum simulator, the external quality factors, Q_{ext} required for achieving the proposed microwave diplexer were extracted and presented in Figure 5.6. From Chapter 4, the theoretical or calculated Q_{ext} values for the *Tx*, the *Rx*, and the *ED* resonators were determined as 24.285, 24.285, and 12.143, respectively. Now, to achieve the simulated Q_{ext} values that correspond to the calculated values, the technique shown in Figure 5.6 and Eqn. (5.2) were employed. The parameter, f_0 in Eqn. (5.2) is the fundamental resonant frequency of the resonator being simulated, and $\delta f@-3dB$ is the 3 dB bandwidth of the simulated curve (Dainkeh et al., 2016). The simulated Q_{ext} values were achieved by adjusting the tapping distance, *t* as shown in Figure 5.6. The *t* values that met the requirements of the proposed microwave diplexer are 1.45 mm, 1.35 mm, and 0.0 mm for the *Tx*, the *Rx*, and the *ED* resonators, respectively.

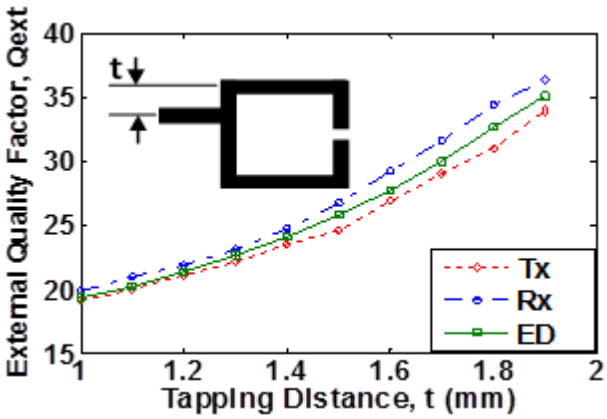

Figure 5.6: External quality factor extraction technique. (Nwajana and Yeo, 2016).

$$Q_{ext} = \frac{f_0}{\delta f @ -3dB} \tag{5.2}$$

5.5 Layout and Simulation

The proposed 10-pole diplexer layout indicating all physical dimensions is shown in Figure 5.7. The microwave diplexer layout arrangement, for a full-wave simulation on the Keysight ADS momentum simulator, is also shown in Figure 5.8. Both Figures 5.7 and 5.8 clearly show that ten multi-coupled resonators were used in achieving the diplexer. Four of the resonators are resonating at the *Tx* centre frequency, another four are at the *Rx* centre frequency, and the last two resonators are resonating at the centre frequency of the diplexer (which also corresponds to the DBF centre frequency). The *Tx* resonators establish the diplexer transmit band, the *Rx* resonators establish the diplexer receive band, and the DBF resonators are for energy distribution between the *Tx* and the *Rx* bands.

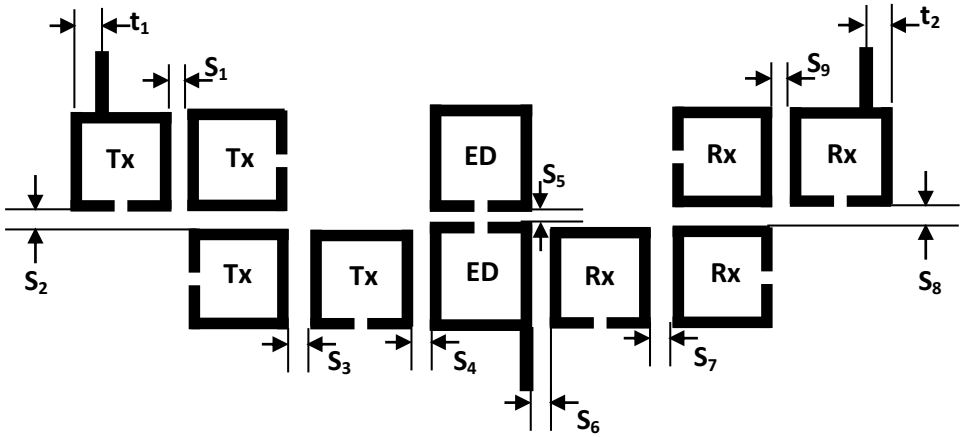

Figure 5.7: 10-pole diplexer layout with physical dimensions indicated (S_1 = 1.5 mm, S_2 = 2.0 mm, S_3 = 2.0 mm, S_4 = 1.6 mm, S_5 = 0.9 mm, S_6 = 1.65 mm, S_7 = 1.95 mm, S_8 = 2.0 mm, S_9 = 1.45 mm, t_1 = 1.45 mm, t_2 = 1.35 mm). (Nwajana and Yeo, 2016).

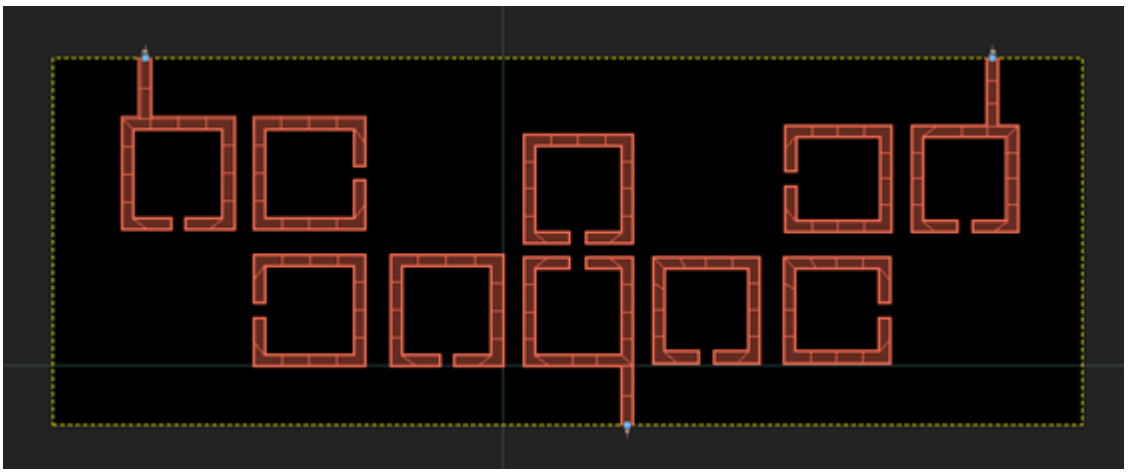

Figure 5.8: 10-pole (10^{th} order) microstrip microwave diplexer layout on a 1.27 mm thick substrate with a dielectric constant of 10.8.

The design was simulated using RT/Duroid 6010LM substrate with a relative permittivity of 10.8 and a thickness of 1.27 mm. The full-wave EM simulation was performed using the Keysight ADS Momentum simulator. A box was used to set the simulation boundaries on the four sides of the substrate as shown in Figure

5.8. Adding a box to the circuit simulation is very important as it enables one to be able to analyse the effects of enclosing the circuit in metal (Keysight Technologies, 2001). The initial simulation was conducted in an ideal condition (i.e. without both conductor and dielectric losses introduced). The lossless simulation responses for the transmit and the receive bands of the diplexer layout, are shown together with the circuit model simulation results from Chapter 4, in Figure 5.9 for ease of comparison. It can be seen from the comparison plot given in Figure 5.9 that the EM simulation results are in good agreement with the circuit model simulation results in Chapter 4. The diplexer layout was re-simulated with both conductor and dielectric losses introduced into the system. The lossy simulation results are shown in Figure 5.10. From the lossy simulation responses, it is clear that the bands isolation (i.e. S_{32}) achieved is very good as it lies at the 50 dB mark. This is very encouraging as it means that a very limited amount of signal may deflect into the wrong path during the operation of the diplexer.

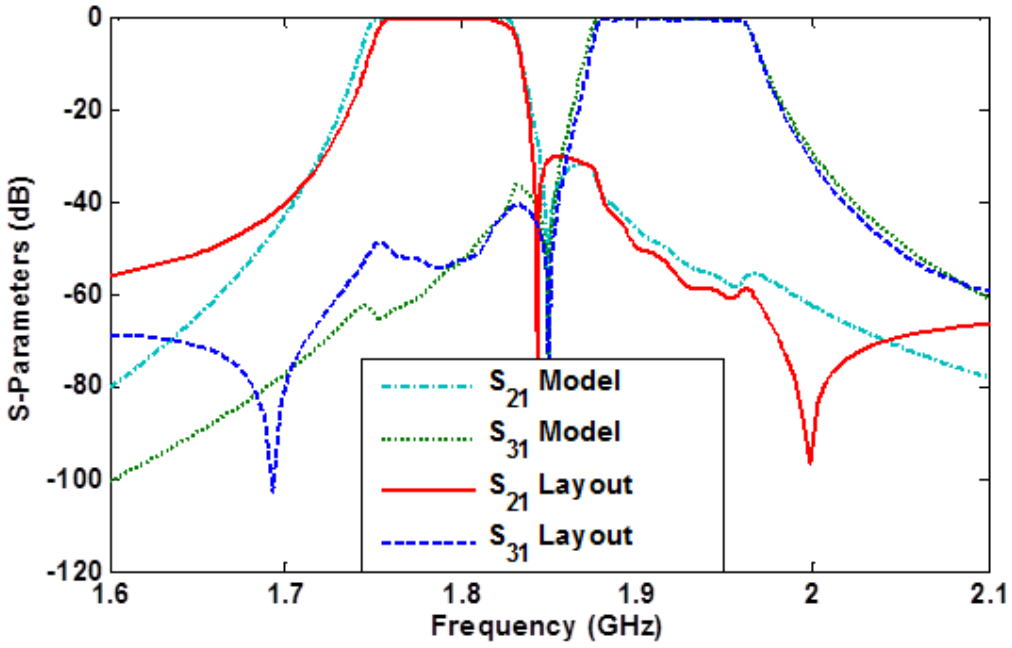

Figure 5.9: Comparison of the transmit and the receive bands responses of the microstrip diplexer layout and the circuit model of Chapter 4 operating in an ideal state (Nwajana and Yeo, 2016).

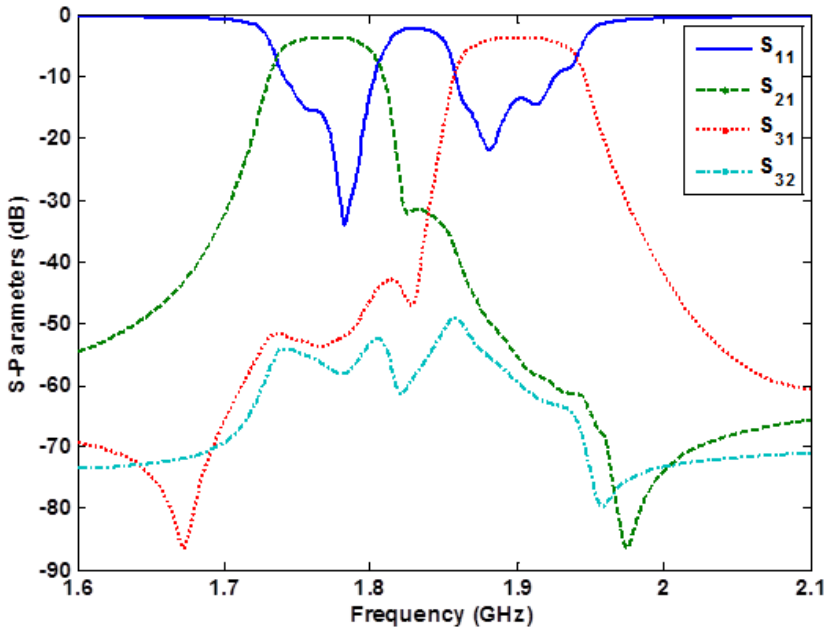

Figure 5.10: Simulation results of the microstrip diplexer with conductor and dielectric losses introduced into the system.

5.6 Fabrication and Measurement

The microstrip diplexer fabrication was based on the same material employed in the full-wave EM simulation, i.e. RT/Duroid 6010LM substrate with a dielectric constant of 10.8 and a thickness of 1.27 mm. The printed circuit board (PCB) milling process fabrication technique was employed. A picture of the fabricated microstrip diplexer is shown in Figure 5.11. Three SMA (Sub-Miniature version A) connectors were fitted onto the three input/output ports of the diplexer, as shown in Figure 5.11. This is to facilitate testing and measurement using the

Agilent Vector Network Analyzer. The measured results showing the transmit and the receive pass-bands, and the bands isolation is shown in Figure 5.12. The measured results clearly show that bands isolation (i.e. S_{32}) of 50 dB was achieved between the *Tx* band (i.e. S_{21}) and the *Rx* band (i.e. S_{31}). The measured minimum insertion loss for the *Tx* band is 2.88 dB, and that of the *Rx* band is 2.95 dB (Nwajana and Yeo, 2016).

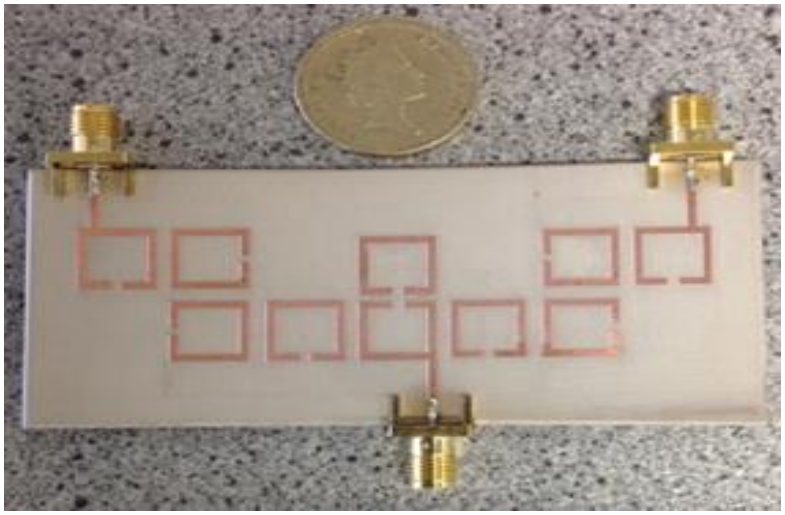

Figure 5.11: A picture of the fabricated 10-pole microstrip diplexer. (Nwajana and Yeo, 2016).

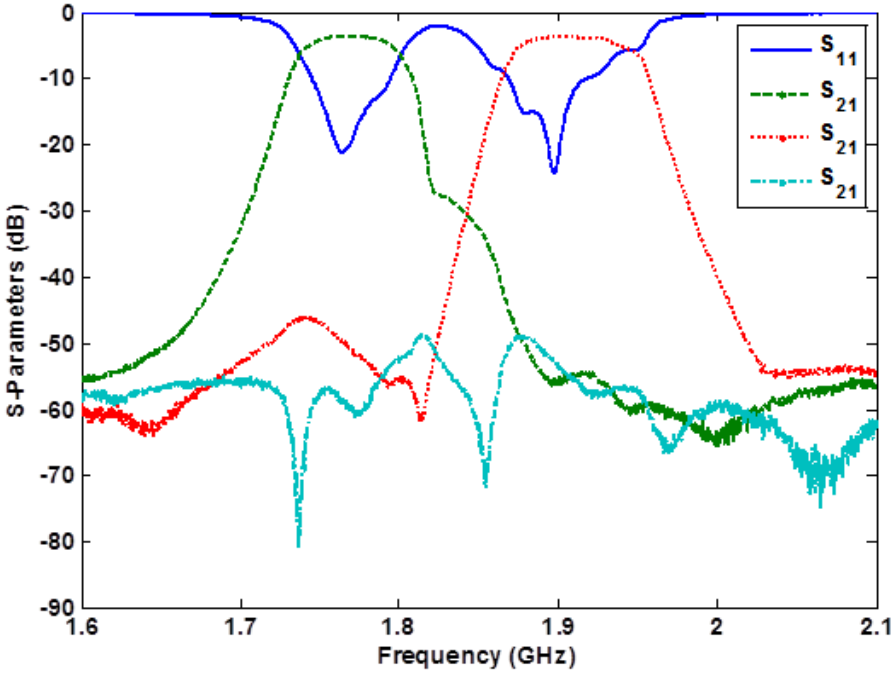

Figure 5.12: Measurement results of the 10-pole (10th order) microstrip diplexer.

To ease comparison between the simulation and measurement results, full-wave EM simulations with losses were performed. The conductor and the dielectric loss parameters were included in the full-wave EM simulations. The RT/Duroid 6010LM substrate with a relative permittivity of 10.8, a loss tangent of 0.0023, and a substrate thickness of 1.27 mm was employed in the loss simulations. The copper conductor used in the top and the bottom metals of the microstrip has a thickness of 16 micron (μm), and conductivity of 5.8 x 10^7 S/m. The loss simulation did not consider the surface roughness and the thickness variation of the substrate material.

The measurement results and the full-wave EM loss simulation results are both presented in Figure 5.13. The graphs obviously show that there is a good

agreement between the simulation and measurement responses. The additional transmission zeros shown in Figure 5.13 is as a result of the unwanted cross-couplings between the non-adjacent resonators which is an artefact.

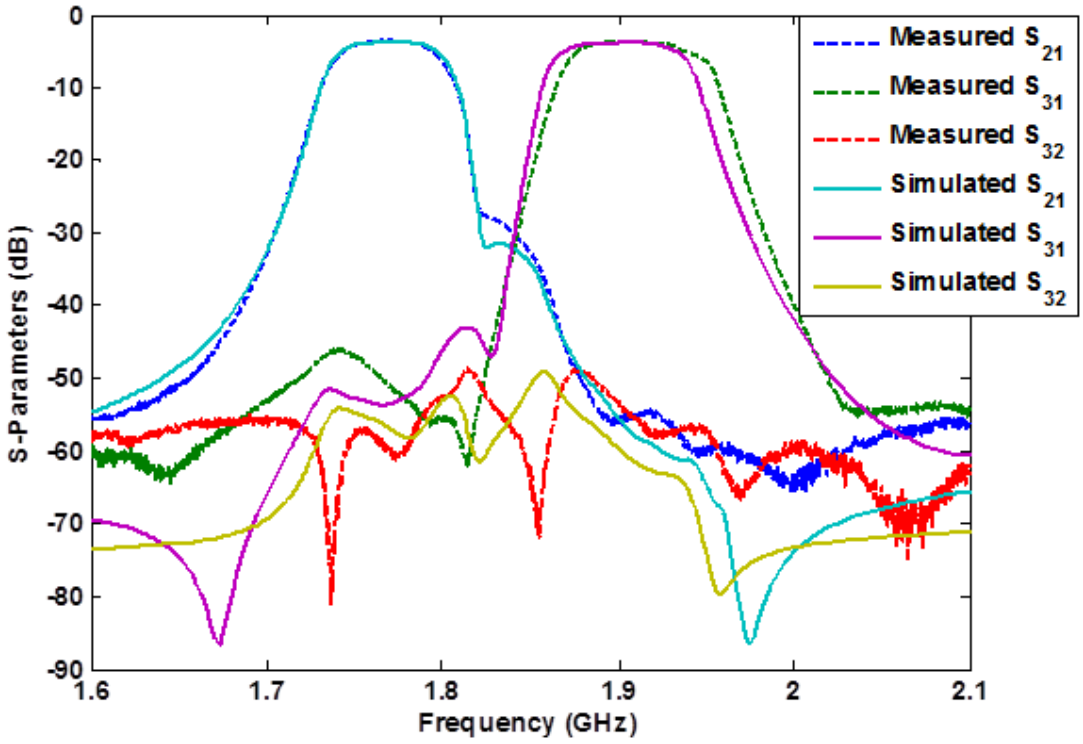

Figure 5.13: Comparison of the full-wave electromagnetic loss simulation results and the measurement results of the 10-pole microstrip diplexer.

5.7 Conclusion

A microstrip diplexer achieved by coupling a dual-band bandpass filter (DBF) with two single-bands bandpass filters (BPFs) has been designed, simulated, measured and presented. In addition to the straight forward design procedure, the design is also shown to have an additional benefit when compared to other designs in the literature, i.e. the energy distributing circuit itself contributes two

resonant poles to the diplexer itself. This is unlike most design methods reported in literature, where the non-resonant energy distributing circuit is primarily for channelling the energy to the correct band; but serve very little function in the selectivity of the diplexer. The design has been experimentally validated and the measured performance of the diplexer presented. The measurement results indicate that the isolation between the *Tx* and the *Rx* bands is about 50 dB, which is very encouraging. The measured minimum insertion loss of the *Tx* and the *Rx* bands are 2.88 dB and 2.95 dB, respectively. Owing to the very good bands isolation of the diplexer, only a very small amount of signal is expected to deflect towards the incorrect direction. The simulation and the measurement results show a very good agreement. The microstrip diplexer can be utilised in either splitting a wide frequency band into two narrow bands, or for combining two narrow bands into one wide frequency band. Even though the example presented here utilised microstrip resonators and is at the mobile communication frequencies, the design approach is applicable at higher frequencies and can be used in the design of diplexers for satellite applications. The method is applicable even when other types of resonators, including dielectric resonators, waveguide resonators, SIW cavities, etc., are employed.

Chapter 6: SIW Diplexer Design

6.1 Introduction

In this chapter, the 10-pole (10th order) microwave diplexer circuit model established in Chapter 4, is being implemented based on the SIW technique. A brief review of literatures that have reported diplexers based on the SIW technique have been covered in Chapter 1 (sub-section 1.4.2).

6.2 SIW Cavity

An overview on the SIW technology has been covered in Chapter 2 (section 2.4). To proceed with the implementation of the SIW diplexer, three separate SIW cavities (i.e. resonators), were designed to resonate at the centre frequencies of the transmit (*Tx*), the receive (*Rx*), and the energy distributor (*ED*) component filters. As explained in Chapter 4; *Tx*, *Rx*, and *ED* correspond to the BPF1, the BPF2, and the DBF resonators, respectively. Using Eqn. (6.1) derived from Han et al. (2007), the *Tx*, the *Rx* and the *ED* cavities were designed to resonate at 1.788 GHz, 1.917 GHz, and 1.849 GHz, respectively.

$$f_{101} = \frac{c_0}{2\pi\sqrt{\mu_r \varepsilon_r}} \sqrt{\left(\frac{\pi}{w_{eff}}\right)^2 + \left(\frac{\pi}{l_{eff}}\right)^2} \qquad (6.1\text{ a})$$

$$w_{eff} = w - 1.08\,\frac{d^2}{p} + 0.1\,\frac{d^2}{w}\;; \quad l_{eff} = l - 1.08\,\frac{d^2}{p} + 0.1\,\frac{d^2}{l} \qquad (6.1\text{ b})$$

The design was fabricated on a Rogers RT/Duroid 6010LM substrate with relative permittivity ε_r = 10.8, substrate thickness h = 1.27 mm and relative permeability

μ_r = 1. The physical design parameters for the three SIW cavities are given in Table 6.1; where *f* is the fundamental resonant frequency of each cavity, *d* is the diameter of each metallic post (also known as via diameter), *p* is the distance between adjacent metallic posts (also popularly known as the pitch), *w* is the width of the SIW cavity, and *l* is the length of the SIW cavity. A full-wave simulation layout and the results, using Keysight EMPro FEM, for the *Tx*, *Rx* and *ED* cavities is shown in Figure 6.1, where f_{Tx}, f_{Rx} and f_{ED} are the fundamental resonant frequencies for the *Tx*, *Rx* and *ED* cavities, respectively.

Table 6.1: Physical design parameters for the substrate integrated waveguide diplexer component filters cavities.

Cavity	***f* (GHz)**	***d* (mm)**	***p* (mm)**	***w* (mm)**	***l* (mm)**
Tx	1.788	2.0	3.725	37.25	37.25
Rx	1.917	2.0	3.490	34.90	34.90
ED	1.849	2.0	3.609	36.09	36.09

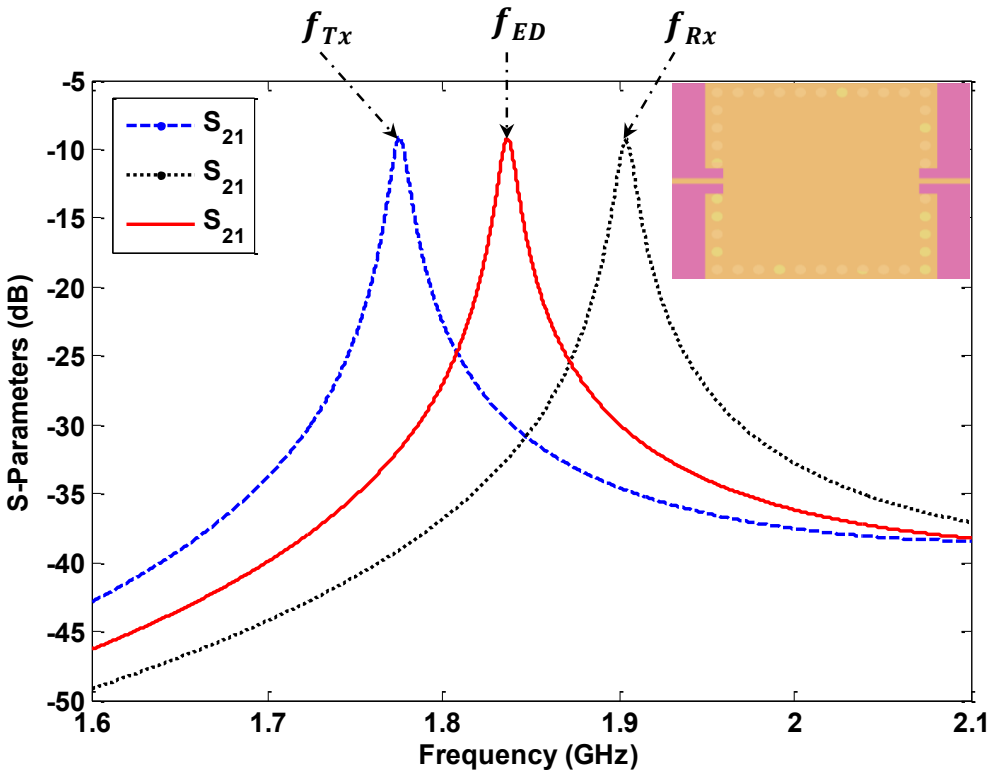

Figure 6.1: Full-wave simulation layout and the results for the *Tx*, the *Rx*, and the *ED* substrate integrated waveguide cavities at their respective fundamental resonant frequencies.

6.3 Coupling Coefficient Extraction

The coupling between adjacent SIW cavities was achieved by simulating two cavities using the methods shown in Figure 6.2. The full-wave simulation was conducted using the Keysight EMPro FEM 3D simulator. Changing the aperture opening *s*, in Figure 6.2, changes the coupling strength between the two cavities. It is clear from Figure 6.2 that an increase in the aperture size *s,* results to an increase in the coupling strength between the two cavities. Similarly, a reduction in the size, *s,* would lead to a reduction in the coupling strength between the two cavities.

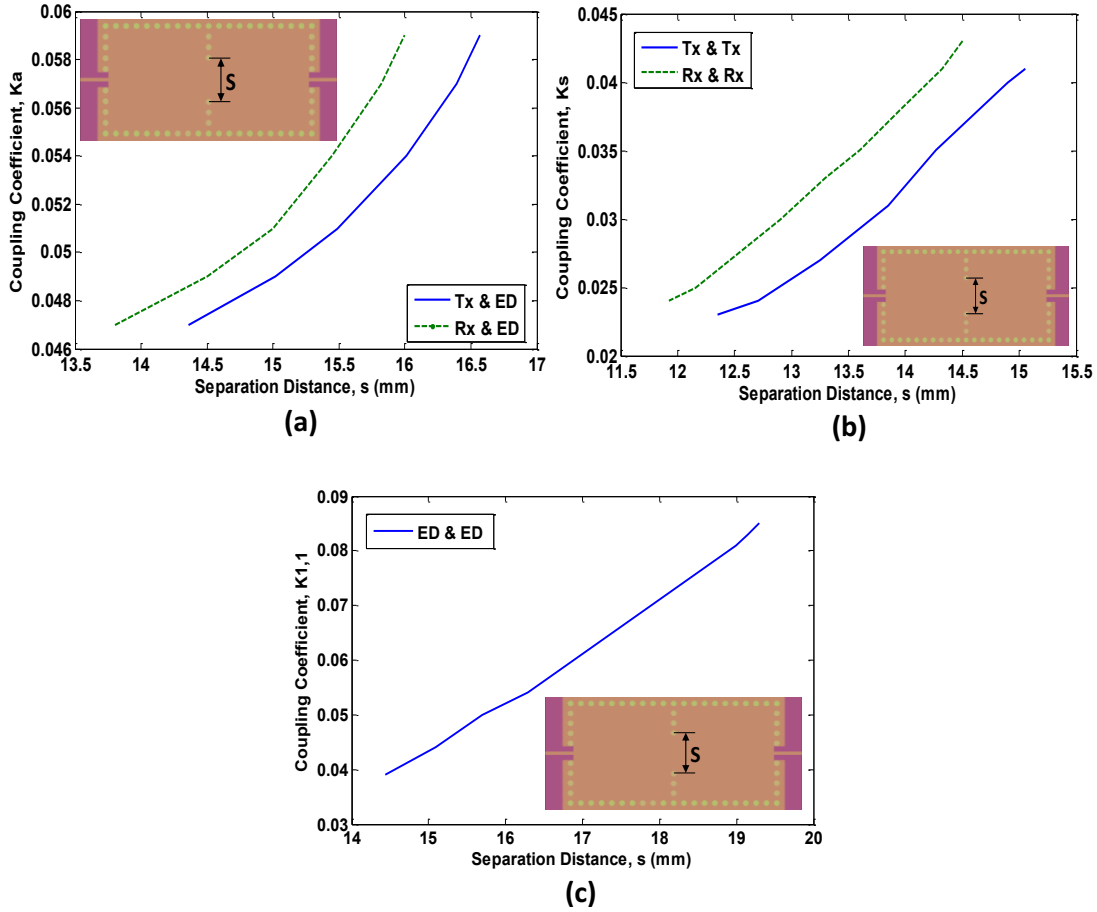

Figure 6.2: Coupling coefficient extraction technique using the substrate integrated waveguide cavities. (a) *Tx* & *ED* and *Rx* & *ED* couplings. (b) *Tx* & *Tx* and *Rx* & *Rx* couplings. (c) *ED* & *ED* coupling.

The type of coupling shown in Figure 6.2 (a) is known as asynchronous coupling since the two cavities involved are of different dimensions. This type of coupling is calculated using Eqn. (6.2) derived from Hong and Lancaster (2001). On the other hand, Figure 6.2 (b) and (c) show a coupling technique referred to as synchronous coupling. This is because the adjacent pair of cavities or resonators involved are exactly of the same dimension. This type of coupling (i.e. synchronous coupling) is calculated using Eqn. (6.3) which is also derived from Hong and Lancaster (2001). The parameters f_1 and f_2 in Eqns. (6.2) and (6.3) are

the eigen-modes from simulating coupled SIW cavities. The f_{r1} and f_{r2} parameters in Eqn. (6.2) are the fundamental resonant frequencies of cavities 1 and 2, respectively. k_s and k_a are the synchronous and asynchronous couplings, respectively.

$$k_a = \frac{1}{2}\left(\frac{f_{r2}}{f_{r1}} + \frac{f_{r1}}{f_{r2}}\right)\sqrt{\left(\frac{f_2^2 - f_1^2}{f_2^2 + f_1^2}\right)^2 - \left(\frac{f_{r2}^2 - f_{r1}^2}{f_{r2}^2 + f_{r1}^2}\right)^2} \tag{6.2}$$

$$k_s = \frac{f_2^2 - f_1^2}{f_2^2 + f_1^2} \tag{6.3}$$

6.4 External Quality Factor Extraction

The theoretical Q_{ext} values for the *Tx*, the *Rx* and the *ED* components of the diplexer have been determined in Chapter 4 as 24.285, 24.285, and 12.143, respectively. To achieve the input / output coupling strength that corresponds to the theoretical / calculated Q_{ext} values, two different techniques were employed. The first technique which was used in achieving the *Tx* and the *Rx* Q_{ext} values have been well documented in Chapter 3 (sub-section 3.6.2). This novel technique was first reported in Nwajana et al. (2017). The second technique which was used to achieve the *ED* Q_{ext} value was proposed in Deslandes and Wu (2001). This technique involves a transition from a coplanar waveguide (CPW) to the SIW using a 90^o bend as shown in Figure 6.3. The only reason for using two different input couplings in the design is to show that any conventional coupling technique could be used, besides the novel Microstrip-CPW-SIW coupling method proposed in this thesis.

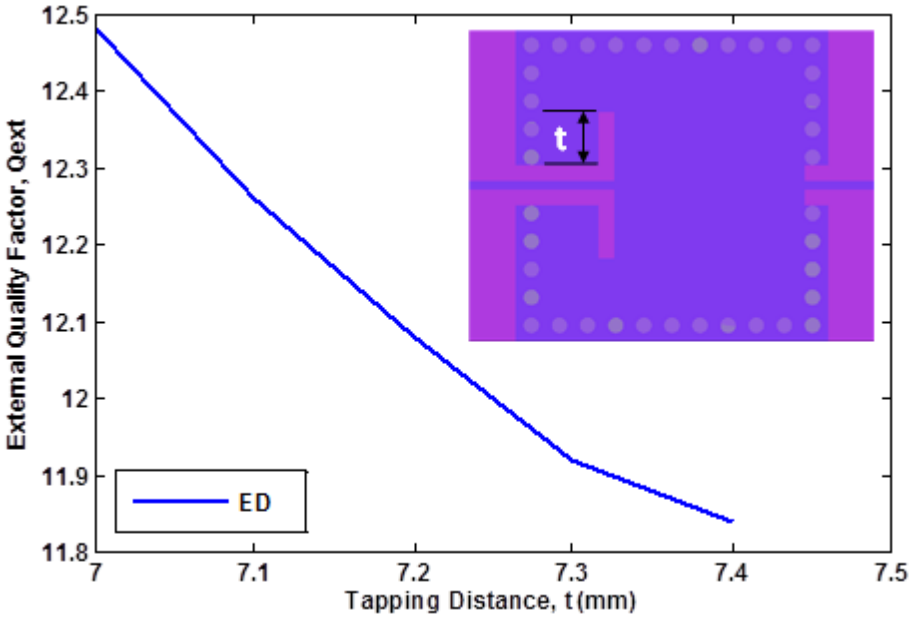

Figure 6.3: External quality factor extraction technique for the *ED* component.

The simulated Q_{ext} value of the *ED* component can be determined from Figure 6.4 which is based on Eqn. (6.4); where f_0 is the fundamental resonant frequency of the cavity being simulated, and $\delta f@-3dB$ is the 3 dB bandwidth of the simulated curve (Dainkeh et al., 2016). The simulation Q_{ext} values were achieved by adjusting the tapping distance, *t* as shown in Figure 6.3. It can be seen from Figure 6.3 that when *t* = 7.2 mm, Q_{ext} = 12.143. Hence, *t* = 7.2 mm corresponds to the calculated Q_{ext} value for the *ED* component of the diplexer.

$$Q_{ext} = \frac{f_0}{\delta f@-3dB} \tag{6.4}$$

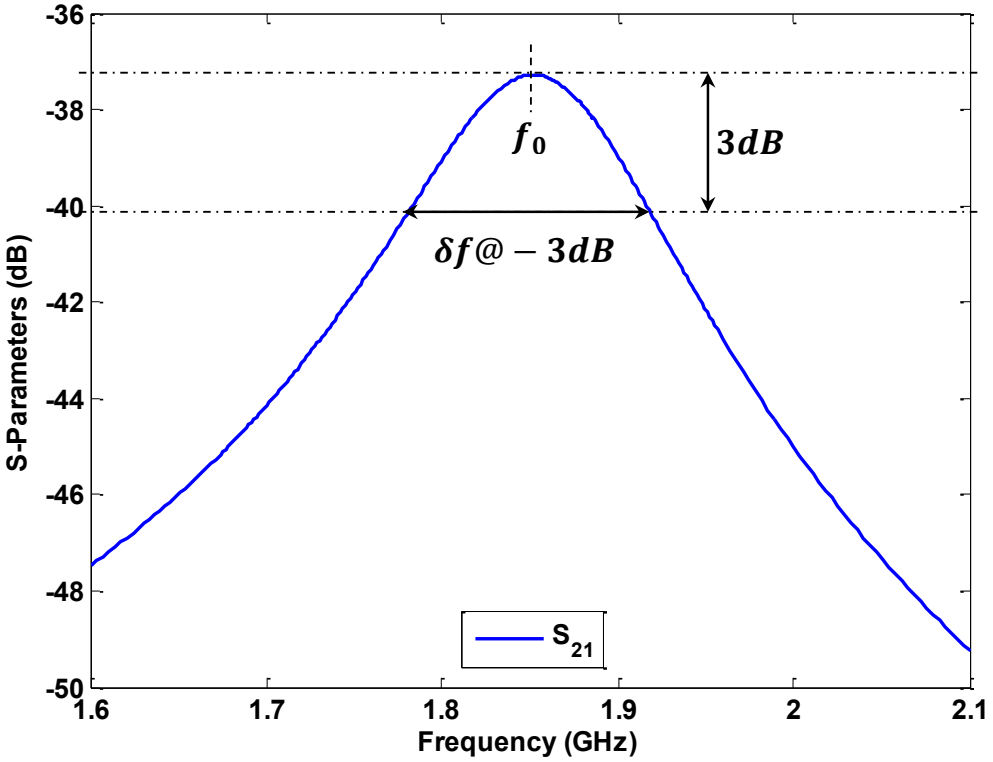

Figure 6.4: Simulation response of the transition from coplanar waveguide to substrate integrated waveguide (i.e. CPW – to – SIW) using a 90° bend.

6.5 Layout and Simulation

The layout of the 10th order SIW diplexer, on a RT/Duroid 6010LM substrate is shown in Figure 6.5. The substrate has a dielectric constant of 10.8, a relative permeability of 1.0 and a thickness of 1.27 mm. The physical dimensions of the diplexer are indicated in Figure 6.5 with the corresponding design values for achieving the design presented in Table 6.2.

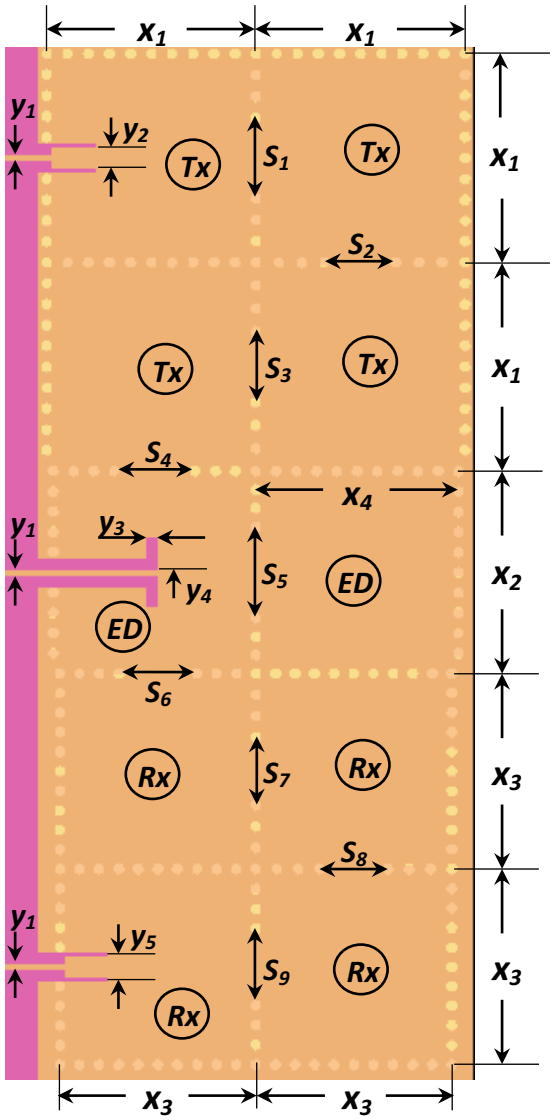

Figure 6.5: 10-pole substrate integrated waveguide diplexer layout indicating physical dimensions, on a 1.27 mm thick RT/Duroid 6010LM substrate with a dielectric constant of 10.8.

Table 6.2: Physical dimensions of the proposed 10-pole substrate integrated waveguide diplexer.

Dimension	Value (mm)	Dimension	Value (mm)
x_1	37.25	s_1	14.27
x_2	34.90	s_2	12.71
x_3	36.09	s_3	12.71
x_4	34.90	s_4	15.02
y_1	1.12	s_5	16.29
y_2	3.70	s_6	14.50
y_3	2.00	s_7	12.16
y_4	9.20	s_8	12.16
y_5	3.70	s_9	13.60

In Figure 6.5, the four cavities marked as *Tx* are resonating at the centre frequency of the diplexer transmit channel filter component (i.e. 1.788 GHz). The four other cavities marked as *Rx,* on the other hand, are resonating at the centre frequency of the diplexer receive channel filter component (i.e. 1.917 GHz). The remaining two cavities marked as *ED* are resonating at the centre frequency of the diplexer (i.e. 1.849 GHz). The function of the four *Tx* cavities is to establish the diplexer transmit band, while the four *Rx* cavities establish the diplexer receive band. The two *ED* cavities are responsible for energy distribution between the *Tx* and the Rx bands.

The full-wave FEM simulation was performed using the Keysight EMPro 3D simulator and the results presented in Figure 6.6. All the loss parameters of the materials used in the design were included in the simulation.

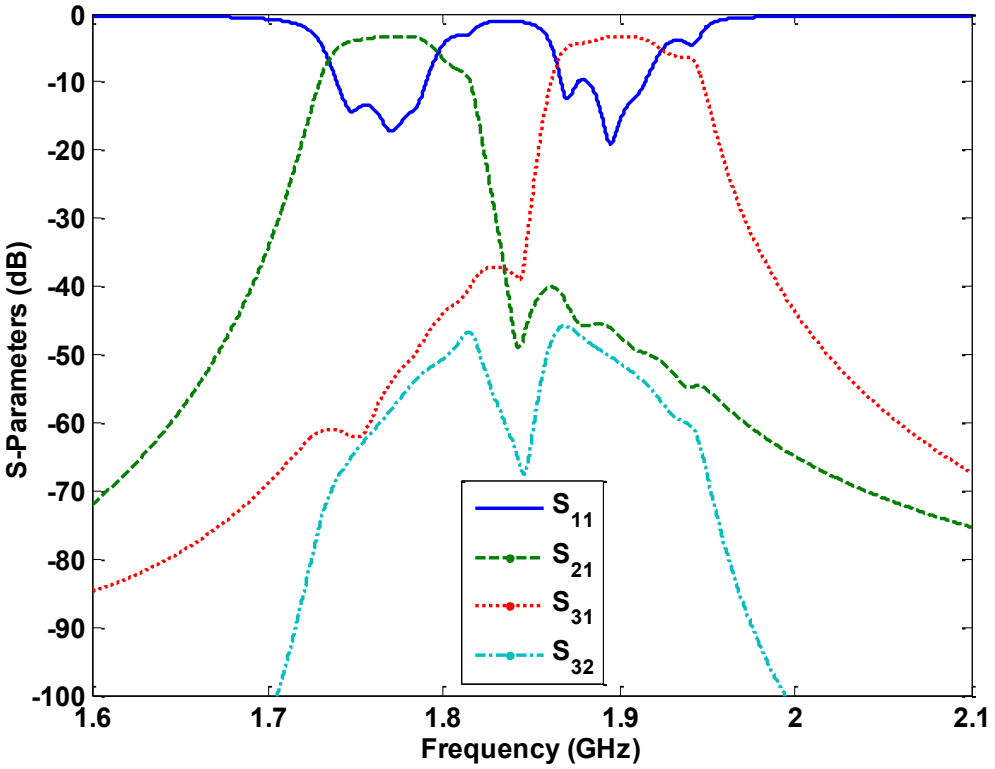

Figure 6.6: Simulation results of the 10-pole substrate integrated waveguide diplexer with both conductor and dielectric losses considered.

FEM padding was also used in the simulation. The FEM padding sets the boundary for the simulation domain by specifying the area that is meshed and solved during the FEM simulation (Keysight Technologies, 2011). The FEM padding value was set to 10 mm in the upper Z-plane as shown in Figure 6.7. This is large enough to avoid any interactions between the object and boundary. Setting the FEM padding too large would mean longer time to mesh and solve (Keysight Technologies, 2011). By default, EMPro sets the FEM padding value to half wavelength of the highest frequency of interest. As waveguide ports were

used for the diplexer simulation, the padding was set to “0” (zero) for the planes where the ports are located as shown in Figure 6.7. The waveguide ports were placed on the boundary of the simulation domain (Keysight Technologies, 2011).

Figure 6.7: FEM padding editor window indicating the settings used for the substrate integrated waveguide diplexer full-wave finite-element method simulations.

The simulated minimum insertion losses across the diplexer transmit (i.e. S_{21}) and the diplexer receive (i.e. S_{31}) bands are 2.86 dB and 2.91 dB, respectively as shown in Figure 6.6. The band isolation between the *Tx* and the *Rx* bands is at 46 dB. One major issue observed while performing the simulation is the enormous amount of time it took the simulation to complete and return converged results. In order to significantly reduce the simulation time and achieve faster results convergence, all the circular metallic posts were replaced with 10-sided polygons (or decagons). This action reduced the simulation time by over 300% as explained in Chapter 3, sub-section 3.6.4. The simulation time can also be

greatly reduced by increasing the diameter of the metallic posts, as this would mean less number of metallic posts present in the design.

6.6 Fabrication and Measurement

The proposed 10-pole SIW diplexer was fabricated using the same material utilised in the finite-element method simulation. The fabrication was based on the PCB micro-milling process by means of the LKPF Protomat C60. Three SMA connectors were fixed onto the input and output ports of the fabricated diplexer as shown in Figure 6.8. The SMA connectors serve as the points of connection between the diplexer and the Agilent Vector Network Analyzer during measurement. Notice that the three ports of the SIW diplexer have been placed on the same side of the substrate. This is an added advantage as having the 3 ports on the side of the substrate would contribute to the diplexer physical size reduction.

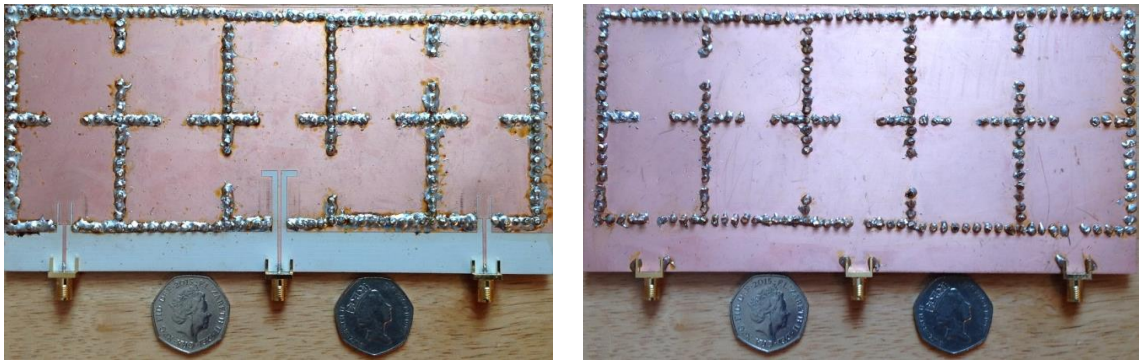

(a) **(b)**

Figure 6.8: Photograph of the fabricated 10-pole substrate integrated waveguide diplexer. (a) Top view. (b) Bottom view.

The measurement results are presented in Figure 6.9 and show that the minimum insertion losses of 2.86 dB and 2.91 dB were achieved on the transmit and the

receive bands, respectively. This is in comparison with the simulation results as shown in Figure 6.10 where both the measurement and simulation results are mutually presented for easiness of comparison. The high insertion loss shown in Figure 6.9 is due to the poor frequency matching among the SIW cavities. The poor matching is as a result of the wide gaps introduced in some cavities while realising the couplings. Note that the simulation results have been shifted by 349 MHz to the left in Figure 6.10. This is to facilitate a better and clear comparison of the simulated and measured results. The frequency shift is mainly due to the variation in dielectric constant of the dielectric materials used in the simulation, and that employed in the actual circuit fabrication. The use of 10-sided polygons in place of the conventional circular metallic posts also contributed to the frequency shift between the simulated and measured results. The measured isolation between the *Tx* and the *Rx* pass-bands is better than 50 dB as shown in Figures 6.9 and 6.10.

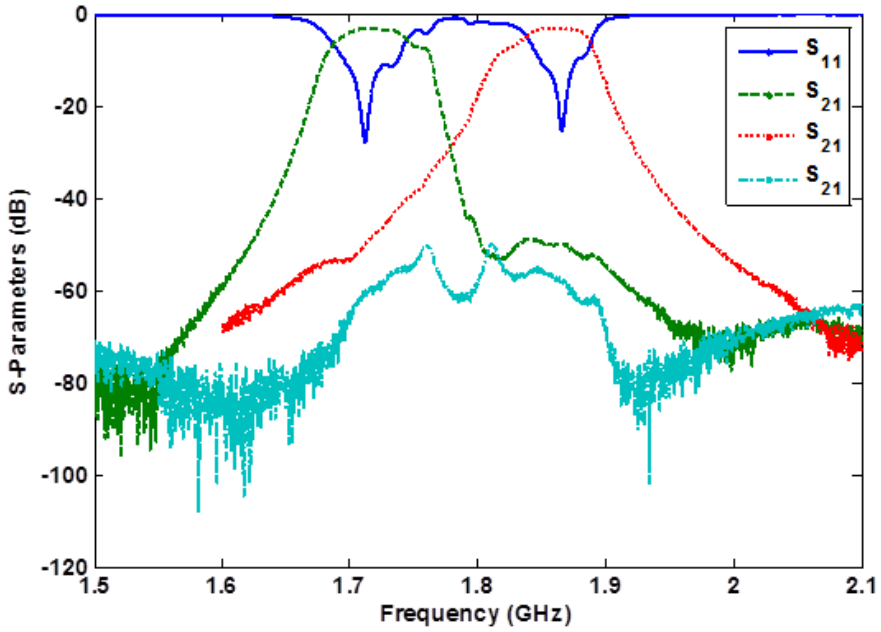

Figure 6.9: Measurement results of the 10-pole (10th order) substrate integrated waveguide diplexer.

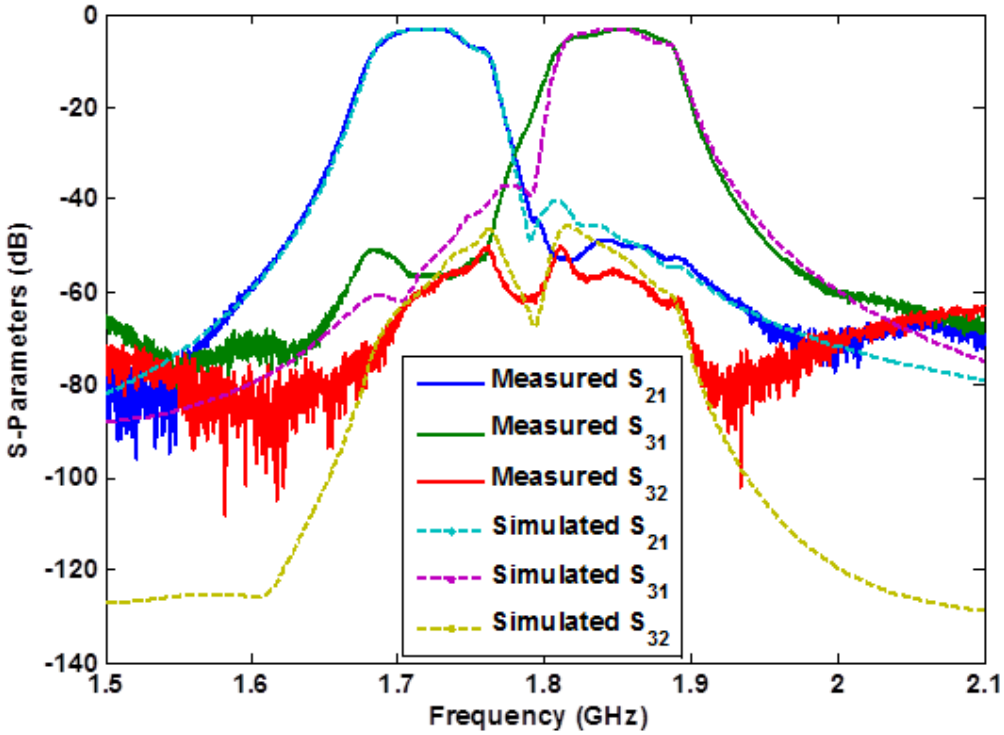

Figure 6.10: Comparison of the full-wave electromagnetic loss simulation responses and the measurement responses of the 10-pole substrate integrated waveguide diplexer.

6.7 Conclusion

The microwave diplexer circuit model achieved in Chapter 4 has been implemented using the SIW transmission line technique. The design benefitted from two different types of SIW transition. The novel Microstrip-CPW-SIW transition presented in Chapter 3 (section 3.6) was utilised at the transmit and the receive ends of the diplexer, while a CPW-to-SIW transition with 90^{o} bend was utilised at the energy distribution end of the diplexer. The design has been experimentally validated with the simulation and measurement results showing good agreement. The minimum measured insertion losses achieved on the SIW

diplexer are 2.86 dB and 2.91 dB across the transmit and the receive bands, respectively. Using Eqn. (2.7), the unloaded quality factors for both passbands of the SIW diplexer, were determined to be 273 and 289 for the *Tx* and *Rx* bands, respectively. The minimum return loss recorded on the SIW diplexer results shown in Figure 6.9 can be further improved by using more sided polygons for the metallic posts employed in the design. The down side is that the more the number of sides of the polygon used for the metallic post, the more time it would take for simulation results to converge as more meshing would be performed by the EM simulator.

Chapter 7: Conclusion and Future Work

7.1 Conclusion

This thesis has successfully modelled a microwave diplexer circuit without the need for using neither an external non-resonant junction, nor an out of band common resonator. The absence of both a non-resonant external junction and an out of band common resonator in the designed circuit model, means that the resultant diplexer is relatively reduced in size when compared to conventional diplexers that depend on T or Y non-resonant junctions or an out of band common resonator for energy distribution. The diplexer design technique reported in this thesis is totally dependent on well-known formulations for achieving bandpass and dual-band bandpass filters, hence, simple design with reduced uncertainties.

The design was initially implemented using asynchronously tuned microstrip square open-loop resonators, where the simulation and measurement results show that an isolation of 50 dB was achieved between the diplexer transmit and receive channels. A minimum insertion loss of 2.88 dB for the transmit band, and 2.95 dB for the receive band, were also achieved in the microstrip diplexer. The design was also implemented using the SIW technique, where the insertion loss of 2.86 dB and 2.91 dB were achieved across the transmit and the receive channels of the SIW diplexer, respectively. The simulation for both the microstrip and the SIW diplexers were based on ideal loss conditions, i.e. the surface roughness and the thickness variation of the substrate were not considered.

This thesis has recommended using polygons in place of the conventional circular metallic posts widely reported in literature. This is a way of reducing simulation time to up to 300% as explained in sub-section 3.6.4. However, care must be taken when deciding on the number of sides the polygon must have for best results comparison between simulated and measured components. As explained in Chapter 3 (sub-section 3.6.4), using fewer sided polygons will achieve the fastest simulation time, but will cause an enormous frequency shift to the left (i.e. reduction in the centre frequency of the component). Based on the results shown in Figure 3.35, this thesis has recommended the use of 10 or more side polygons as metallic posts, for good result comparison and improved simulation time of up to 300% less. Using fewer side polygons as metallic posts also degrades the return loss of the component being simulated as shown in Figure 3.35.

Another novelty achieved in this thesis is the implementation of a new type of SIW transition technique that was first demonstrated in a 3-pole bandpass filter (Nwajana and Yeo, 2017). The Microstrip-CPW-SIW transition technique exploited the step impedance between a 50 Ohms input/output feedline to control the input/output coupling of the filter. The minimal milling or etching requirements of the SIW ensured that fabrication errors were kept at the barest minimum. Both the SIW bandpass filter and the SIW diplexer reported were fabricated using the low cost and commercially available PCB technology. The micro-milling process was performed on the LKPF Protomat C60 which is also commercially available and not so expensive.

7.2 Future Work

The microstrip implementation of the diplexer circuit can be further reduced in size by employing the dual-mode resonator reported in Yeo and Nwajana (2013). This would be an important improvement as fewer resonators would lead to reduction in simulation time. Dual-mode resonators can achieve up to 50% reduction in the physical size of the microstrip diplexer.

The SIW implementation of the diplexer circuit, on the other hand, can also achieve further reduction in size by employing the half-mode substrate integrated waveguide (HMSIW) proposed in literature (Hong et al., 2006; Lai et al., 2009). The HMSIW cavity has a width that is half that of the conventional SIW, hence, it could achieve up to 50% reduction in device size while still maintaining the characteristics of the traditional SIW. Folded substrate integrated waveguide (FSIW) cavities (Wang et al., 2009; Wang et al., 2008) could also be used to achieve further miniaturisation in the size of the SIW diplexer.

Further investigations can also be conducted in deciding on the initial design parameters to be selected when working with SIW. For example, choosing a smaller diameter for the metallic posts could mean a better insertion loss. However, care must be taken in making such decisions as the smaller the diameter of the metallic posts, the longer it takes for the simulation results to converge. The larger the diameter of the metallic posts chosen, the faster the simulation time. This is due to the reduced number of metallic posts involved in the meshing process.

List of Publications

Journal Articles:

Nwajana, A. O., Dainkeh, A. and Yeo, K. S. K. (2017) 'Substrate Integrated Waveguide (SIW) Bandpass Filter with Novel Microstrip-CPW-SIW Input Coupling', *Journal of Microwaves, Optoelectronics and Electromagnetic Applications,* 16(2), pp. 393-402. doi: http://dx.doi.org/10.1590/2179-10742017v16i2793.

Nwajana, A. O. and Yeo, K. S. K. (2016) 'Microwave Diplexer Purely Based on Direct Synchronous and Asynchronous Coupling', *Radioengineering*, 25(2), pp. 247-252. doi: 10.13164/re.2016.0247.

Dainkeh, A., **Nwajana, A. O.** and Yeo, K. S. K. (2016) 'Filtered power splitter using microstrip square open loop resonators', *Progress in Electromagnetics Research C*, 64, pp. 133-140. doi: 10.2528/PIERC16042005.

Yeo, K. S. K. and **Nwajana, A. O.** (2013) 'A novel microstrip dual-band bandpass filter using dual-mode square patch resonators', *Progress in Electromagnetic Research C*, 36, pp. 233-247. doi: 10.2528/PIERC12120312.

Conference Papers:

Nwajana, A. O., Yeo, K. S. and Dainkeh, A. (2016), 'Low cost SIW Chebyshev bandpass filter with new input/output connection', In *Proceedings of the IEEE 16th Mediterranean Microwave Symposium (MMS)*, Abu Dhabi, UAE, 14-16 November, pp. 1-4. doi: 10.1109/MMS.2016.7803795.

Nwajana, A. O. and Yeo, K. S. K. (2016) 'Multi-coupled resonator microwave diplexer with high isolation', In *Proceedings of the IEEE 46st European Microwave Conference (EuMC),* London, UK, 4-6 October, pp. 1167-1170. doi: 10.1109/EuMC.2016.7824556.

Paper – In preparation at the Time of Thesis Submission:

Nwajana, A. O., Dainkeh, A. and Yeo, K. S. K. (2017) 'Substrate Integrated Waveguide (SIW) Diplexer with no Separate Non-Resonant Junction', *IEEE Transactions on Microwave Theory and Techniques*, pp. 1-6.

References

Adabi, A. and Tayarani, M. (2008) 'Substrate integration of dual inductive post waveguide filter', *Progress in Electromagnetic Research B*, 7, pp. 321-329. doi: 10.2528/PIERB08051002.

Ahn, H. R. and Tentzeris, M. M. (2016) 'Comments on "On-chip miniaturized diplexer using joint dual-mode right-/left-handed synthesized coplanar waveguides on GIPD process"', *IEEE Microwave and Wireless Components Letters*, 26(6), pp. 380-382. doi: 10.1109/LMWC.2016.2562632.

Araujo, L. S. and Belfort de Oliveira, A. B. (2013) 'A triplexer design based on coupled resonators approach for wireless communication', In *Proceedings of the SBMO/IEEE MTT-S International Microwave and Optoelectronics Conference (IMOC),* Rio de Janeiro, Brazil, 4-7 August, pp. 1-4. doi: 10.1109/IMOC.2013.6646595.

Ashiq, I. and Khanna, A. S. (2015) 'A novel planar contiguous diplexer DC-67-100 GHz using organic liquid crystal polymer (LCP)', In *Proceedings of the IEEE MTT-S International Microwave Symposium Digest,* Phoenix, AZ, USA, 17-22 May, pp. 1-4. doi: 10.1109/MWSYM.2015.7167091.

Athanosopoulos, N., Makris, D. and Voudouris, K. (2011) 'Development of a 60 GHz substrate integrated waveguide planar diplexer', In *Proceedings of the IEEE MTT-S International Microwave Workshop Series on Millimeter Wave Integration Technologies*, Sitges, Spain, 15-16, September, pp. 128-132. doi: 10.1109/IMWS3.2011.6061855.

Bao, Z. H., Chen, J. X., Lim, E. H. and Xue, Q. (2010) 'Compact microstrip diplexer with differential outputs', *IET Electronics letters*, 46(11), pp. 766-768. doi: 10.1049/el.2010.0260.

Bastioli, S., Marcaccioli, L. and Sorrentino, R. (2009) 'An original resonant Y-junction for compact waveguide diplexers' In *Proceedings of the IEEE MTT-S International Microwave Symposium Digest*, Boston, MA, USA, 7-12 June, pp. 1233-1236. doi: 10.1109/MWSYM.2009.5165926.

Behagi, A. (2015) *RF and microwave circuit design: a design approach using (ADS).* New York, NY: TECHNO Search. ISBN: 9780996446617.

Bozzi, M., Georgiadis, A. and Wu, K. (2011) 'Review of substrate-integrated waveguide circuits and antennas', *IET Microwaves, Antennas & Propagation,* pp. 909-920. doi: 10.1049/iet-map.2010.0463.

Bozzi, M., Pasian, M. and Perregrini, L. (2014) 'Modeling of losses in substrate integrated waveguide components', In *Proceedings of the IEEE International Conference on Numerical Electromagnetic Modeling and Optimization for RF, Microwave, and Terahertz Applications (NEMO),* Pavia, Italy, 14-16 May, pp. 1-4. doi: 10.1109/NEMO.2014.6995688.

Bozzi, M., Pasian, M., Perregrini, L. and Wu, K. (2007) 'On the losses in substrate integrated waveguides', In *Proceedings of the European Microwave Conference (EuMC),* Munich, Germany, 9-12 October, pp. 384-387. doi: 10.1109/EUMC.2007.4405207.

Bozzi, M., Pasian, M., Perregrini, L. and Wu, K. (2009) 'On the losses in substrate-integrated waveguides and cavities', *International Journal of Microwave and Wireless Technologies*, 1(5), pp. 395-401. doi: doi.org/10.1017/S1759078709990493.

Bozzi, M., Perregrini, L. and Wu, K. (2008) 'Modeling of conductor, dielectric, and radiation losses in substrate integrated waveguide by the boundary integral-resonant mode expansion method', *IEEE Transactions on Microwave Theory and Techniques*, 56(12), pp. 3153-3161. doi: 10.1109/TMTT.2008.2007140.

Bozzi, M., Perregrini, L. and Wu, K. (2008) 'Modeling of losses in substrate integrated waveguide by boundary integral-resonant mode expansion method', In *Proceedings of the IEEE MTT-S International Microwave Symposium Digest,* Atlanta, GA, USA, 15-20 June, pp. 515-518. doi: 10.1109/MWSYM.2008.4633216.

Bozzi, M., Perregrini, L., Wu, K. and Arcioni, P. (2009) 'Current and future research trends in substrate integrated waveguide technology', *Radioengineering*, 18(2), pp. 201-209.

Cameron, R. I. and Yu, M. (2007) 'Design of manifold-coupled multiplexers', *IEEE microwave magazine*, 8(5), pp. 46-59. doi: 10.1109/MMM.2007.904715.

Carceller, C., Soto, P., Boria, V., Guglielmi, M. and Gil, J. (2015) 'Design of compact wideband manifold-coupled multiplexers', *IEEE Transactions on Microwave Theory and Techniques*, 63(10), pp. 3398-3407. doi: 10.1109/TMTT.2015.2460738.

Chan, H. L., Lee, C. H. and Hsu, C. I. G. (2015) 'Balanced dual-band diplexer design using microstrip and slot-line resonators', In *Proceedings of the IEEE Asia-Pacific Microwave Conference (APMC)*, Nanjing, China, 6-9 December, 3, pp. 1-3. doi: 10.1109/APMC.2015.7413543.

Chen, C. F., Huang, T. Y., Chou, C. P. and Wu, R. B. (2006) 'Microstrip diplexer design with common resonator sections for compact size, but high isolation', *IEEE Transactions on Microwave Theory and Techniques*, 54(5), pp. 1945-1952. doi: 10.1109/TMTT.2006.873613.

Chen, C. F., Huang, T. Y., Shen, T. M. and Wu, R. B. (2006) 'A miniaturized microstrip common resonator triplexer without extra matching network', In *Proceedings of the IEEE Asia-Pacific Microwave Conference (APMC)*, Yokohama, Japan, 12-15 December, pp. 1439-1442.

Chen, C. F., Lin, C. Y., Tseng, B. H. and Chang, S. F. (2014) 'High-isolation and high-rejection microstrip diplexer with independently controllable transmission zeros', *IEEE Microwave and Wireless Components Letters*, 24(12), pp. 851-853. doi: 10.1109/LMWC.2014.2361684.

Chen, C. F., Wang, G. Y., Tseng, B. H. and Lin, T. A. (2016) 'Design of compact microwave diplexer for system-in-a-package applications', In *Proceedings of the IEEE International Conference on Consumer Electronics-Taiwan (ICCE-TW),* Nantou County, Taiwan, 27-29 May, pp. 1-2. doi: 10.1109/ICCE-TW.2016.7520955.

Chen, C. H., Wu, H. and Wu, W. (2011) 'High isolation DBR diplexer using in-line SCMRC', *Progress in Electromagnetics Research C*, 22, pp. 97-108. doi: 10.2528/PIERC11051208.

Chen, C., Chen, L. and Zhao, P. (2014) 'A waveguide diplexer based on E-plane T-junction', In *Proceedings of the IEEE 15th International Conference on Electronic Packaging Technology (ICEPT)*, Chengdu, China, 12-15 August, pp. 1390-1391. doi: 10.1109/ICEPT.2014.6922912.

Chen, D., Zhu, L., Bu, H. and Cheng, C. (2015) 'A Novel Planar Diplexer Using Slotline-Loaded Microstrip Ring Resonator', *IEEE Microwave and Wireless Components Letters*, 25(11), pp. 706-708. doi: 10.1109/LMWC.2015.2479836.

Chen, J. X., Zhang, X. Y. and Xue, Q. (2008) 'Dual-band bandpass filter and diplexer based on double-sided parallel-strip line', In *Proceedings of the IEEE*

MTT-S International Microwave Symposium Digest pp. Atlanta, GA, USA, 15-20 June, pp. 675-678. doi: 10.1109/MWSYM.2008.4632922.

Chen, M. H., Cheng, H. S., Chou, P. J. and Chang, C. Y. (2015) 'W-band T-Junction and bifurcated substrate integrated waveguide diplexers', In *Proceedings of the IEEE International Workshop on Electromagnetics: Applications and Student Innovation Competition (iWEM),* Hsin-Chu, Taiwan, 16-18 November, pp. 1-2. doi: 10.1109/iWEM.2015.7365091.

Chen, X. P. and Wu, K. (2014) 'Substrate integrated waveguide filter: basic design rules and fundamental structure features', *IEEE Microwave Magazine*, 15(5), pp. 108-116. Doi: 10.1109/MMM.2014.2321263.

Chen, X., Hong, W., Cui, T., Chen, J. and Wu, K. (2005) 'Substrate integrated waveguide (SIW) linear phase filter', *IEEE Microwave and Wireless Components Letters*, 15(11), pp. 787-789. doi: 10.1109/LMWC.2005.859021.

Cheng, F., Lin, X. Q., Jiang, Y., Song, K. J. and Fan, Y. (2014) 'A compact substrate integrated waveguide diplexer using dual-mode filters', In *Proceedings of the Progress in Electromagnetics Research Symposium (PIERS)*, Guangzhou, China, 25-28 August, pp. 1351-1355.

Cheng, F., Lin, X. Q., Zhu, Z. B., Wang, L. Y. and Fan, Y. (2012) 'High isolation diplexer using quarter-wavelength resonator filter', *IET Electronic Letters*, 48(6), pp. 330-331. doi: 10.1049/el.2012.0031.

Cheng, F., Lin, X., Song, K., Jiang, Y. and Fan, Y. (2013) 'Compact diplexer with high isolation using the dual-mode substrate integrated waveguide resonator', *IEEE Microwave and Wireless Components Letters*, 23(9), pp. 459-461. doi: 10.1109/LMWC.2013.2274036.

Cheng, Y. J. (2015) *Substrate integrated antennas and arrays*. New York, NY: CRC Press. ISBN: 9781498714532.

Chu, H., Guo, Y. X., Song, Y. L. and Wang, Z. L. (2011) '40/50 GHz diplexer design in LTCC technology', *IET Electronic Letters*, 47(4), pp. 260-262. doi: 10.1049/el.2010.3644.

Chuang, M. L. and Wu, M. T. (2011) 'Microstrip diplexer design using common T-shaped resonator', *IEEE Microwave and Wireless Components Letters*, 21(11), pp. 583-585. doi: 10.1109/LMWC.2011.2168949.

Cogollos, S., Soto, P., Boria, V. E., Guglielmi, M., Brumos, M., Gimeno, B. and Raboso, D. (2015) 'Efficient design of waveguide manifold multiplexers based on low-order EM distributed models', *IEEE Transactions on Microwave Theory and Techniques*, 63(8), pp. 2540-2549. doi: 10.1109/TMTT.2015.2442990.

Collin, R. E. (2000) *Foundations for microwave engineering*. 2nd edn. New York, NY: IEEE Press. ISBN: 9780780360310.

Dainkeh, A., Nwajana, A. O. and Yeo, K. S. K. (2016) 'Filtered power splitter using microstrip square open loop resonators', *Progress in Electromagnetics Research C*, 64, pp. 133-140. doi: 10.2528/PIERC16042005.

Deng, H. W., Zhao, Y. J., Fu, F., Zhou, X. J. and Liu, Y. Y. (2013) 'Compact and high isolation microstrip diplexer for GPS and UWB application', *IET Electronics Letters*, 49(10), pp. 659-661. doi: 10.1049/el.2012.3247.

Deng, K., Che, W., Li, C. and Russer, P. (2008) 'Novel microwave diplexer system based on planar waveguide and metamaterial technologies', In *Proceedings of the IEEE Asia-Pacific Microwave Conference (APMC)*, Hong Kong, 16-20 December, pp. 1-4. doi: 10.1109/APMC.2008.4958656.

Deng, P. H. and Tsai, J. T. (2013) 'Design of microstrip lowpass-bandpass diplexer', *IEEE Microwave and Wireless Components Letters*, 23(7), pp. 332-334. doi: 10.1109/LMWC.2013.2262264.

Deng, P. H., Wang, C. H. and Chen, C. H. (2006) 'Compact microstrip diplexer based on a dual-passband filter', In *Proceedings of the IEEE Asia-Pacific Microwave Conference (APMC)*, Yokohama, Japan, 12-15 December, pp. 1228-1232. doi: 10.1109/APMC.2006.4429629.

Denlinger, E. J. (1980) 'Losses of microstrip lines', *IEEE Transactions on Microwave Theory Techniques*, 28(6), pp. 513-522. doi: 10.1109/TMTT.1980.1130112.

Deslandes, D. (2010) 'Design equations for tapered microstrip-to-substrate integrated waveguide transitions', In *Proceedings of the IEEE MTT-S International Microwave Symposium Digest,* Anaheim, CA, USA, pp. 704-707. doi: 10.1109/MWSYM.2010.5517884.

Deslandes, D. and Wu, K. (2001) 'Integrated microstrip and rectangular waveguide in planar form', *IEEE Microwave and Wireless Components Letters*, 11(2), pp. 68-70. doi: 10.1109/7260.914305.

Deslandes, D. and Wu, K. (2001) 'Integrated transition of coplanar to rectangular waveguides', In *Proceedings of the IEEE MTT-S International Microwave Symposium Digest,* Phoenix, AZ, USA, 20-25 May, 2, pp. 619-622. doi: 10.1109/MWSYM.2001.966971.

Deslandes, D. and Wu, K. (2002) 'Design consideration and performance analysis of substrate integrated waveguide components', In *Proceedings of the European Microwave Conferenc (EuMC),* Milan, Italy, 23-26 September, pp. 1-4. doi: 10.1109/EUMA.2002.339426.

Deslandes, D. and Wu, K. (2003) 'Millimeter-wave substrate integrated waveguide filters', In *Proceedings of the IEEE 16th Canadian Conference in Electrical and Computer Engineering (CCECE)*, Montreal, Canada, 4-7 May, 3, pp. 1917-1920. doi: 10.1109/CCECE.2003.1226288.

Deslandes, D. and Wu, K. (2003) 'Single-substrate integrated technique of planar circuits and waveguide filters', *IEEE Transactions on Microwave Theory and Techniques*, 51(2), pp. 593-596. doi: 10.1109/TMTT.2002.807820.

Deslandes, D. and Wu, K. (2005) 'Analysis and design of current probe transition from grounded coplanar to substrate integrated rectangular waveguides', *IEEE Transactions on Microwave Theory and Techniques*, *53*(8), pp. 2487-2494. doi: 10.1109/TMTT.2005.852778.

Deslandes, D. and Wu, K. (2006) 'Accurate modelling, wave mechanisms, and design considerations of a substrate integrated waveguide', *IEEE Transactions on Microwave Theory and Techniques,* 54(6), pp. 2516-2526. doi: 10.1109/TMTT.2006.875807.

Ding, Y. and Wu, K. (2007) 'Substrate integrated waveguide-to-microstrip transition in multilayer substrate', *IEEE Transactions on Microwave Theory and Techniques*, 55(12), pp. 2839-2844. doi: 10.1109/TMTT.2007.909878.

Dong, Y. and Itoh, T. (2011) 'Substrate integrated waveguide loaded by complementary split-ring resonators for miniaturized diplexer design', *IEEE Microwave and Wireless Components Letters*, 21(1), pp. 10-12. doi: 10.1109/LMWC.2010.2091263.

Duong, T. V., Hong, W., Hao, Z. C., Huang, W. C., Zhuang, J. X. and Vo, V. P. (2016) 'A millimeter wave high-isolation diplexer using selectivity-improved dual-mode filters', *IEEE Microwave and Wireless Components Letters*, *26*(2), pp. 104-106. doi: 10.1109/LMWC.2016.2517135.

Feng, W., Gao, X. and Che, W. (2014) 'Microstrip diplexer for GSM and WLAN bands using common shorted stubs', *IET Electronics Letters*, 50(20), pp. 1486-1488. doi: 10.1049/el.2014.2500.

Fritz, M. and Wiesbeck, W. (2006) 'A diplexer based on transmission lines, implemented in LTCC', *IEEE Transactions on Advanced Packaging*, 29(3), pp. 427-432. doi: 10.1109/TADVP.2006.872997.

García-Lampérez, A., Salazar-Palma, M. and Yeung, S. H. (2014) 'Compact diplexer with dual-mode SIW resonators', In *Proceedings of the IEEE 44th European Microwave Conference (EuMC),* Rome, Italy, 6-9 October, pp. 857-860. doi: 10.1109/EuMC.2014.6986570.

García-Lampérez, A., Salazar-Palma, M. and Yeung, S. H. (2014) 'SIW compact diplexer', In *Proceedings of the IEEE MTT-S International Microwave Symposium Digest,* Tampa, FL, USA, pp. 1-4. doi: 10.1109/MWSYM.2014.6848514.

Gouget, P., Duchamp, G. and Pistre, J. (2003) 'Optimisation and comparison of three diplexers based on a new slot to microstrip junction', In *Proceedings of the IEEE MTT-S International Microwave Symposium Digest,* Philadelphia, PA, USA, 2, pp. 1231-1234. doi: 10.1109/MWSYM.2003.1212591.

Govind, V., Monajemi, P., Carastro, L., Lapushin, S., Russell, C., Dalmia, S., Vickers, J., Sundaram, V. and White, G. (2006) 'Design of novel highly integrated passive devices for digital broadcasting satellite/802.11 home networking solution in liquid crystal polymer (LCP) based organic substrates', In *Proceedings of the IEEE MTT-S International Microwave Symposium Digest,* San Francisco, CA, USA, 11-16 June, pp. 1157-1160. doi: 10.1109/MWSYM.2006.249396.

Guan, X., Huang, W., Liu, H., Wen, P. and Chen, Q. (2016) 'A novel microstrip diplexer with a common square ring resonator for WCDMA', In *Proceedings of the IEEE International Workshop on Electromagnetics: Applications and Student Innovation Competition (iWEM),* Nanjing, Jiansu, China, 16-18 May, pp. 1-3. doi: 10.1109/iWEM.2016.7504877.

Guan, X., Yang, F., Liu, H. and Zhu, L. (2014) 'Compact and high-isolation diplexer using dual-mode stub-loaded resonators', *IEEE Microwave and Wireless Components Letters*, *24*(6), pp. 385-387. doi: 10.1109/LMWC.2014.2313591.

Guan, X., Yang, F., Liu, H., Ma, Z., Ren, B., Huang, W. and Wen, P. (2016) 'Compact, low Insertion-loss, and wide stopband HTS diplexer using novel coupling diagram and dissimilar spiral resonators', *IEEE Transactions on Microwave Theory and Techniques*, 64(8), pp. 2581-2589. doi: 10.1109/TMTT.2016.2580143.

Guglielmi, M. (1993) 'Optimum CAD procedure for manifold diplexers', In *Proceedings of the IEEE MTT-S International Microwave Symposium Digest,* Atlanta, GA, USA, pp. 1081-1084. doi: 10.1109/MWSYM.1993.277054.

Han, S. H., Wang, X. L., Fan, Y., Yang, Z. Q. and He, Z. N. (2007) 'The generalized Chebyshev substrate integrated waveguide diplexer', *Progress in Electromagnetic Research*, 73, pp. 29-38. doi: 10.2528/PIER07032002.

Hao, Z. C., Hong, W., Chen, J. X., Chen, X. P. and Wu, K. (2005) 'Planar diplexer for microwave integrated circuits', *IEE Proceedings on Microwaves, Antennas and Propagation*, 152(6), pp. 455-459. doi: 10.1049/ip-map:20050014.

Hao, Z., Hong, W., Li, H., Zhang, H. and Wu, K. (2005) 'A broadband substrate integrated waveguide (SIW) filter', In *Proceedings of the IEEE Antennas and Propagation Society International Symposium Digest*, Washington, DC, USA, 3-8 July, pp. 598-601. doi: 10.1109/APS.2005.1551629.

Harfoush, O., Yazbek, K. and Alkhoder, A. (2009) 'Diplexer design for switched frequency diversity applications in wireless communications systems', In *Proceedings of the IEEE 9th Mediterrannean Microwave Symposium (MMS)*, Tangiers, Morocco, 15-17 November, pp. 1-3. doi: 10.1109/MMS.2009.5409782.

He, J., Gao, K. and Shao, Z. (2012) 'A novel compact Ka-band high-rejection diplexer based on substrate integrated waveguide', In *Proceedings of the IEEE International Conference on Computational Problem-solving (ICCP)*, Leshan, China, 19-21 October, pp. 193-197. doi: 10.1109/ICCPS.2012.6384320.

He, N., Ji, J. and Fei, Y. (2010) 'A compact millimeter-wave stripline diplexer with two modified hairpin filters', In *Proceedings of the IEEE Asia-Pacific International Symposium on Electromagnetic Compatibility (APEMC),* Beijing, China, 12-16 April, pp. 1370-1373. doi: 10.1109/APEMC.2010.5475569.

Heng, Y., Guo, X., Cao, B., Wei, B., Zhang, X., Zhang, G., Song, X. and Feng, C. (2013) 'Design and optimization of a superconducting contiguous diplexer

comprising doubly terminated filters', *IEEE Transactions on Applied Superconductivity*, 23(4), pp.1-6. doi: 10.1109/TASC.2013.2250284.

Heng, Y., Guo, X., Cao, B., Wei, B., Zhang, X., Zhang, G. and Song, X. (2014) 'A narrowband superconducting quadruplexer with high isolation', *IEEE Transactions on Applied Superconductivity*, 24(2), pp. 21-26. doi: 10.1109/TASC.2014.2304886.

Hill, M. J., Papapolymerou, J. and Ziolkowski, R. W. (2001) 'High-Q micromachined resonant cavities in a K-band diplexer configuration', *IEE Proceedings-Microwaves, Antennas and Propagation*, 148(5), pp. 307-312. doi: 10.1049/ip-map:20010644.

Hong, J. S. and Lancaster, M. J. (2000) 'Microstrip triangular patch resonator filters', In *Proceedings of the IEEE MTT-S International Microwave Symposium Digest,* Boston, MA, USA, 11-16 June, 1, pp. 331-334. doi: 10.1109/MWSYM.2000.861002.

Hong, J. S. (2011) *Microstrip filters for RF/microwave applications*. 2nd edn. New York, NY: John Wiley & Sons. ISBN: 9780470408773.

Hong, J. S. and Lancaster, M. J. (1996) 'Couplings of microstrip square open-loop resonators for cross-coupled planar microwave filters', *IEEE Transactions on Microwave Theory and Techniques*, 44(11), pp. 2099-2109. Doi: 10.1109/22.543968.

Hong, J. S., and Lancaster, M. J. (2001) *Microstrip filters for RF/microwave applications*. New York, NY: John Wiley & Sons. ISBN: 9780471388777.

Hong, W., Liu, B., Wang, Y., Lai, Q., Tang, H., Yin, X. X., Dong, Y. D., Zhang, Y. and Wu, K. (2006) 'Half mode substrate integrated waveguide: a new guided wave structure for microwave and millimeter wave application', In *proceedings of the IEEE Joint 31st International Conference on Infrared Millimeter Waves and 14th International Conference on Teraherz Electronics,* Shanghai, China 18-22 September, pp. 219-219. doi: 10.1109/ICIMW.2006.368427.

Huang, Y. and Wu, K. L. (2003) 'A broad-band LTCC integrated transition of laminated waveguide to air-filled waveguide for millimeter-wave applications', *IEEE Transactions on Microwave Theory and Techniques*, 51(5), pp. 1613-1617. doi: 10.1109/TMTT.2003.810146.

Hung, W. T., Chang, S. Y. and Chen, S. Y. (2010) 'High isolation, compact microstrip diplexers using quarter-wave stepped-impedance resonators', In *Proceedings of the IEEE Asia-Pacific Microwave Conference (APMC),* Yokohama, Japan, 7-10 December, pp. 1747-1750.

Hunter, I. C., Billonet, L., Jarry, B. and Guillon, P. (2002) 'Microwave filters-applications and technology', *IEEE Transactions on microwave theory and techniques*, 50(3), pp. 794-805. doi: 10.1109/22.989963.

Ismail, M. A., Wang, Y. and Yu, M. (2012) 'Advanced design and optimization of large scale microwave devices', In *Proceedings of the IEEE MTT-S International Microwave Symposium Digest,* Montreal, Canada, 17-22 June, pp. 1-3. doi: 10.1109/MWSYM.2012.6259535.

Karim, M. F., Ong, L. C., Chiam, T. M. and Seah, K. H. (2011) 'SIW bandpass filter based on negative order resonance', In *Proceedings of the IEEE Asia-Pacific Microwave Conference (APMC)*, Melbourne, Victoria, Australia, 5-8 December, pp. 1098-1101.

Keysight Technologies (2001) *Adding a box*. Available at: http://literature.cdn.keysight.com/litweb/pdf/ads2001/mom/mom052.html (Accessed: 25/07/2017).

Keysight Technologies (2011) *Defining FEM Paddings*. Available at: http://edadocs.software.keysight.com/display/empro2011/Defining+Outer+Boundary+Conditions (Accessed: 27/07/2017).

Khanna, A. P. S. and Garault, Y. (1983) 'Determination of loaded, unloaded, and external quality factors of a dielectric resonator coupled to a microstrip line', *IEEE Transactions on Microwave Theory and Techniques*, 31(3), pp 261-264. doi: 10.1109/TMTT.1983.1131473.

Kim, D. H., Kim, D., Ryu, J. I., Kim, J. C., Park, J. C. and Park, C. D. (2010) 'A novel integrated Tx-Rx diplexer for dual-band WiMAX system', In *Proceedings of the IEEE MTT-S International Microwave Symposium Digest,* Anaheim, CA, USA, 23-28 May, pp. 1736-1739. doi: 10.1109/MWSYM.2010.5514675.

King, T. S., Ying, A. T. Y. and Tiong, S. H. (2011) 'A microstrip diplexer using folded hairpins', In *Proceedings of the IEEE International RF and Microwave Conference (RFM),* Seremban, Malaysia, 12-14 December, pp. 226-229. doi: 10.1109/RFM.2011.6168735.

Kodera, T. and Caloz, C. (2010) 'Integrated leaky-wave antenna–duplexer/diplexer using CRLH uniform ferrite-loaded open waveguide', *IEEE Transactions on Antennas and Propagation*, 58(8), pp. 2508-2514. doi: 10.1109/TAP.2010.2050449.

Kordiboroujeni, Z., Bornemann, J. and Sieverding, T. (2014) 'K-band substrate integrated waveguide T-junction diplexer design by mode-matching techniques', In *Proceedings of the IEEE Asia-Pacific Microwave Conference (APMC),* Sandai, Japan, 4-7 November, pp. 1297-1299.

Kordiboroujeni, Z. and Bornemann, J. (2015) 'K-band backward diplexer in substrate integrated waveguide technology', *IET Electronics Letters*, 51(18), pp. 1428-1429. doi: 10.1049/el.2015.0948.

Kuan, H., Yang, R.-Y., Weng, M.-H. and Chen, W.-L. (2009) 'A novel parallel-coupled line diplexer excited using slot-line resonators for ultra-wideband communications', *Microwave and Optical Technology Letters*, 51(6), pp. 1552-1555. doi: 10.1002/mop.24356.

Lai, C. H., Zhou, G. T. and Ma, T. G. (2014) 'On-chip miniaturized diplexer using jointed dual-mode right-/left-handed synthesized coplanar waveguides on GIPD process', *IEEE Microwave and Wireless Components Letters*, 24(4), pp. 245-247. doi: 10.1109/LMWC.2014.2299553.

Lai, Q., Fumeaux, C., Hong, W. and Vahldieck, R. (2009) 'Characterization of the propagation properties of the half-mode substrate integrated waveguide', *IEEE Transactions on Microwave Theory and Techniques*, 57(8), pp. 1996-2004. doi: 10.1109/TMTT.2009.2025429.

Lee, C. H., Hsu, C. I. G., Wu, S. X. and Wen, P. H. (2016) 'Balanced quad-band diplexer with wide common-mode suppression and high differential-mode isolation', *IET Microwaves, Antennas & Propagation*, 10(6), pp. 599-603. doi: 10.1049/iet-map.2015.0538.

Lee, T. H. (2004) *Planar microwave engineering: a practical guide to theory, measurement, and circuits*. New York, NY: Cambridge University Press. ISBN: 9780521835268.

Lerdwanittip, R., Namsang, A. and Akkaraekthalin, P. (2011) 'Bandpass filters using T-shape stepped impedance resonators for wide harmonics suppression and their application for a diplexer', *Journal of Semiconductor Technology and Science*, 11(1), pp. 65-72. doi: 10.5573/JSTS.2011.11.1.065.

Li, J., Huang, H., Zhang, Z., Song, W., Shao, H., Chen, C. and Huang, W. (2013) 'A novel x-band diplexer based on overmoded circular waveguides for high-power microwaves', *IEEE Transactions on Plasma Science*, 41(10), pp. 2724-2728. doi: 10.1109/TPS.2013.2258473.

Lin, S. C. and Yeh, C. Y. (2015) 'Design of microstrip triplexer with high isolation based on parallel coupled-line filters using T-shaped short-circuited resonators', *IEEE Microwave and Wireless Components Letters*, 25(10), pp.648-650. doi: 10.1109/LMWC.2015.2463215.

Lin, Y. S. and Chen, C. H. (2002) 'Lumped-element coplanar-waveguide diplexer', In *Proceedings of the IEEE 32nd European Microwave Conference (EuMC),* Milan, Italy, 23-26 September, pp. 1-4. doi: 10.1109/EUMA.2002.339254.

Liu, H., Xu, W., Zhang, Z. and Guan, X. (2013) 'Compact diplexer using slotline stepped impedance resonator', *IEEE Microwave and Wireless Components Letters*, 23(2), pp. 75-77. doi: 10.1109/LMWC.2013.2238912.

Loras-Gonzalez, F., Sobrino-Arias, S., Hidalgo-Carpintero, I., García-Lampérez, A. and Salazar-Palma, M. (2010) 'A novel Ku-band dielectric resonator triplexer based on generalized multiplexer theory', In *Proceedings of the IEEE MTT-S International Microwave Symposium Digest,* Anaheim, CA, USA, 23-28 May, pp. 884-887. doi: 10.1109/MWSYM.2010.5515905.

Macchiarella, G. and Tamiazzo, S. (2006) 'Novel approach to the synthesis of microwave diplexers', *IEEE Transactions on Microwave Theory and Techniques*, 54(12), pp. 4281-4290. doi: 10.1109/TMTT.2006.885909.

Macchiarella, G. and Tamiazzo, S. (2006) 'Synthesis of diplexers based on the evaluation of suitable characteristic polynomials', In *Proceedings of the IEEE MTT-S International Microwave Symposium Digest,* San Francisco, CA, USA, 11-16 June, pp. 111-114. doi: 10.1109/MWSYM.2006.249406.

Macchiarella, G. and Tamiazzo, S. (2010) 'Design of triplexer combiners for base stations of mobile communications', In *Proceedings of the IEEE MTT-S International Microwave Symposium Digest,* Anaheim, CA, USA, 23-28 May, pp. 429-432. doi: 10.1109/MWSYM.2010.5515617.

Macchiarella, G. and Tamiazzo, S. (2010) 'Synthesis of star-junction multiplexers', *IEEE Transactions on Microwave Theory and Techniques*, 58(12), pp. 3732-3741. doi: 10.1109/TMTT.2010.2086570.

Mansour, M. M., Shalaby, A. A. T., El-Rabaie, E. S. M. and Messiha, N. W. (2014) 'Design and simulation of microwave diplexer based on D-CRLH metamaterials', In *Proceedings of the IEEE 2nd International Conference on Engineering and Technology (ICET),* Cairo, Egypt, 19-20 April, pp. 1-5. doi: 10.1109/ICEngTechnol.2014.7016782.

Mansour, R. R., Jolley, B., Ye, S., Thomson, F. S. and Dokas, V. (1996) 'On the power handling capability of high temperature superconductive filters', *IEEE Transactions on Microwave Theory and Techniques*, 44(7), pp. 1322-1338. doi: 10.1109/22.508237.

Matthaei, G., Young, L. and Jones, E. M. T. (1980) *Microwave Filters, Impedance-Matching Networks, and Coupling Structures*. Norwood: Artech House. ISBN: 9780890060995.

Meng, M. and Wu, K. L. (2010) 'Direct synthesis of general Chebyshev bandpass filters with a frequency variant complex load', In *Proceedings of the IEEE MTT-S International Microwave Symposium Digest,* Anaheim, CA, USA, 23-28 May, pp. 433-436. doi: 10.1109/MWSYM.2010.5517836.

Menzel, W. and Balalem, A. (2005) 'Quasi-lumped suspended stripline filters and diplexers', *IEEE Transactions on Microwave Theory and Techniques*, 53(10), pp. 3230-3237. doi: 10.1109/TMTT.2005.855139.

Mohottige, N., Glubokov, O., Jankovic, U. and Budimir, D. (2016) 'Ultra compact inline E-plane waveguide bandpass filters using cross coupling', *IEEE Transactions on Microwave Theory and Techniques*, 64(8), pp. 2561-2571. Doi: 10.1109/TMTT.2016.2578329.

Morini, A., Baldelli, M., Venanzoni, G., Cifola, L., Farina, M., Iglesias, P. M., Ernst, C. and Macchiarella, G. (2015) 'Improvement of dual-manifold architecture for the design of reconfigurable diplexers', In *Proceedings of the IEEE MTT-S International Microwave Symposium Digest,* Phoenix, AZ, USA, pp. 1-4. doi: 10.1109/MWSYM.2015.7167119.

Nwajana, A. O. and Yeo, K. S. K. (2016) 'Microwave diplexer purely based on direct synchronous and asynchronous coupling', *Radioengineering*, 25(2), pp. 247-252. doi: 10.13164/re.2016.0247.

Nwajana, A. O. and Yeo, K. S. K. (2016) 'Multi-coupled resonator microwave diplexer with high isolation', In *Proceedings of the IEEE 46th European Microwave Conference (EuMC),* London, UK, 4-6 October, pp. 1167-1170. doi: 10.1109/EuMC.2016.7824556.

Nwajana, A. O., Dainkeh, A. and Yeo, K. S. K. (2017) 'Substrate integrated waveguide (SIW) bandpass filter with novel microstrip-CPW-SIW input coupling', *Journal of Microwaves, Optoelectronics and Electromagnetic Applications,* 16(2), pp. 393-402. doi: http://dx.doi.org/10.1590/2179-10742017v16i2793.

Nwajana, A. O., Yeo, K. S. K. and Dainkeh, A. (2016), 'Low cost SIW Chebyshev bandpass filter with new input/output connection', In *Proceedings of the IEEE 16th Mediterranean Microwave Symposium (MMS)*, Abu Dhabi, UAE, 14-16 November, pp. 1-4. doi: 10.1109/MMS.2016.7803795.

Packiaraj, D., Ramesh, M. and Kalghatgi, A. T. (2005) 'Cavity diplexer using tapped line interdigital filters', In *Proceedings of the IEEE Asia-Pacific Microwave Conference (APMC),* Suzhou, China, 4-7 December, 1, pp. 1-3. doi: 10.1109/APMC.2005.1606274.

Palma, L. D., Bilotti, F., Toscano, A. and Vegni, L. (2012) 'Design of a waveguide diplexer based on connected bi-omega particles', *IEEE Microwave and Wireless Components Letters*, 22(3), pp. 126-128. doi: 10.1109/LMWC.2012.2186560.

Pasian, M., Bozzi, M. and Perregrini, L. (2013) 'Radiation losses in substrate integrated waveguides: a semi-analytical approach for a quantitative determination', In *Proceedings of the IEEE MTT-S International Microwave Symposium Digest,* Seattle, WA, USA, 2-7 June, pp. 1-3. doi: 10.1109/MWSYM.2013.6697593.

Peng, H. S. and Chiang, Y. C. (2015) 'Microstrip diplexer constructed with new types of dual-mode ring filters', *IEEE Microwave and Wireless Components Letters*, 25(1), pp. 7-9. doi: 10.1109/LMWC.2014.2365740.

Pozar, D. M. (2004) *Microwave engineering*. 3rd edn. New York, NY: John Wiley & Sons. ISBN: 9780471448785.

Pucel, R. A., Masse, D. J. and Hartwig, C. P. (1968) 'Losses in microstrip', *IEEE Transactions on Microwave Theory and Techniques*, *16*(6), pp. 342-350. doi: 10.1109/TMTT.1968.1126691.

Rakic, M., Jokanovic, B. and Budimir, D. (2004) 'Waveguide E-plane all-metal inserted diplexer', *Serbian Journal of Electrical Engineering*, 1(3), pp. 79-87. doi: 10.2298/SJEE0403079R.

Ranjkesh, N. and Shahabadi, M. (2008) 'Loss mechanism in SIW and MSIW', *Progress in Electromagnetic Research B*, 4, pp. 299-309. doi: 10.2528/PIERB08012807.

Reid, J. R., Hanna, D. and Webster, R. T. (2008) 'A 40/50 GHZ diplexer realized with three dimensional copper micromachining', In *Proceedings of the IEEE MTT-S International Microwave Symposium Digest,* Atlanta, GA, USA, 15-20 June, pp. 1271-1274. doi: 10.1109/MWSYM.2008.4633291.

Rezaee, M., Zaman, A. U. and Kildal, P. S. (2015) 'V-band groove gap waveguide diplexer', In *Proceedings of the IEEE 9th European Conference on Antennas and Propagation (EuCAP),* Lisbon, Portugal, 13-17 April, pp. 1-4.

Rhodes, J. D. and Levy, R. (1979) 'Design of general manifold multiplexers', *IEEE Transactions on Microwave Theory and Techniques*, 27(2), pp. 111-123. doi: 10.1109/TMTT.1979.1129571.

Saavedra, C. E. (2008) 'Diplexer using a circulator and interchangeable filters', In *Proceedings of the IEEE 7th International Caribbean Conference on Devices, Circuits and Systems (ICCDCS)*, Cancun, Mexico, 28-30 April, pp. 1-5. doi: 10.1109/ICCDCS.2008.4542631.

Schorer, J., Bornemann, J. and Rosenberg, U. (2016) 'Mode-matching design of substrate mounted waveguide (SMW) components', *IEEE Transactions on Microwave Theory and Techniques*, 64(8), pp. 2401-2408. doi: 10.1109/TMTT.2016.2582484.

Setoodeh, S., Mansour, R. R. and Gupta, D. (2013) 'Multi-layer low temperature superconducting K-band filter and diplexer design', In *Proceedings of the IEEE MTT-S International Microwave Symposium Digest,* Seattle, WA, USA, 2-7 June, pp. 1-4. doi: 10.1109/MWSYM.2013.6697798.

Shang, X., Wang, Y., Xia, W. and Lancaster, M. J. (2013) 'Novel multiplexer topologies based on all-resonator structures', *IEEE Transactions on Microwave Theory and Techniques*, 61(11), pp. 3838-3845. doi: 10.1109/TMTT.2013.2284496.

Shen, T., Zaki, K. A. and Dolan, T. G. (2003) 'Rectangular waveguide diplexers with a circular waveguide common port', *IEEE Transactions on Microwave Theory and Techniques*, 51(2), pp. 578-582. doi: 10.1109/TMTT.2002.807811.

Shi, J., Chen, J. X. and Bao, Z. H. (2011) 'Diplexers based on microstrip line resonators with loaded elements', *Progress in Electromagnetics Research*, 115, pp. 423-439. doi: 10.2528/PIER11031516.

Shimonov, G., Garb, K. and Kastner, R. (2010) 'Mode matching analysis and design of waveguide E-plane filters and diplexers', In *Proceedings of the IEEE International Workshop on Antenna Technology (iWAT),* Lisbon, Portugal, 1-3 March, pp. 1-4. doi: 10.1109/IWAT.2010.5464745.

Sirci, S., Martínez, J. D., Vague, J. and Boria, V. E. (2015) 'Substrate integrated waveguide diplexer based on circular triplet combline filters', *IEEE Microwave and Wireless Components Letters*, 25(7), pp. 430-432. doi: 10.1109/LMWC.2015.2427516.

Skaik, T. (2012) 'Novel star-junction coupled-resonator multiplexer structures', *Progress in Electromagnetics Research Letters*, 31, pp. 113-120. doi: 10.2528/PIERL12030114.

Skaik, T. and AbuHussain, M. (2013) 'Design of diplexers for E-band communication systems', In *Proceedings of the IEEE 13th Mediterranean Microwave Symposium (MMS)*, Saida, Lebanon, 2-5 September, pp. 1-4. doi: 10.1109/MMS.2013.6663087.

Skaik, T. and Lancaster, M. (2011) 'Coupled resonator diplexer without external junctions', *Journal of Electromagnetic Analysis and Applications*, 3, pp. 238-241. doi: 10.4236/jemaa.2011.36038.

Skaik, T. F. and Tubail, D. A. (2015) 'Novel multiplexer topologies based on coupled resonator structures', In *Proceedings of the IEEE 15th Mediterranean Microwave Symposium (MMS),* Lecce, Italy, 30 November – 2 December, pp. 1-4. doi: 10.1109/MMS.2015.7375393.

Skaik, T. F., Lancaster, M. J. and Huang, F. (2011) 'Synthesis of multiple output coupled resonator circuits using coupling matrix optimisation', *IET Microwaves, Antennas & Propagation*, 5(9), pp. 1081-1088. doi: 10.1049/iet-map.2010.0447.

Skaik, T., Lancaster, M., Ke, M. and Wang, Y. (2011) 'A micromachined WR-3 band waveguide diplexer based on coupled resonator structures', In *Proceedings of the IEEE 41st European Microwave Conference (EuMC),* Manchester, UK, 10-13 October, pp. 770-773.

Steer, M. (2009) *Microwave and RF design*. North Carolina: SciTech. ISBN: 9781891121883.

Tang, H. J., Hong, W., Chen, J. X., Luo, G. Q. and Wu, K. (2007) 'Development of millimeter-wave planar diplexers based on complementary characters of dual-mode substrate integrated waveguide filters with circular and elliptic cavities', *IEEE Transactions on Microwave Theory and Techniques*, 55(4), pp. 776-782. doi: 10.1109/TMTT.2007.893655.

Tantiviwat, S., Intarawiset, N. and Jeenawong, R. (2013) 'Wide-stopband, compact microstrip diplexer with common resonator using stepped-impedance resonators', In *Proceedings of the IEEE TENCON Spring Conference,* Sydney, Australia, 17-19 April, pp. 174-177. doi: 10.1109/TENCONSpring.2013.6584435.

Taroncher, M., Hueso, J., Cogollos, S., Gimeno, B., Vidal, A., Boria, V. E. and Guglielmi, M. (2006) 'Accurate consideration of ohmic losses in passive waveguide circuits for microwave and millimeter-wave applications', In *Proceedings of the IEEE Mediterranean Electrotechnical Conference (MELECON),* Malaga, Spain, 16-19 May, pp. 180-183. doi: 10.1109/MELCON.2006.1653066.

Taroncher, M., Hueso, J., Cogollos, S., Vidal, A., Boria, V. E. and Gimeno, B. (2006) 'Efficient and accurate consideration of ohmic losses in waveguide diplexers and multiplexers', In *Proceedings of the IEEE MTT-S International Microwave Symposium Digest,* San Francisco, CA, USA, 11-16 June, pp. 1241-1244. doi: 10.1109/MWSYM.2006.249435.

Teberio, F., Arregui, I., Guglielmi, M., Gomez-Torrent, A., Soto, P., Laso, M. A. G. and Boria, V. E. (2016) 'Compact broadband waveguide diplexer for satellite applications', In *Proceedings of the IEEE MTT-S International Microwave Symposium Digest,* San Francisco, CA, USA, 22-27 May, pp. 1-4. doi: 10.1109/MWSYM.2016.7540231.

Thirupathaiah, K., Iyer, B., Pathak, N. P. and Rastogi, V. (2014) 'Concurrent dualband diplexer for nanoscale wireless links', *IEEE Photonics Technology Letters*, 26(18), pp. 1832-1835. doi: 10.1109/LPT.2014.2337016.

Tsai, W. L., Shen, T. M., Chen, B. J., Huang, T. Y. and Wu, R. B. (2013) 'Design of single-branch laminated waveguide diplexers using modal orthogonality', *IEEE Transactions on Microwave Theory and Techniques*, 61(12), pp. 4079-4089. doi: 10.1109/TMTT.2013.2287476.

Tu, W. H. and Hung, W. C. (2014) 'Microstrip eight-channel diplexer with wide stopband', *IEEE Microwave and Wireless Components Letters*, 24(11), pp. 742-744. doi: 10.1109/LMWC.2014.2348499.

Tubail, D. A. and Skaik, T. F. (2015) 'Synthesis of coupled resonator-based multiplexers with generalised structures using coupling matrix optimisation', *IET Electronics Letters*, 51(23), pp. 1891-1893. doi: 10.1049/el.2015.2274.

Wang, R. and Xu, J. (2012) 'Synthesis and design of microwave diplexers with a common resonator junction', In *Proceedings of the IEEE International Conference on Microwave and Millimeter Wave Technology (ICMMT),* 2, pp. 1-4. doi: 10.1109/ICMMT.2012.6230019.

Wang, R., Wu, L. S. and Zhou, X. L. (2008) 'Compact folded substrate integrated waveguide cavities and bandpass filter', *Progress in Electromagnetics Research*, 84, pp. 135-147. doi: 10.2528/PIER08071501.

Wang, R., Xu, J., Wang, M. Y. and Dong, Y. L. (2012) 'Synthesis of microwave resonator diplexers using linear frequency transformation and optimization', *Progress in Electromagnetic Research*, 124, pp. 441-455. doi: 10.2528/PIER12011108.

Wang, R., Zhou, X. L. and Wu, L. S. (2009) 'A folded substrate integrated waveguide cavity filter using novel negative coupling', *Microwave and Optical Technology Letters*, 51(3), pp. 866-871. doi: 10.1002/mop.24181.

Wang, W., Zhang, Q., Lin, X., Wang, F. and Liao, W. (2015) 'Diplexer with high isolation using multi-order resonances', In *Proceedings of the IEEE Asia-Pacific Microwave Conference (APMC),* 6-9 December, Nanjing, China, 3, pp. 1-3. doi: 10.1109/APMC.2015.7413542.

Wang, Y. and Lancaster, M. J. (2013) 'An investigation on the coupling characteristics of a novel multiplexer configuration', In *Proceedings of the IEEE 43rd European Microwave Conference (EuMC),* Nuremberg, Germany, 6-10 October, pp. 900-903.

Watkins, J. (1969) ‘Circular resonant structures in microstrip’, *IET Electronics Letters*, *5*(21), pp. 524-525. doi: 10.1049/el:19690393.

Wen, C. P. (1969) ‘Coplanar waveguide: a surface strip transmission line suitable for nonreciprocal gyromagnetic device applications’, *IEEE Transactions on Microwave Theory and Techniques*, 17(12), pp. 1087-1090. doi: 10.1109/TMTT.1969.1127105.

Wolff, I. and Knoppik, N. (1971) ‘Microstrip ring resonator and dispersion measurement on microstrip lines’, *IET Electronics Letters*, 26(7), pp. 779-781. doi: 10.1049/el:19710532.

Wu, H. W., Huang, S. H. and Chen, Y. F. (2013) ‘Design of new quad-channel diplexer with compact circuit size’, *IEEE Microwave and Wireless Components Letters,* 23(5), pp. 240-242. doi: 10.1109/LMWC.2013.2253314.

Wu, K. L. and Meng, W. (2007) ‘A Direct synthesis approach for microwave filters with a complex load and its application to direct diplexer design’, *IEEE Transactions on Microwave Theory and Techniques*, 55(5), pp. 1010-1016. doi: 10.1109/TMTT.2007.895175.

Wu, Z. L., Lee, C. H. and Chen, H. H. (2015) ‘Balun diplexer design in hybrid structure of microstrip line and slot-line’, In *Proceedings of the IEEE Asia-Pacific Microwave Conference (APMC)*, Nanjing, China, 6-9 December, 3, pp. 1-3. doi: 10.1109/APMC.2015.7413541.

Xia, L., Xu, R., Yan, B., Li, J., Guo, Y. and Wang, J. (2006) ‘Broadband transition between air-filled waveguide and substrate integrated waveguide’, *IET Electronics Letters*, *42*(24), p. 1403-1405. doi: 10.1049/el:20062228.

Xia, W., Shang, X. and Lancaster, M. J. (2014) ‘All-resonator-based waveguide diplexer with cross-couplings’, *IET Electronics Letters*, *50*(25), pp.1948-1950. doi: 10.1049/el.2014.3659.

Xiao, J. K., Zhu, M., Li, Y., Tian, L. and Ma, J. G. (2015) ‘High selective microstrip bandpass filter and diplexer with mixed electromagnetic coupling’, *IEEE Microwave and Wireless Components Letters*, 25(12), pp. 781-783. doi: 10.1109/LMWC.2015.2495194.

Xu, F. and Wu, K. (2005) 'Guided-wave and leakage characteristics of substrate integrated waveguide', *IEEE Transactions on Microwave Theory and Techniques*, 53(1), pp. 66-73. doi: 10.1109/TMTT.2004.839303.

Xu, J. (2016) 'Compact switchable bandpass filter and its application to switchable diplexer design', *IEEE Microwave and Wireless Components Letters*, *26*(1), pp. 13-15. doi: 10.1109/LMWC.2015.2505612.

Xu, W. Q. and Ho, M. H. (2007) 'UMTS diplexer design using combined coplanar waveguide and microstrip', In *Proceedings of the IEEE Region 10 Conference (TENCON 2007),* Taipei, Taiwan, 30 October – 2 November, pp. 1-4. doi: 10.1109/TENCON.2007.4428793.

Xu, W. Q., Ho, M. H. and Hsu, C. G. (2007) 'UMTS diplexer design using dual-mode stripline ring resonators', *IET Electronics Letters*, 43(13), pp. 721-722. doi: 10.1049/el:20070747.

Xu, W. Q., Ho, M. H. and Hsu, C. I. (2009) 'Quasi-lumped design of UMTS diplexer using combined CPW and microstrip', *Microwave and Optical Technology Letters*, 51(1), pp. 150-152. doi: 10.1002/mop.23952.

Xue, Q. and Chen, J. X. (2008) 'Compact diplexer based on double-sided parallel-strip line', *IET Electronic Letters*, 44(2), pp. 123-124. doi: 10.1049/el:20083117.

Yang, T. and Rebeiz, G. M. (2013) 'Three-pole 1.3–2.4-GHz diplexer and 1.1–2.45-GHz dual-band filter with common resonator topology and flexible tuning capabilities', *IEEE Transactions on Microwave Theory and Techniques*, 61(10), pp. 3613-3624. doi: 10.1109/TMTT.2013.2279381.

Yang, T. and Rebeiz, G. M. (2016) 'A simple and effective method for 1.9–3.4-GHz tunable diplexer with compact size and constant fractional bandwidth. *IEEE Transactions on Microwave Theory and Techniques*, 64(2), pp. 436-449. doi: 10.1109/TMTT.2015.2504937.

Yang, T., Chi, P. L. and Itoh, T. (2010) 'High isolation and compact diplexer using the hybrid resonators', *IEEE Microwave and Wireless Components Letters*, 20(10), pp. 551-553. doi: 10.1109/LMWC.2010.2052793.

Ye, S. and Mansour, R. R. (1994) 'Design of manifold-coupled multiplexers using superconductive lumped element filters', In *Proceedings of the IEEE MTT-S*

International Microwave Symposium Digest, San Diego, CA, USA, 23-27 May, pp. 191-194. doi: 10.1109/MWSYM.1994.335255.

Yeo, K. S. K. and Lancaster, M. J. (2001) 'The design of microstrip six-pole quasi-elliptic filter with linear phase response using extracted-pole technique', *IEEE Transactions on Microwave Theory and Techniques*, 49(2), pp. 321-327. doi: 10.1109/22.903092.

Yeo, K. S. K. and Nwajana, A. O. (2013) 'A novel microstrip dual-band bandpass filter using dual-mode square patch resonators', *Progress in Electromagnetic Research C*, 36, pp. 233-247. doi: 10.2528/PIERC12120312.

Yiming, L. and Xing, J. (2010) 'Design of a Ku-band cavity diplexer with an E-plane T-junction', In *Proceedings of the IEEE 9th International Symposium on Antennas, Propagation and EM Theory (ISAPE),* Guangzhou, China, 29 November – 2 December, pp. 1105-1108. doi: 10.1109/ISAPE.2010.5696670.

Yun, S. H., Uhm, M. S. and Yom, I. B. (2005) 'Design of multiplication free high power Ka-band diplexer with an E-plane T-junction', In *Proceedings of the IEEE Asia-Pacific Conference on Communications*, Perth, Western Australia, 3-5 October, pp. 582-585. doi: 10.1109/APCC.2005.1554128.

Zhang, D., Zhao, Y., Liu, W., Zhao, W. and Sun, Q. (2010) 'A fast synthesis approach for diplexer with E-plane T-junction design', *In Proceedings of the IEEE 3rd International Symposium on Information Science and Engineering (ISISE),* Shanghai, China, 24-26 December, pp. 133-136. doi: 10.1109/ISISE.2010.32.

Zhang, Y., Ruiz-Cruz, J. A. and Zaki, K. A. (2006) 'Ridge waveguide coupled stripline resonator filters and multiplexers', In *Proceedings of the IEEE MTT-S International Microwave Symposium Digest,* San Francisco, CA, USA, 11-16 June, pp. 681-684. doi: 10.1109/MWSYM.2006.249724.

Zhao, P. and Wu, K.L. (2016) 'Model-based vector-fitting method for circuit model extraction of coupled-resonator diplexers', *IEEE Transactions on Microwave Theory and Techniques*, 64(6), pp. 1787-1797. doi: 10.1109/TMTT.2016.2558639.

Zheng, T., Guo, X., Cao, B., Wei, B., Zhang, X., Feng, C. and Zhang, G. (2014) 'Design of compact superconducting diplexer with spiral short-circuited stubs', *IEEE Transactions on Applied Superconductivity*, 24(2), pp. 16-20. doi: 10.1109/TASC.2014.2302375.

Zheng, T., Wei, B., Cao, B., Guo, X., Zhang, X., Jiang, L., Xu, Z. and Heng, Y. (2015) 'Compact superconducting diplexer design with conductor-backed coplanar waveguide structures', *IEEE Transactions on Applied Superconductivity*, *25*(2), pp. 1-4. doi: 10.1109/TASC.2015.2409204.

Zhou, Y., Deng, H. W. and Zhao, Y. (2014) 'Compact balanced-to-balanced microstrip diplexer with high isolation and common-mode suppression', *IEEE Microwave and Wireless Components Letters*, *24*(3), pp. 143-145. doi: 10.1109/LMWC.2013.2291856.

Zhu, L., Mansour, R. R. and Yu, M. (2014) 'A compact waveguide diplexer employing dual-band resonators', In *Proceedings of the IEEE MTT-S International Microwave Symposium Digest*, Tampa, FL, USA, 1-6 June, pp. 1-4. doi: 10.1109/MWSYM.2014.6848499.